UiT
THE ARCTIC UNIVERSITY OF NORWAY

Faculty of science and technology

Department of Geoscience

The effect of lithology and microstructure on the deformation of unstable rock slopes in northern Norway

—

Emilie Jensen Aamodt

Master's thesis in Geology (GEO-3900), May 2022

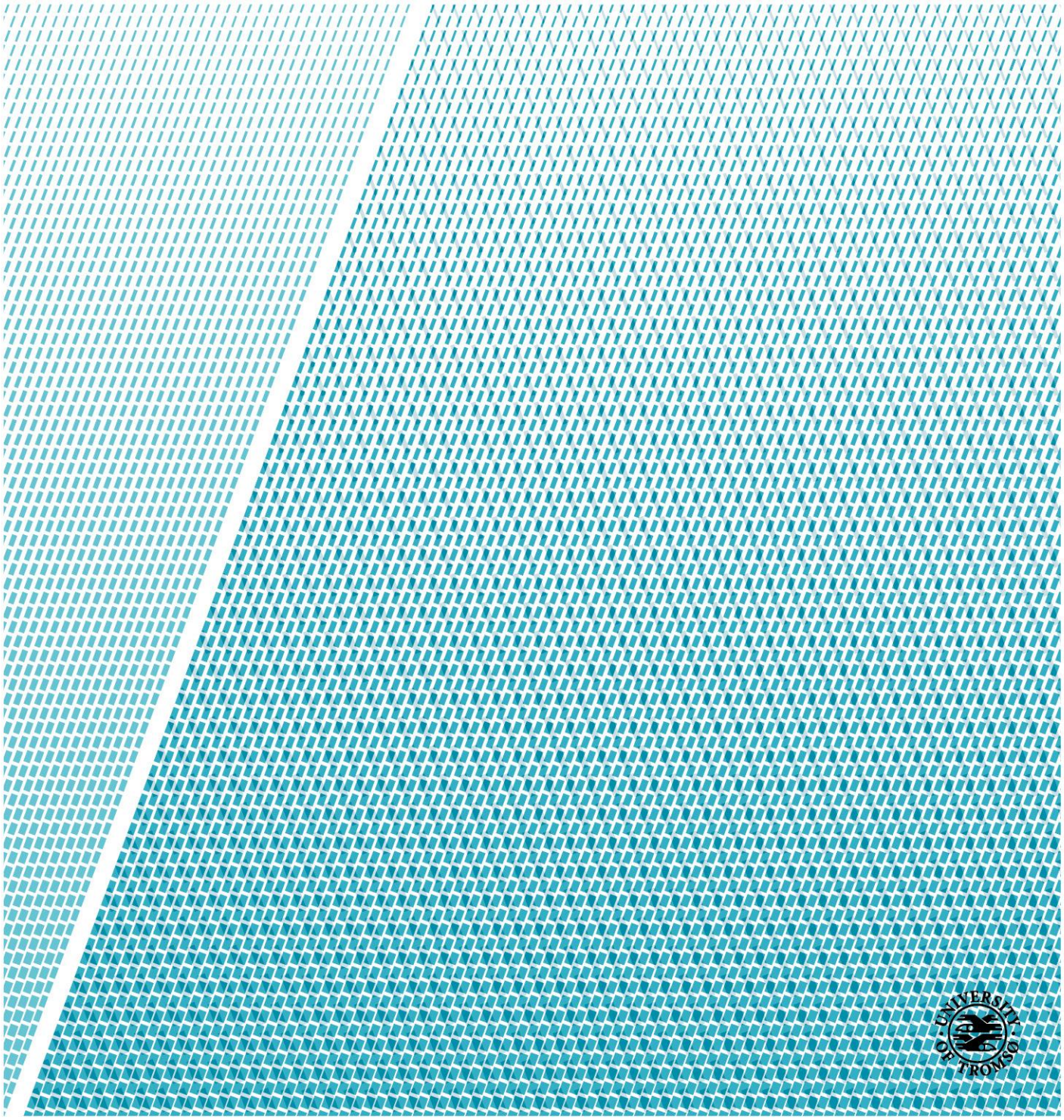

Abstract

The alpine landscape in Troms and Finnmark County makes it a region with a high frequency of unstable rock slopes. Catastrophic failure and the possibility of subsequent displacement waves pose a direct threat if a failure occurs at an unstable rock slope, which can cause a great loss of life and damage to infrastructure. The study of geology and its effect on unstable rock slope failures is therefore considered essential for the understanding of future instabilities.

Pre-existing structural discontinuities are considered a necessity for the point of rupture initiation, and important to understand in terms of correct characterization of the failure process and risk evaluation. To retrieve more information about the effect of discontinuities at different scales, two unstable rock slopes have been studied in this thesis. Dusnjarga in Kvænangen municipality and Gámanjunni 3 in Kåfjord municipality both consist of metamorphosed bedrock, but each has completely different lithological properties. Dusnjarga consists of meta-igneous metagabbro and amphibolite, and Gámanjunni 3 of meta-sedimentary mica-schist with layers of metapsammite and amphibolite.

A total of 76 samples and 3000 structural measurements were collected from fieldwork. To retrieve information about the small-scale discontinuities' effect on strength, a selection of samples from each locality have been studied under the microscope and undergone mechanical testing. The processed rock material resulted in 20 uniaxial compression tests, 263 point load tests, and 22 thin sections.

Both localities have a high frequency of pre-existing structural discontinuities in the back scarp region. Dusnjarga has a 50 m thick mylonitic zone in the back scarp together with lenses and folds, and a highly metamorphosed rock mass. Ductile shear zones, brittle faults, and consistent joint sets are observed throughout the unstable area. At Gámanjunni 3, layers of amphibolite and metapsammite together with sigma clasts and folds are centered around the back scarp region. The toe area is heavily affected by several brittle faults. Both Dusnjarga and Gámanjunni 3 consist of anisotropic rock, making the rock more prone to fail along foliation.

Microfractures and their behavior with respect to mineralogy, fabric, and structural discontinuities were investigated. At Dusnjarga, plagioclase is favored by microfracture propagation in metagabbro. These rocks also display a high frequency of small-scale ductile shear zones that microfractures utilize, propagating straight and often displaying dilation. The observed mylonite displays a highly densified system of randomly oriented microfractures. At Gámanjunni 3, the mica-rich samples are not very affected by microfractures and the samples with a lower mica content appear to have more favorable conditions for fracture propagation. Quartz is found to affect the sample by inducing more

brittle behavior, which is advantageous for fracture propagation, especially combined with small proportions of mica minerals.

All investigated thin sections present consistent small-scale joint sets parallel and normal to foliation. Each rock type displays different structures and mineralogy, and the fracture behavior is not random. In addition, observed microfractures appear to propagate easier in a metamorphosed fabric and favor changes in texture. All small-scale observations can be linked to large-scale discontinuities in unstable rock slopes. Lithology has a strong control on the development and evolution of URS-related structures.

Acknowledgements

First of all, I would like to thank my supervisor at the University of Tromsø (UiT), Louise M. Vick, for brilliant ideas, valuable guidance and helpful feedback. Secondly, I would like to thank my co-supervisors Carly Faber and Andreas Grumstad for educational and motivational feedback. A special thank you to the brilliant Carly Faber, for sharing your knowledge and the amount of time and effort you have put into my thesis. I am very grateful.

I would like to thank Kristine Halvorsen and the Norwegian Geotechnical Institute (NGI), for letting us use the rock lab, and for valuable guidance during testing.

I would also like to thank Martina Böhme, at the Geological Survey of Norway (NGU), for educational days at Dusnjarga and for sharing Gámanjunni data.

Thanks to The Norwegian Water Resources and Energy Directorate (NVE) for guidance and helicopter transport at Gámanjunni 3.

I would also like to thank co-student Simen Bekkevoll for the fun days in field and help with carrying rocks down Dusnjarga.

Lastly, a big thank you to my family and friends in Tromsø. Your support has truly made this year easier.

Emilie Jensen Aamodt – May 2022, Tromsø

Contents

1 Introduction

1.1 Introduction – motivational background

Norway is a country with beautiful nature, from alpine mountains ending in deep fjords to large plateaus with glaciers. The dramatic and mountainous nature of Norway is continuously changing from glacial uplift, wind, precipitation, and weathering. As a result of intense weather and geological history, avalanches have become one of the most active and prominent geological processes (Eikenæs, 2015). These avalanches occur as rockfall, snow-, soil, and rock avalanches. The recurrence interval for rock avalanches is infrequent, but history shows that the effects of rock avalanches are the most catastrophic to nature, life, and infrastructure. The chance of rock avalanches happening remains small, but such an event will have a catastrophic effect on life and infrastructure. The Norwegian Water Resources and Energy Directorate (NVE) therefore ordered the Geological Survey of Norway (NGU) to identify and map all, if possible, potentially unstable rock slopes (URS). In this report, a total of 66 URS was investigated (Bunkholt et al., 2011), and in total there are more than 130 rock slope deformations identified in Troms County, northern Norway (NGU, 2019a).

Northern Norway is a region with a high frequency of large and unstable rock slope deformations. The landscape is alpine, and the bedrock is mostly metamorphic, usually with anisotropic properties, which appear to easily cause or trigger instabilities. The bedrock geology is highly relevant to assess and understand the failure mechanisms and mechanical properties that influence deformation in rock slopes. In this case, it is also beneficial to investigate regional geology to understand the pre-existing structures and lithological changes that have the potential to affect mechanical properties on a larger scale. Point of rupture initiation often follows pre-existing structures in the bedrock, these structures are identified as discontinuities and linked directly to the unstable slopes (Vick et al., 2020). Understanding the effect and magnitude of discontinuities at all scales gives a more adequate understanding of the mechanical behavior that causes large instabilities.

Each unstable rock slope is affected by local petrology, structures, morphology, and periglacial processes, and the failure mechanisms can therefore be difficult to recognize and understand. These factors are important to define in order to decide the magnitude of the unstable mass, runout zone, and likelihood of failing. However, every investigated URS is different. Information about failure mechanisms and internal deformations are therefore fundamental knowledge in the process of understanding the reason for failure.

Dusnjarga was classified as an unstable rock slope in 2008, after observing the movement for a year. Gámanjunni 3 is a URS in the Manndalen and a was classified a high-risk object in 2016, because of

the likelihood of failure combined with consequence. When Gámanjunni 3 got classified as a high-risk object, it became methodically studied and is today heavily monitored. Dusnjarga has been investigated by NGU and a master student (Bunkholt et al., 2011; Blau, 2020). It is clear from earlier publications that Dusnjarga and Gámanjunni 3 are vastly different from a petrological perspective, so a further study of the discontinuities and their connection to small-scale structures would give a wider perspective and understanding of the deformation mechanisms. The understanding of how fractures behave and utilize discontinuities at all scales will give a broader understanding of the failure mechanism.

1.2 Definitions

ASTM = American Society for Testing and Materials

B.P. = Before Present

DEM = Digital Elevation Model

GIS = Geographic Information System

JN = Joint Set

KNC = Kalak Nappe Complex

LGM = Last Glacial Maximum

NGI = Norwegian Geotechnical Institute

NGU = The Geological Survey of Norway

NVE = The Norwegian Water Resources and Energy Directorate

PLT = Point Load Test

RNC = Reisa Nappe Complex

SIP = Seiland Igneous Province

UCS = Uniaxial Compression Strength test

URS = Unstable Rock Slope

1.3 Study area

Dusnjarga and Gámanjunni 3 are located in Troms and Finnmark county, northern Norway. Dusnjarga URS is located on Dusnjarga peninsula in Kvænangen municipality. Gámanjunni 3 is located in Manndalen in Kåfjord municipality. Locations marked in figure 1.

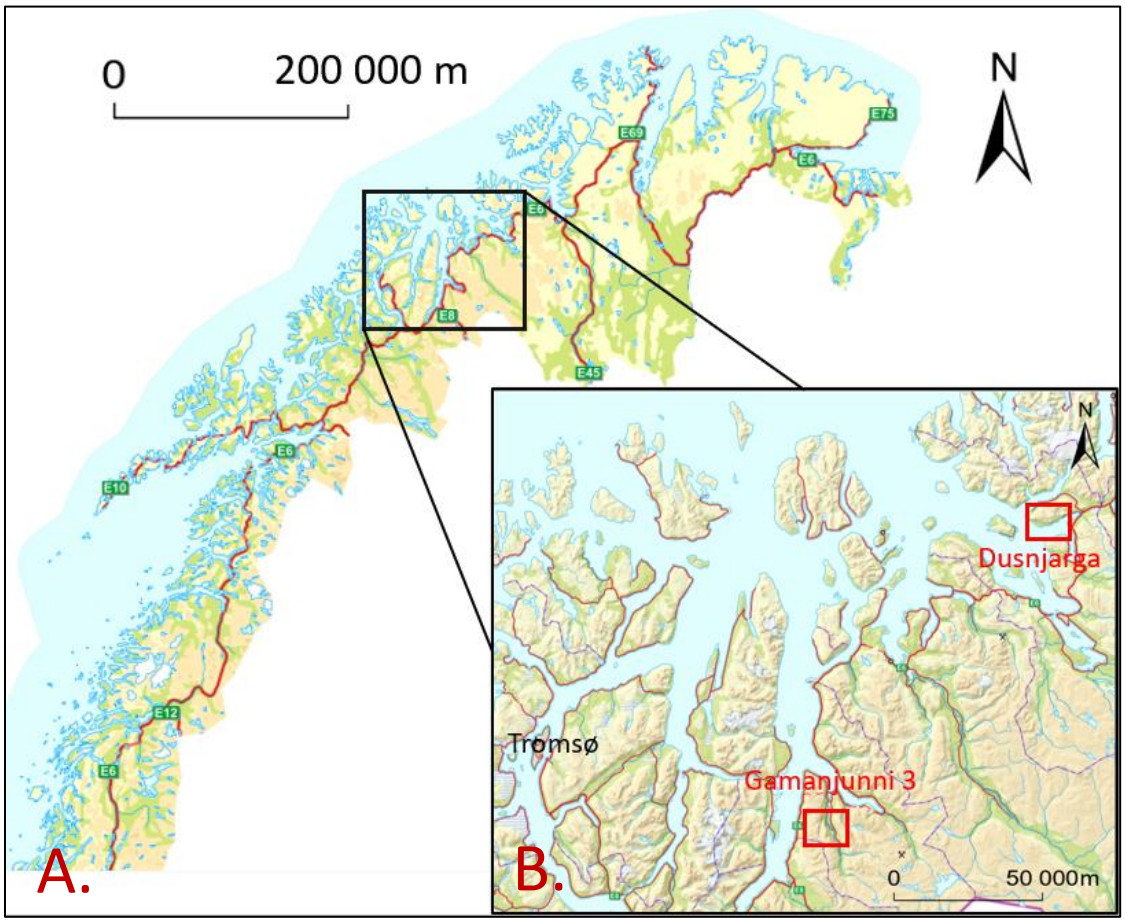

FIGURE 1: OVERVIEW OF THE TWO STUDY AREAS. A: NORTH OF NORWAY IN A 1: 200 000 SCALE. B: SECTION OF THE TWO INVESTIGATED AREAS: DUSNJARGA AND GÁMANJUNNI 3. TROMSØ IS ALSO MARKED IN AS A REFERENCE POINT. THE MAP IS IN 1:50 000 SCALE. BOTH MAPS ARE DEVELOPED USING THE APPLICATION ARCGIS PRO, BASELAYER IS TOPOGRAFISK NORGESKART 4 FROM KARTVERKET.NO

1.3.1 Dusnjarga

The URS Dusnjarga is located on the mountain Dusnjarga (figure 2 A and B). It is situated in Kvænangen municipality, Troms and Finnmark county. The unstable rock slope is located on the south face of the Dusnjarga peninsula, situated between the northern Lille Altafjorden and southern Jøkulfjorden. Both fjords are connected to the large Kvænangen fjord. The peninsula is approximately 11 km long and 5 km wide, with the highest mountain being Koppartind (923 m asl.). The nearest residential area, Alteidet, is located 400 m west of the base of Dusnjarga, where approximately 100 people live.

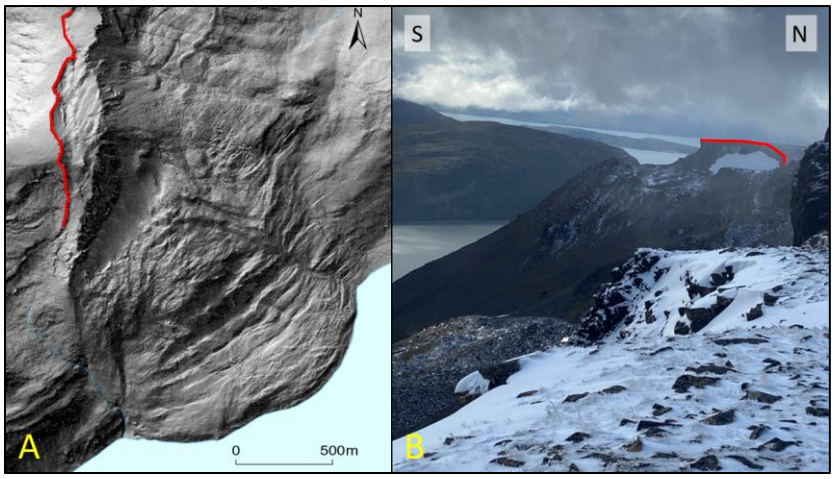

FIGURE 2: DUSNJARGA URS. A: HILLSHADE MAP OF DUSNJARGA URS WITH BACKSCARP MARKED IN RED. THE HILLSHADE IS GENERATED FORM A HIGH-RESOLUTION DIGITAL ELEVATION MODEL (DEM) OF A 0.5 M RASTER, DEVELOPED IN ARCGIS PRO. B: PHOTOGRAPH OF THE BACKSCARP AND PLATEAU AT DUSNJARGA URS, RED LINE ILLUSTRATES THE TOP EDGE AT THE BACKSCARP. PHOTOGRAPH TAKEN 5/9.2021 BY MYSELF.

1.3.2 Gámanjunni 3

Gámanjunni 3 (figure 3 A and B) is a URS in Manndalen Valley in Kåfjord municipality, Troms and Finnmark county. Manndalen is 15 km long and N-S oriented, with Gámanjunni 3 facing west. The plateau containing Gámanjunni 3 also contains six other URS, including Gámanjunni 1, Gámanjunni 2. Gámanjunni is a plateau mountain with a summit 1200 m asl. and steep mountain faces. Manndalen is an inhabited area with 900 people living in the valley (Pedersen, 2015). Olmmáiváteatnu, or Manndalselva, is a meandering river stretching 23 km through the Manndalen Valley.

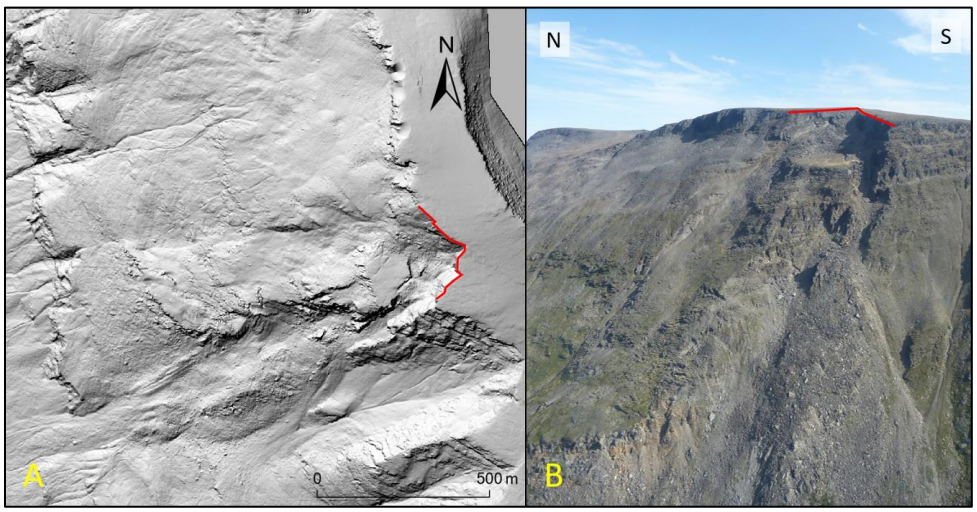

FIGURE 3: GÁMANJUNNI 3. A: HILLSHADE MAP OF GÁMANJUNNI 3 URS, WITH A RED LINE TO ILLUSTRATE THE BACKSCARP. THE HILLSHADE IS DEVELOPED WITH A 1 M RASTER DEM IN ARCGIS PRO. B: PHOTOGRAPH FROM GÁMANJUNNI 3, WITH A RED LINE ILLUSTRATES THE BACKSCARP. THE PICTURE IS ADAPTED BY H. BUNKHOLT, NVE (2019).

1.4 Climate

Climate factors, such as rainfall and permaprost, have been known to have a significant impact on URS development in Norway (Hilger et al., 2021; Pless et al., 2021; Etzelmuller et al., 2022). The URS sensitivity to rainfall is also suggested to have a thermal control on pore-water pressure (Hilger, 2019; Kristensen et al, 2021).

The topographical variation and vicinity to the coastal regions influence Troms' climate. The weather is dominated by long winters and short, cool summers. The winters are long with seven or more months snow-covered ground (Meteorologisk Institutt, 2021). In January, the average temperature in Troms is – 2 °C at the coast and – 7 °C in the interior regions. In July, the coastal regions have a temperature of 11-12 °C, and in the inner regions the average temperature is 14 °C. Northern Norway's coastal areas are less humid than coastal regions in the south. In the coastal regions of Troms and Finnmark, the average annual precipitation is 750 mm. Along the mountains at the coast, there is a zone of maximum precipitation, and this zone often has an annual precipitation rate of 1000-1500 mm (Dannevig, 2020). The low-altitude area in the coastal regions consists of sheltered valleys. Therefore, the annual precipitation can be as low as 300 mm. Both Dusnjarga and Gámanjunni -3 are in this low-altitude zone and experience a combination of coastal and continental climates. The temperature is not as cold as the continental climate but is often lower than the coastal climate.

The closest weather station to Dusnjarga is 15 km east in Sopnesbukta (8 m asl). The records show average annual precipitation of 745 mm within the period 1998-2021 (Meterologisk Institutt et al. 2021). The average temperature for the last decade measured at the Sopnesbukta weather station is 2.6 °C.

A weather station is located at the top of Gámanjunni -3 (1230 m asl). This station shows an average temperature of – 3.5 °C between 2017-2021 and average precipitation of 1074 mm in 2020-2021. A weather station in Manndalen reveals annual precipitation of 651 mm with a middle temperature of -6 °C in January and 11.9 °C in July (Meterologisk Institutt, 2019).

1.5 Regional geology

The bedrock geology is highly relevant to assess and understand the failure mechanisms and mechanical properties that influence deformation in rock slopes. In this case, it is also beneficial to investigate regional geology to understand the pre-existing structures and lithological changes that have the potential to affect the mechanical properties on a larger scale. The bedrock at both sites is

part of the Scandinavian Caledonides. The Scandinavian Caledonides are comprised of a series of allochthons (lower, middle, upper, and uppermost) including metasedimentary and magmatic rocks. The degree of metamorphism in the allochtons increases upwards and westward, from greenschist facies in in the east to amphibolite/granulite facies in the west.

1.5.1 Dusnjarga

The Dusnjarga peninsula has not been mapped in detail. Currently, the only desktop resource is a 1:250 000 geological survey presented by Roberts (1974). The Dusnjarga peninsula is mapped as undifferentiated gabbro with layers of clinopyroxene gabbro (figure 4, NGU).

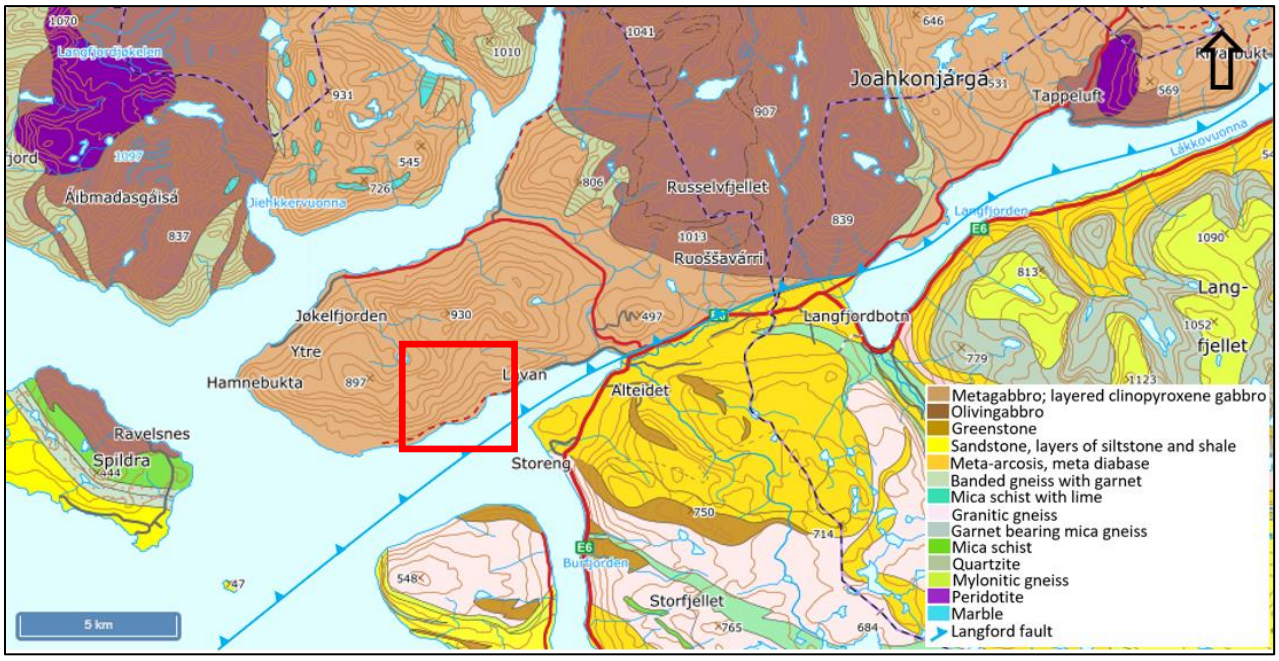

FIGURE 4 – BEDROCK GEOLOGY MAP (1:250 000) OVER DUSNJARGA PENINSULA. THE BLUE LINE REPRESENTS THE MAJOR LANGFJORD FAULT, TOGETHER WITH THE RED FRAME TO MARK DUSNJARGA URS. THE MAP IS ADAPTED FROM NGU (2015) (BERGGRUNNSKART ØKSFJORDEN)

The Dusnjarga peninsula is part of the Kalak Nappe Complex (KNC) within the middle allochthon of the Scandinavian Caledonides. The KNC consists of a Precambrian basement and late Precambrian to Cambrian cover deposited on the margin of the Iapetus Ocean (Kirkland et al., 2007), later metamorphosed during Caledonian continental collision. It is interpreted as a tectonically shortened margin of the ancient Baltica continent. The metasedimentary rocks of the KNC are intruded by the Seiland Igneous Province (SIP)(Ramsay, 1979) (figure 5), which is within the upper part of the KNC.

The SIP has been the subject of several published studies and is a collective term for deep-seated magmatic rocks with a wide range of compositions. The SIP is linked to extensional tectonic activity, but its origin is highly discussed. Age dating indicates that the SIP intruded the surrounding metasediments between 560 to 520 Ma (Roberts et al., 2006).

The SIP comprises gabbroic plutons with subordinate ultramafic syenitic and felsic intrusions (Roberts et al., 2006). An alkaline plutonic suite consisting of syenites, carbonatites, and feldspathoidal syenites is believed to have concluded the magmatic development of the SIP (Sturt et al., 1965). The mafic and ultramafic intrusions in the gabbro are iron-rich, with amphibole and plagioclase in olivine pyroxenites. Wehrlites and dunites are also observed (Stephens, 1985). Syenite pegmatites and sodic nepheline syenite pegmatites are widespread in the SIP, and can be up to 100 m wide, several km long, and intrude metasediments, gabbro, and ultramafic rocks. After intrusion, a regional event metamorphosed and deformed the KNC and SIP locally at amphibolite facies conditions, resulting in the formation of a penetrative foliation. This was most likely during the Scandian phase of the Caledonian Orogeny, c. 430 Ma ago (Roberts et al., 2006).

The area is also affected by more recent normal and transtensional faulting (Koehl et al., 2019). The Langfjord fault is a more than 120 km long fault located directly south of Dusnjarga (figure 4, NGU). The fault truncates the SIP (to the north) and a Precambrian section of the upper KNC (to the south) (figure 5). The Langfjord fault strikes WSW-ENE, is oriented parallel to Lille Altafjorden, and continues through Langfjorden to the east. It has been active during Permo-/Devon-Carboniferous rifting and then reactivated by dextral strike-/oblique-slip during the Mesozoic (Roberts & Lippard, 2005).

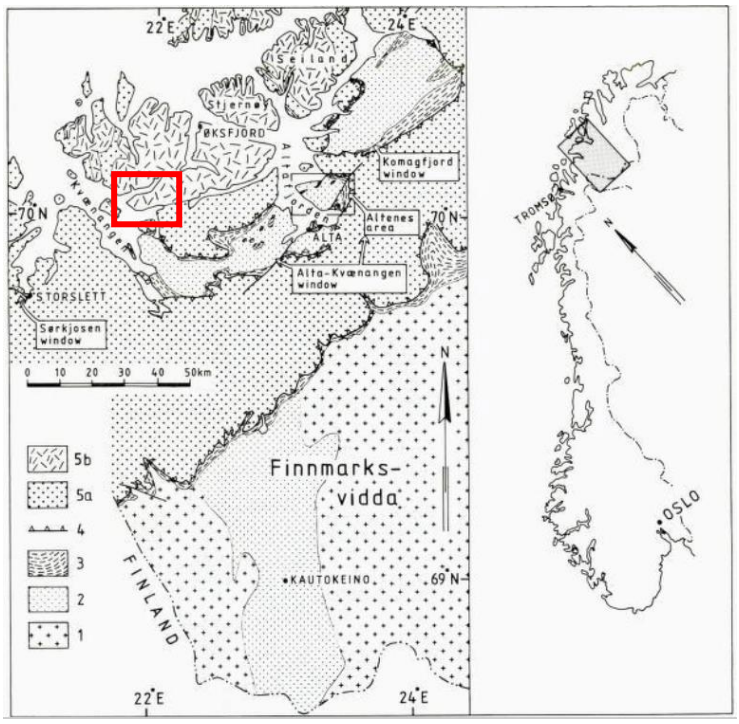

FIGURE 5: MAP SHOWING REGIONAL GEOLOGY TOGETHER WITH A RED ILLUSTRATED LOCATION FRAME. THE DIFFERENT BEDROCK LAYERS OF A LOWER CAMBRIAN AGE IS: 1) PRECAMBRIAN BASEMENT ROCKS OLDER THAN RAIPAS GROUP, 2) RAIPAS GROUP AND PROBABLE CORRELATIVES, 3) AUTOCHTHONOUS/PARAUTOCHTHONOUS LATE PRECAMBRIAN-CAMBRIAN ROCKS, 4) THRUST PLANE, 5A) KALAK NAPPE COMPLEX (=REISA NAPPE COMPLEX), 5B) KALAK NAPPE COMPLEX, IGNEOUS ROCKS OF THE SEILAND PETROGRAPHIC PROVINCE. ADAPTED FROM RAMSAY (1979).

1.5.2 Gámanjunni 3

The bedrock at Gámanjunni comprises metasedimentary rocks from the uppermost allochthon of the northern Scandinavian Caledonides, the Reisa Nappe Complex (RNC). The RNC, from bottom to top, is comprised of the Vaddas, Kåfjord and Nordmannvik Nappes (figure 6) (Andresen, 1988). Gámanjunni is underlain by both the Vaddas and Kåfjord Nappes, and the rockslide area involves rocks from both nappes and the nappe thrust boundary between them (the Cappis thrust; Andersen, 1988).

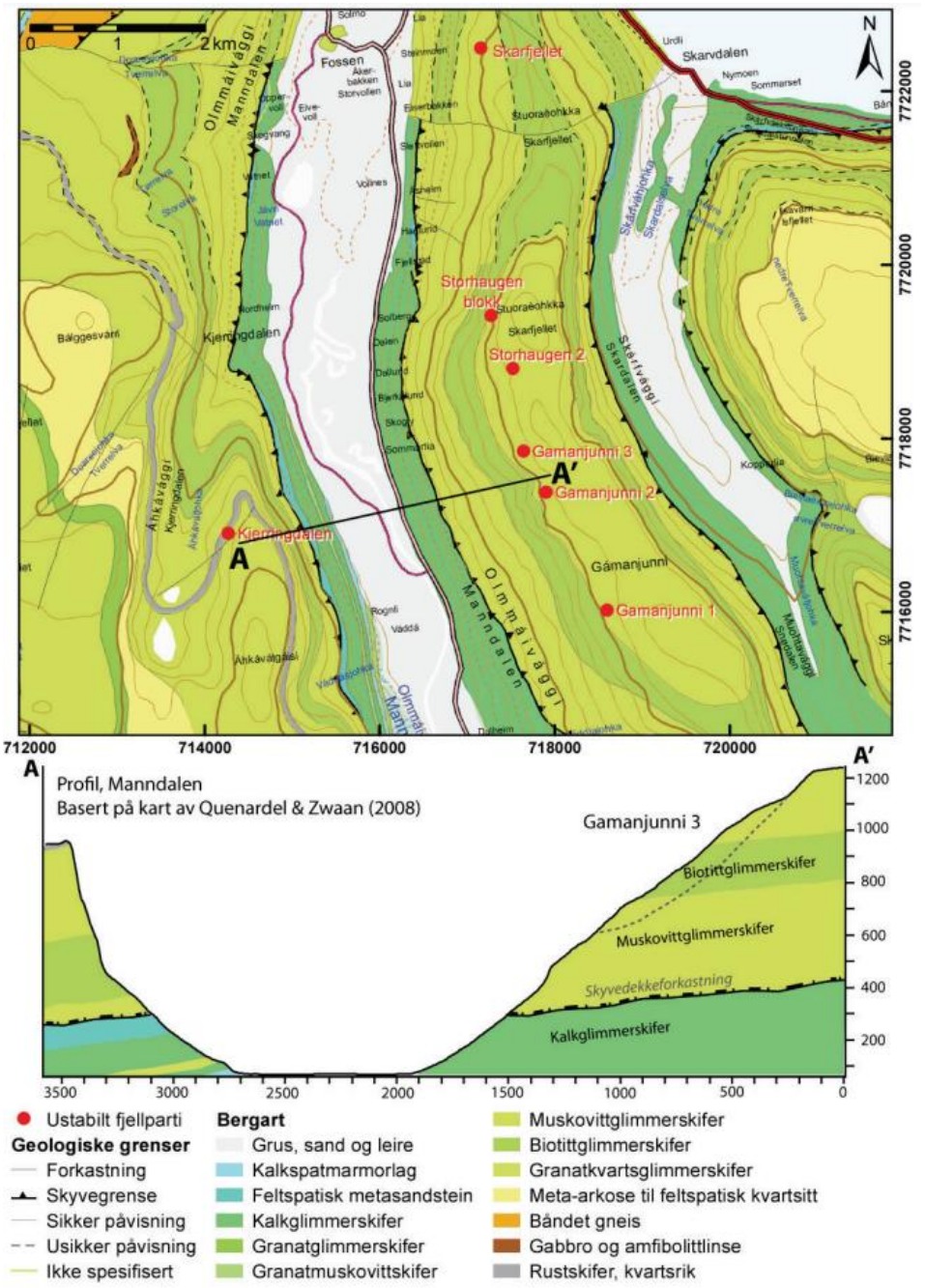

FIGURE 6: TOP: A GEOLOGICAL MAP OF MANNDALEN, GÁMANJUNNI 3. FIGURE IS ADAPTED FROM QUENARDEL & ZWAAN (2006). BOTTOM: A PROFILE A-A' OF GÁMANJUNNI 3 AND MANNDALEN, WITH THE CAPPIS THRUST NAMED "SKYVEGRENSE". KÅFJORD NAPPE ABOVE THE THRUST BOUNDARY. ADAPTED FROM BÖHME ET AL. (2016).

The Vaddas Nappe consists of metasediments (metapsammites, mica schists) and metavolcanics with local layers and lenses of amphibolite. These rocks are metamorphosed into amphibolite facies conditions (Faber et al., 2018). The uppermost section of the Vaddas Nappe in the Kåfjord area includes greenschist and a more massive amphibolite (Andersen, 1988). The Vaddas Nappe is intruded by 440 Ma gabbro's, and peak metamorphism is dated to 432 Ma (Faber et al., 2018).

In the Kåfjord Nappe marbles, meta-psammites and garnet mica schist dominate the lower section, while mylonitic gneisses with layers of amphibolite and some granite dominate the upper section (Padget, 1955). The Kåfjord Nappe is also metamorphosed to amphibolite facies conditions, and metamorphism is interpreted to have taken place during the Scandian phase of the Caledonian Orogeny (Faber et al., 2018) (figure 7).

Within both the Vaddas and Kåfjord nappe rocks, there are clear signs of ductile deformation, with folds at large and small scale, a penetrative ductile foliation, and multiple thrust zones. While these ductile structures are associated with Caledonian deformation, the area is also crosscut by younger Mesozoic brittle faults that trend NNE-SSW to NE-SW and NW-SE (Bredal, 2016).

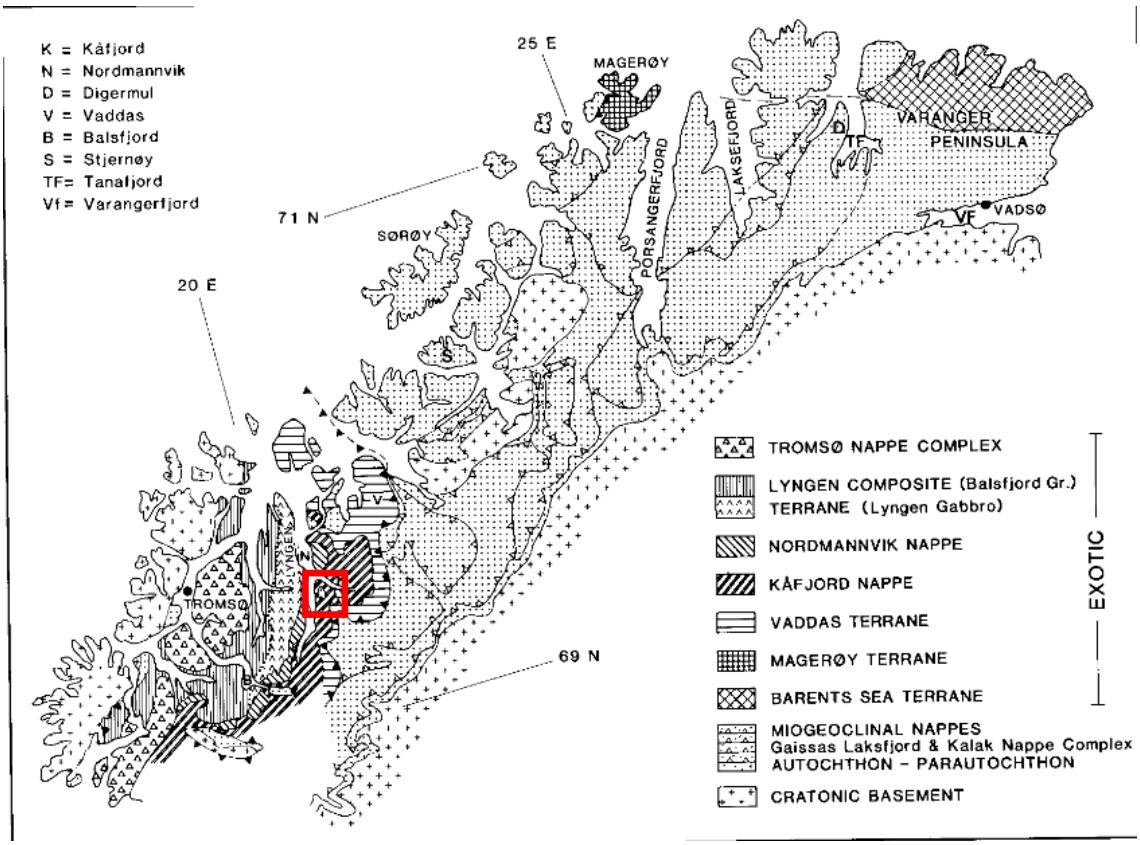

FIGURE 7: A GEOLOGICAL BEDROCK MAP OF TROMS AND FINNMARK COUNTY. RED FRAME MARKS LOCATION OF GÁMANJUNNI 3. ADAPTED FROM ANDERSEN, 1988.

1.6 Quaternary geology

Alpine mountains and deep fjords are dominated the nature in north of Troms County. Glaciers have and in some places are still changing the landscape. Information about local Quaternary deposits and landforms is therefore important to understand previous and ongoing temporal variations that is forming today's landscape.

1.6.1 Glaciation – and deglaciation history of northern Norway

The destabilization of several unstable rock slopes in Norway have been linked to the effect of debuttressing (i.e. removal of the glacial counterweight in steep rock slopes) (Gräminger et al., 2017; Hilger, 2019; Glueer et al., 2020; Storni et al., 2020). The study of earlier rock slope failure concludes with a peak in rock slope failure in the beginning of Holocene (i.e. 12 – 9 ka ago) as a response of deglaciation activity (Hilger, 2019). Therefore, as several URS failures are linked to deglaciation, the glacial impact at Dusnjarga and Gámanjunni 3 is considered important to study.

The Quaternary period is defined by the current and most recent period in Earth's history, roughly the past 2.6 million years. The geological period is characterized by major climate fluctuations and variations from glacial and inter- glacial periods (Lysså, 2015).

The Neogene period lasted 23 – 2.5 Ma, and during this period there was a series of glaciations as a result of a significant drop in global temperature. The series of glaciations has lasted 2.5 Ma – present and is defined as the Quaternary period. The Eurasian ice sheet did not reach its maximum simultaneously, but it took place during the period 29 and 21 ka (Böse et al., 2012; Patton et al., 2017). The time of glacial maximum is important to decide, as the last glacial maximum (LGM) can be defined. LGM in north Norway is set to be in the period 23 000 – 21 000, in which the Fennoscandian ice sheet coalesced and merged with the Barents Sea ice (figure 8) (Patton et al., 2017). As illustrated in figure 8, the entire Troms County was covered by ice, but some mountain peaks remained ice free, nunataks, above 1000 m asl. (Sveian, 2004). This correlates with the observations of no erosion at certain elevations in the nature.

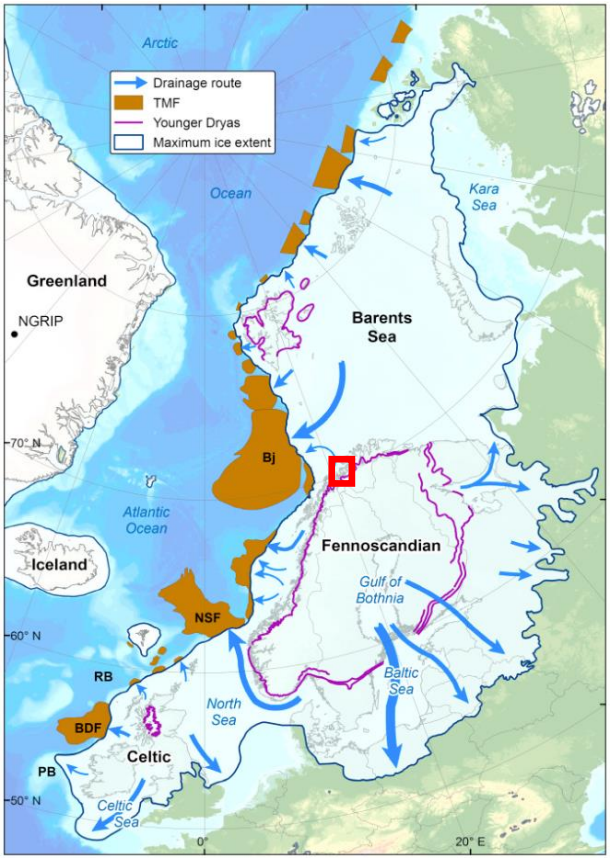

FIGURE 8: A MAP OF THE EURASIAN ICE SHEET COMPLEX WITH GLACIERS: BARENTS SEA, FENNOSCANDIAN AND CELTIC ICE SHEETS. THE MAJOR DRAINAGE ROUTES ARE MARKED. RED FRAME ILLUSTRATES LOCATION OF BOTH LOCALITIES. ADAPTED FROM PATTON ET AL., 2017.

After the LGM the ice sheets retracted, and the ice sheets reached the coast of Troms roughly around 17 ka (Hughes et al., 2015; Patton et al., 2017). The ice sheet re-advanced several times, and this phase is named the Late glacial interstadial (15.3 – 12.9 ka) and can be subdivided into smaller interstitials (Hughes et al., 2016; Patton et al., 2017). This period is characterized by ice streams filling the fjords and overall significant ice retreat. A scenario representing the extent of the retreat from DATED-1 time slice reconstruction suggests that Dusnjarga peninsula and Lille Altafjorden was deglaciated before 14 ka, or 15 ka depending on different extent calculations (Hughes et al., 2015). The study suggests that Gámanjunni 3 and Manndalen became ice free around 12 ka, possibly before 13 ka if minimum extent is representative.

The following period, the Younger Dryas (11 – 10 ka), is a phase of strong climatic cooling and glacial re-advancing. This period represents some of the most notable glacial formations in the region (Vorren and Mangerud, 2007). At the end of Younger Dryas the glaciers retreated rapidly, resulting in the prominent and easily traceable 'Lyngen-Tromsø moraines' (Patton et al., 2017). Studies from the Troms-area conclude that there have been local re-advances during the Preboreal period (Ørnes event 9.8-9.9 $\pm$ 0,15 ka, the Skibotn event 9.5-9.6 $\pm$ 0,25 ka and a younger event 9.4 $\pm$ 0.25 ka)

(Corner, 1980). The major ice fronts have been dated from investigations and plotting from the marine limit.

The deglaciation caused a global sea level rise, and at the same time an isostatic uplift from the unloading and retreating of the Fennoscandian ice sheet (Vorren et al., 2008). The isostatic uplift is a response to Earth's crust being elastic, and the depression caused by the Fennoscandian ice sheet. During the deglaciation and melting water runoff, the crust experiences heavy unloading and reacts with uplifting to the level before glacial loading. The isostatic rebound started after LGM and is still happening in Fennoscandia and can be observed as seismic events (figure 9). The degree of isostatic uplift increases towards inland areas, as the ice was thinner at the coast (Dehls et al., 2000; Vorren et al., 2008).

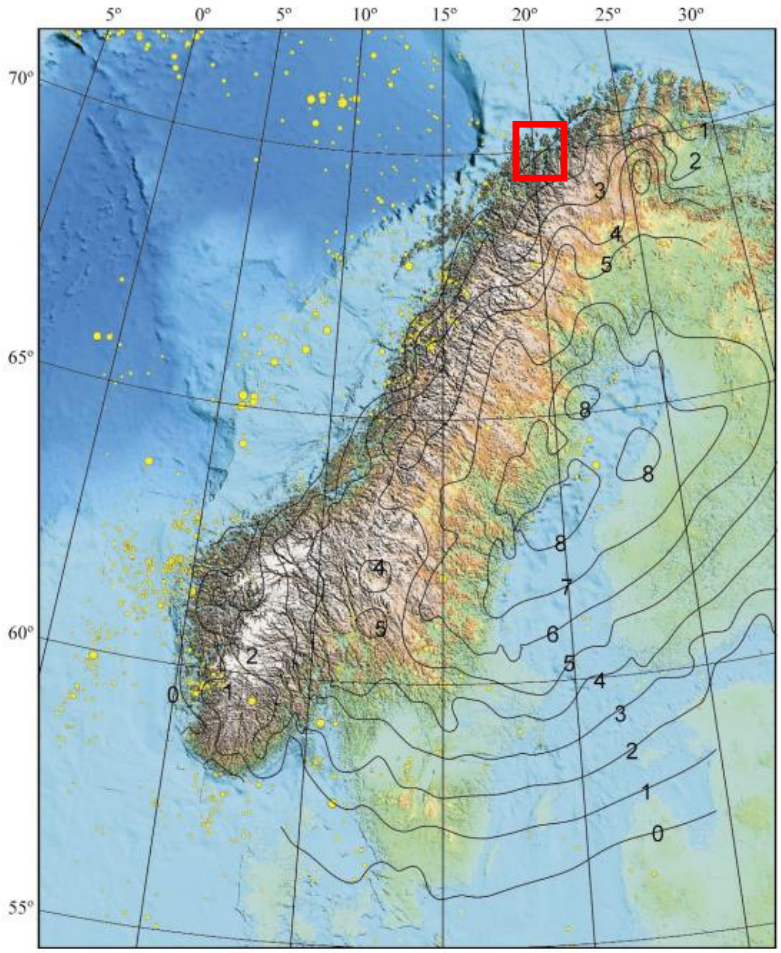

FIGURE 9: MAP PRESENTING THE EXTENT OF THE FENNOSCANDIAN ICE SHEET, WITH REPRESENTATIVE DATA, FROM 2000, ON UPLIFT RATES IN MM/YR. YELLOW MARKS ARE EARTHQUAKES WITH A MAGNITUDE GREATER THAN 3.0, SINCE 1965. RED FRAME MARKS LOCATION OF THE INVESTIGATED AREA. ADAPTED FROM DEHLS ET AL. (2000).

1.6.2 Geomorphology and quaternary geology - local

In this section the focus will be on local characteristics for geomorphology and quaternary geology.

A Quaternary map are published from NGU in 1:250 000 (Riiber, 2000) and is presented for both Dusnjarga and Gámanjunni 3 (figure 10 and 11). This is a national geological quaternary map, and the data is based on aerial photographs. As the map is published in a 1:250 000 scale, it gives adequate general information about the local quaternary geology, but it is not considered to be of a very detailed scale.

1.6.2.1 Dusnjarga

There is not much research done in the Kvænangen area regarding quaternary geology, but the findings that have been made are relevant for the Dusnjarga peninsula. There have been some marine limits identified nearby from marine deltas, the lower and closest identifications are one from Jøkulfjordeidet at 34 m asl. and one at Alteidet at 47 m asl. (Evans et al., 2002). These marine limit observations are in contrast to observations of marine limits made from the end of Jøkulfjorden at 66 m asl and Burfjorden at 67 m asl. Further south the marine limits are observed to be even higher, with the highest at Badderen (72 m asl.). The lower marine limit has been discussed and interpreted to be incorrect, as the propagation of distal sediments would be stronger from glaciers in the surrounding area (Evans et al., 2002). In the national Quaternary database from NGU, marker points indicate that the marine limit at Dusnjarga is between 65 – 66 m asl. (Høgaas et al., 2012). It should be mentioned that the closest marker points are situated approximately 10 km towards the coast.

The quaternary geology of the Dusnjarga peninsula is not well defined in NGU's database (figure 10) (Riiber, 2000). Avalanche- and weathering material are the only deposits identified.

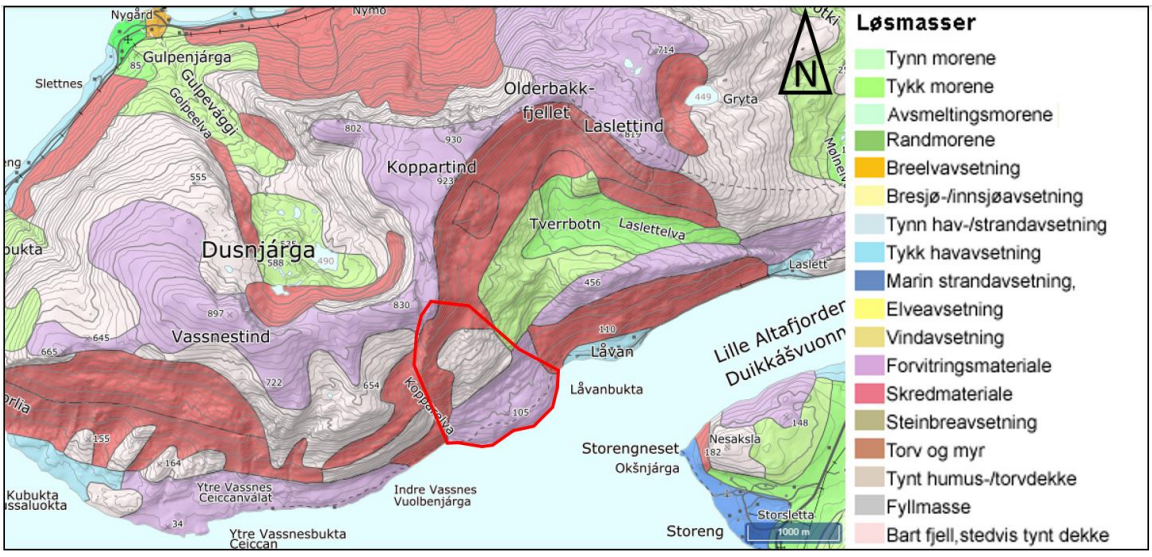

FIGURE 10: THE RED POLYGON MARKS THE URS DUSNJARGA. QUATERNARY MAP PUBLISHED BY THE GEOLOGICAL SURVEY OF NORWAY (NGU). THE QUATERNARY MAP IS PRESENTED AS A PARTLY TRANSPARENT LAYER WITH DEM AS A BASE LAYER. ADAPTED FROM RIIBER (2000).

1.6.2.2 Gámanjunni 3

The quaternary deposits in Manndalen are found to be predominantly glaciofluvial and fluvial deposits in the valley bottom, and the valley sides are primarily consisting of avalanche-, moraine- and marine materials (figure 11) (Eilertsen et al., 2012).

Three earlier avalanche events are registered in immediate area to Gámanjunni 3 (Eilertsen et al., 2012; Böhme et al., 2016). Two of these events have been dated to occur during or just after deglaciation (avalanches; 11 ka $\pm$ 250 B.P. and 4.25 ka $\pm$ 270 B.P.), but the circumstances linked to the avalanches are not connected to the deglaciation (Böhme et al., 2016). There are several avalanche scars in Manndalen, but all of these are believed to occur before or during the last glacial period, as the deposits have likely been removed by glaciers (Bunkholt et al., 2011; Böhme et al., 2016).

The marine limit near Manndalen (Gámanjunni 3) varies somewhat, from 50 m asl. in the outer parts of Lyngen to 100 m asl. in the inner parts of Storfjorden (Corner, 1980).

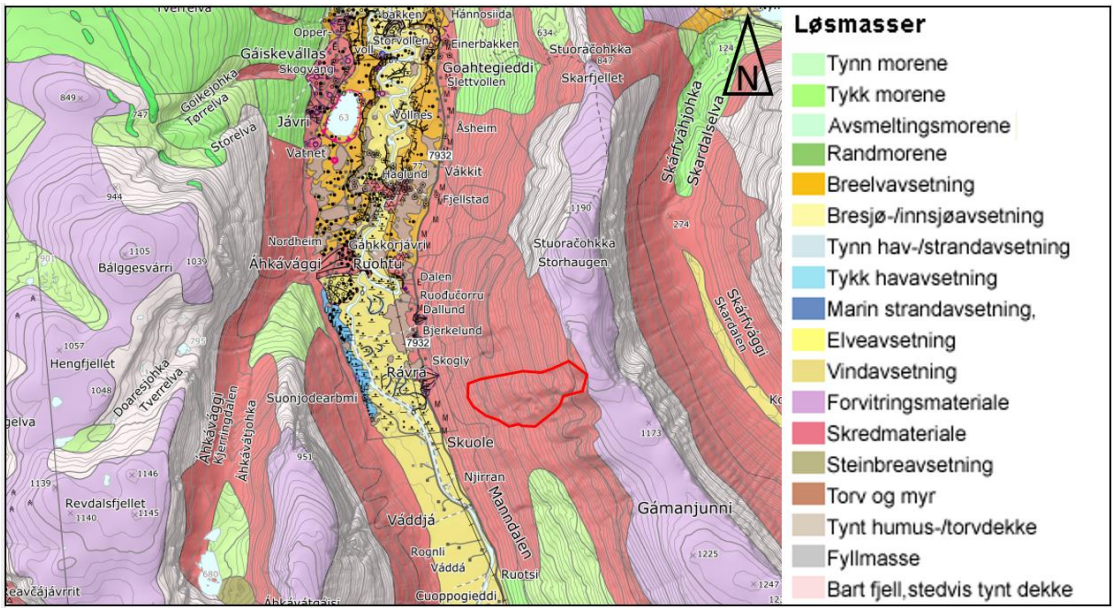

FIGURE 11: THE RED POLYGON MARKS THE URS GÁMANJUNNI 3. QUATERNARY MAP PUBLISHED BY THE GEOLOGICAL SURVEY OF NORWAY (NGU). THE QUATERNARY MAP IS PRESENTED AS A PARTLY TRANSPARENT LAYER WITH DEM AS A BASE LAYER. ADAPTED FROM RIIBER (2000).

1.7 Previous work and monitoring history

In this section the previous work will briefly be discussed for each URS together with their monitoring history. Dusnjarga and Gámanjunni 3 are investigated to very different extents, but both URS have in common that a potential failure will be catastrophic and are therefore monitored based on their to risk evaluation.

1.7.1 Dusnjarga

Previous studies from Dusnjarga are limited, but the URS is a part of NGU's regional mapping projects (Henderson et al., 2008; Bunkholt et al., 2011; Bunkholt et al., 2012; Bunkholt et al., 2013). A master thesis is also completed from Dusnjarga and the neighboring URS Låvan (Blau, 2020).

During NGU's first fieldwork at Dusnjarga in 2007, four new GPS monitoring points where installed. The overall movement has a direction of 125° and measurements from 2012 suggests a movement of 7 mm/yr (Bunkholt et al., 2012). Since DUS-2 and DUS-3 were installed after 2012, the data has been chaotic, so average movement is set to be 2.1 and 2.3 mm/yr (figure 12). Dusnjarga URS has been calculated to have a volume of 16 Mm^3 (Bunkholt et al., 2011). Figure 13 represents a profile of the URS.

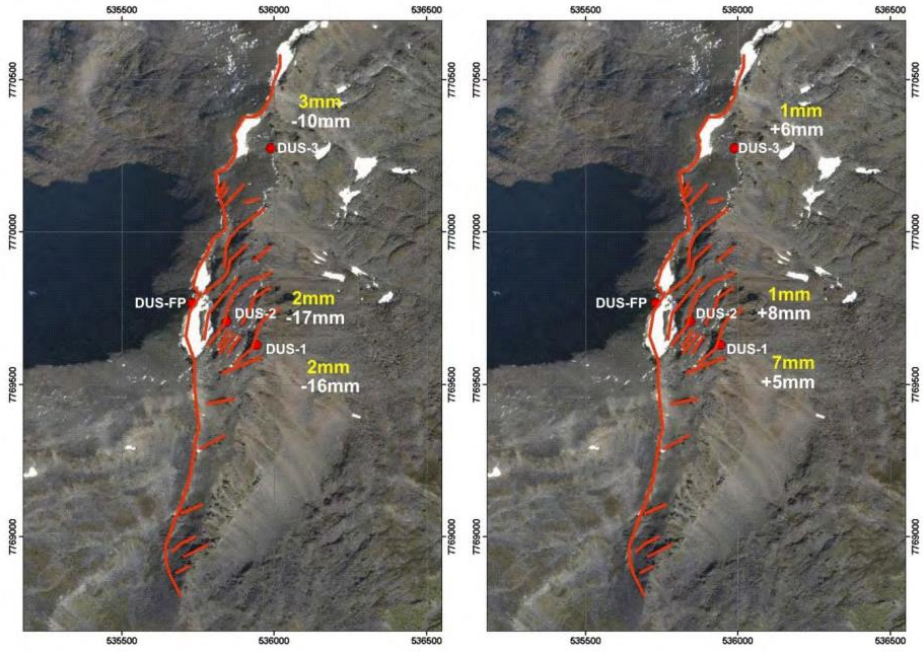

FIGURE 12: GPS MONITORS AT DUSNJARGA, DATA REPRESENTS 2007-08. YELLOW TEXT ARE HORIZONTAL MOVEMENT AND VERTICAL MOVEMENT IN WHITE TEXT. DUS-FP IS MONITORED IN STABLE GROUND FOR REFERENCE. ADAPTED FROM HENDERSON ET AL. (2010).

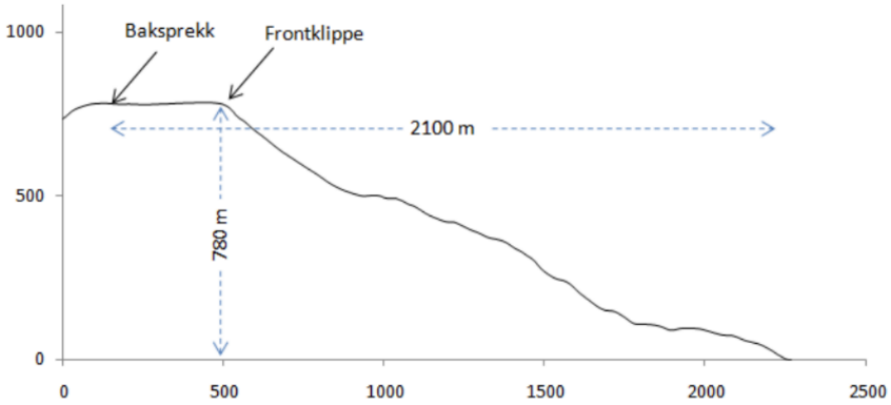

FIGURE 13: A PROFILE OF DUSNJARGA URS. ADAPTED FROM BUNKHOLT ET AL. (2011).

Dusnjarga is not a very well investigated URS, and the failure mechanism is poorly understood. Especially the understanding of what role geology and discontinuities play in facilitating for an instability to occur. There are earlier studies done on the strength of the rock types: amphibolite and metagabbro, but not how the rock behavior responds to development of fractures in micro- and macroscale (Segaetsho & Zvarivadza, 2006; Ali et al., 2013).

1.7.2 Gámanjunni 3

In 2016 NGU completed a risk- and hazard analysis from Gámanjunni 3 (Böhme et al., 2016). Calculations of volume and runout in this report indicate that a possible scenario, if the slope fails simultaneously, where the extent of the avalanche deposit can reach the opposite of the valley and potentially cause a dam. A dam of this sort can have a potential height of 20-30 m (Böhme et al., 2016) or 62-137 m and width of 900 m, and can easily fail and cause a flood, as a secondary effect (figure 14) (Oppikofer et al., 2016). The predicted height of the dam differs, depending on the calculations. The damage on human life can be up to tens of people, as the impacted area is inhabited. The combination of risk and consequence gives Gámanjunni 3 the highest possible risk and hazard classification (Böhme et al., 2016).

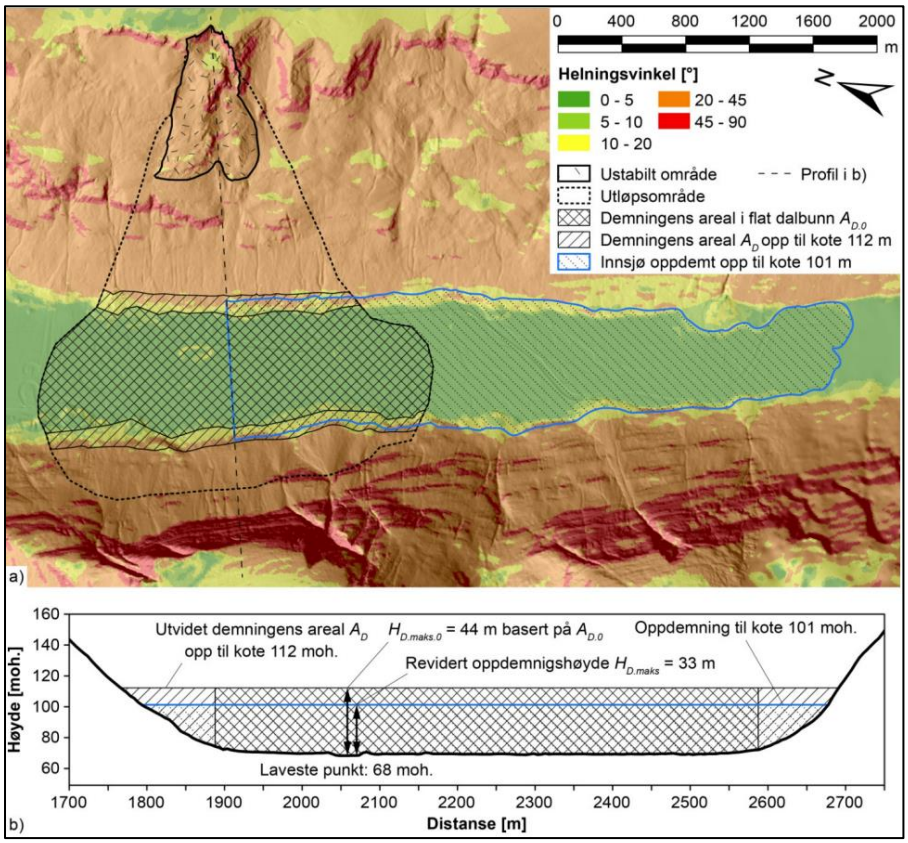

FIGURE 14: A: DIGITAL ELEVATION MODEL (DEM) USED AS A BASELAYER COVERED WITH A SEMI-TRANSPARENT INCLINATION LAYER OVER. ILLUSTRATED ARE DIFFERENT RUNOUT SCENARIOS WITH POTENTIAL FLOODED AREA. B: CALCULATIONS FROM A IN PROFILE WITH MEASUREMENTS. ADAPTED FROM OPPIKOFER (2016).

The Gámanjunni 3 top section moves at the speed of 50mm/yr, the movement decreases downwards and is 30mm/yr in the lower section (Böhme et al., 2016).

Numerous studies have been completed at Gámanjunni 3, for a better understanding of the URS. Cosmogenic nuclide dating has been done as a comparison of monitoring data with paleo-slip rates, and results indicate that the displacement initiated between 6.6 and 4.3 ka, with a fast displacement rate initially before decelerating after a few hundred years (Böhme et al., 2019). The movement has a median age of 5.3 ka, which gives a movement of 28 mm/yr. The cause is therefore not considered to be directly linked to glaciation.

There is currently an ongoing campaign at Gámanjunni 3 to measure internal temperature in the URS. Logging equipment was first installed in 2013 and show that temperature is slightly higher within the URS than at the surface. Results indicate that permafrost is still active in both the URS and the neighboring rock glacier (Eriksen, 2018).

Geophysical measurements have been extensive. The resistivity measurements found permafrost in the top section of the URS, and a drained zone at the toe section.

Hybrid seismic mapping is completed in two profiles of the subsurface structures at Gámanjunni 3 (GeoExpert, 2016). The investigation is a combination of high-resolution reflection seismic with inversion of refraction seismic tomography. In other words, a seismic signal penetrates the bedrock as a spherical wave front. A geophone records the reflected signals by acoustic sensors. The results indicate that the area is intensely tectonized with small scale fold structures. Findings also indicate a well-developed tectonic fault system striking N-S in a 100 m deep decomposed zone (GeoExpert, 2016).

The 4-model estimates content of ice in a mass, or content in pores, based on a geoelectrical and refraction seismic tomographic survey. At Gámanjunni 3 this method was conducted based on available electric and seismic data, and results indicate that the top 5-10 m are melted previous permafrost with high content of air (Hauck & Hilbich, 2018).

There has also been several structural investigations and kinematic analysis completed. Two main joint sets have been identified at Gámanjunni 3 (Böhme et al., 2016). JN 1 faces SSW with 200/84$\pm$18°, and JN 2 faces NV with 124/89$\pm$17°. Foliation dips shallowly towards NW with 312/08$\pm$13°. Backscarp 1 has a dip/dip direction of 217/51, and backscarp 2 are oriented 305/58.

3D-processed satellite images (TerraSAR-X) and ground-based radar data are used to calculate 3D movement vectors, giving movement direction and speed. Some sections of Gámanjunni 3 appears

to move up to 50-100 mm/yr to the southwest (Eriksen et al., 2017a). The central parts of the URS moves faster than the rock glacier.

Gámanjunni 3 is a heavily investigated URS in terms of monitoring and calculations of different failure scenarios. The detailed geology and discontinuities with their effect on instabilities is not studied in the same degree.

2 Methods

Methods used in this thesis include desktop data investigation, fieldwork to collect samples and map structures and bedrock, rock mechanical testing of samples, and thin section investigation. Fieldwork focused on bedrock geology and sampling for mechanical testing. Mechanical testing of the rocks is intended to investigate rock strength and how this might vary based on lithology, pre-existing structures, and location within the URS area. Thin section investigation was used to identify potential small-scale weakness zones and identify microscale contributing factors to weakness in the rocks.

Most of the fieldwork was in collaboration with co-student Simen Bekkevoll, who focused on the rock slope failure mechanism of Dusnjarga. This thesis occasionally utilizes data provided by Bekkvoll and is highlighted where this is the case.

2.1 Desktop data

The digital data sources used in this thesis include Digital Elevation Models (DEMs) provided from Hoydedata.no. Quaternary maps are provided by Riiber (2000) and bedrock map in 1:250 000 provided by Norges Geologiske Undersøkelser (NGU, 2015), The digital maps were assembled using a geographical information system (GIS) with ArcGIS Pro (ESRI) version 2.7.0. Coordinate system is Euret89 UTM33 for all figures including a map.

For Dusnjarga; the DEM has a resolution of 0.5 m (2016), name: NDH Kvænangen 2pkt 2016. The orthophotos, also from Kartverket, are of the Finnmark 2015 series with a resolution of 0.25 m.

For Gámanjunni 3; the DEM has a resolution of 0.5 m (2014), name: Troms 2pkt 2014. The orthophotos from Kartverket are Troms 2016, resolution 0.25 m.

2.2 Fieldwork

The fieldwork was conducted during four excursions in September of 2021. At Dusnjarga, the field data were collected on foot over a total of 13 days. Due to limited access to the unstable section at

Gámanjunni 3, the Norwegian Water Resources and Energy Directorate (NVE) provided a helicopter for the two field days spent at this locality.

Structural measurements, lithological mapping, and rock sampling were the main fieldwork tasks at Dusnjarga and Gámanjunni 3. All structural measurements were obtained using the application FieldMove Clino v1.5.2.152001. The measurements were restricted to foliation planes, joint sets and faults. Roughly 3000 structural measurements were collected at Dusnjarga using FieldMove in cooperation with Bekkevoll and the supervisors. Lithological structures and boundaries were mapped and combined with morphological features and signs of gravitational deformation. NGU's structural data were used to supplement field data collected at Gámanjunni 3, as field days spent at this locality caused our own data to be limited.

Structural measurements were taken in the form of dip and dip directions, and the structural data were processed in the application Rocscience Dips 7.0 [05-04-22]. Structural analysis and rose diagrams were done in DIPS.

2.3 Sampling

Both sites were sampled for lithological analysis and rock mechanics testing. A large portion of the fieldwork was focused on finding and extracting samples for a representative collection of the rock slope constituents. It was essential to sample both stable and unstable parts of the slope, to get comparable results. Lithological anomalies and average rock samples were also prioritized to obtain a representative selection of the bedrock.

The extraction of rock samples was done with a geological hammer, chisel, marker, and protective goggles. Pictures and structural measurements were taken at every sample location. Each sample was oriented and marked with the sample name. Samples were only taken from areas where the rock material was known to be in-situ, meaning valid sample locations showed no signs of severe movement or rotation; however, due to the nature of the unstable slopes this was sometimes challenging. The degree of rotation for samples within the rockslides was checked against local foliation orientation.

Seventy-six samples were collected from both localities, with a total mass of 300kg. Fifty-six of the total samples were taken from Dusnjarga.

2.4 Bedrock mapping - Dusnjarga peninsula

The area covered is 49 $km^{2,}$ and a bedrock map was produced on a scale of 1:250 000.

A map of 1:250 000 scale already exists (NGU, 2015), but mapped on a regional scale. The current bedrock map is a lithological interpretation based on surrounded area but is mapped without capturing the lithological variation at an unstable rock slope-scale.

The mapping of the Dusnjarga peninsula was completed simultaneously with the rest of the fieldwork. Investigate of the lithological variation within the unstable section of Dusnjarga was prioritized. The surroundings and the outcrops near the road were investigated, and structural measurements were taken from selected outcrops.

The primary source of information was field observations. Identifying bedrock types, deformation mechanisms, and structural measurements were done to get an adequate representation of the lithological changes within the peninsula.

2.5 Laboratory analysis

A selection of the rock samples was investigated using petrographic microscopy at the UiT lab. Thin sections were prepared from blocks by trained technical staff, with a total of 11 samples prepared from Dusnjarga and 10 prepared from Gámanjunni 3. Importantly, thin sections were taken from Dusnjarga before mechanical testing, but from Gámanjunni 3 after mechanical testing. The reason for the latter was a short time gap between Gámanjunni 3 fieldwork and postage of samples to Oslo.

A total of 76 samples, or 300 kg of rock, was shipped to Oslo for test preparation. Many samples failed during sample preparation (block cutting and core drilling) and could therefore not be tested.

Rock mechanical testing was conducted in October 2021 to review the behavioral strength properties of the rock material. The tests, point load, and uniaxial compressive strength test (UCS) were conducted by myself, with assistance from supervisor Andreas Grumstad and lab technicians at the Norwegian Geotechnical Institute (NGI) in Oslo.

2.5.1 Thin sections

The rock samples are cut with a diamond saw. A 40x20x10 mm block is cut ideally parallel to lineation and foliation. The block is then glued to a glass slide using epoxy and polished to 30 µm thickness to enable examination using polarizing light microscopy.

A Zeiss Axio Lab A1 microscope was used for the thin section analysis to investigate samples from Dusnjarga and Gámanjunni (figure 15). Mineralogy and microstructures, including fracture patterns, were investigated. A Canon EOS DSLR camera was used to capture magnified images up to 20 times.

Thin sections are used to identify minerals and examine microstructures. By examining a thin section using a polarizing light microscope, it is possible to observe the optical properties of minerals that are not visible in hand specimen (color, relief, cleavage, extinction angle, pleochroism, birefringence), typical habits, dynamic recrystallization, grain boundaries, and microstructures. The mineralogy and microstructures interpreted from the thin section description will be used to interpret rock strength (qualitatively) and possible failure mechanisms at the microscale/grain scale.

FIGURE 15: ZEISS AXIO LAB A1 MICROSCOPE USED FOR THINS SECTION STUDY.

2.5.2 Point Load Strength Index

The point load strength test (PLT) is an index to classify the rock specimen's compressive strength (ASTM, 2016). It is cheaper and less time-consuming than the UCS test. However, it should be considered more as a semi-quantitative indicator of strength rather than an absolute value, as it is less accurate than the UCS test. This test is done with industry standards and follows the American Society for Testing and Materials guidelines (ASTM, 2016). All observed and measured values were documented in a spreadsheet provided by NGI, which calculates the point load index. The method is different depending on whether the samples are cubic or irregular. Only irregular blocks were used in this project, as we utilized cast-offs from UCS core drilling and natural shaped samples. Samples ranged between 30 and 120 mm in diameter, and samples larger than 120 mm where cut to smaller pieces.

The point load apparatus consists of a measuring system for load indication and specimen length, a loading frame, a hydraulic pump to help manually apply pressure, and two cones for uniaxial rock contact.

The irregular block can be tested in two directions, depending on the angle of foliation (fig. 16). Diametral is the test direction when the foliation is parallel to the load direction, and axial is when the foliation is normal to the load. The test index does not accept foliation with an angle of 30-60° to the load direction. To get the best test results, it is preferable to test the samples to get the weakest and strongest result possible for each sample, hence the diametral and dextral testing with a preferred foliation completely parallel or perpendicular to the load direction. The height-diameter ratio should not be greater than 1:3, and a preferred ratio is 1. This is determined both with a caliper and sensors in the device.

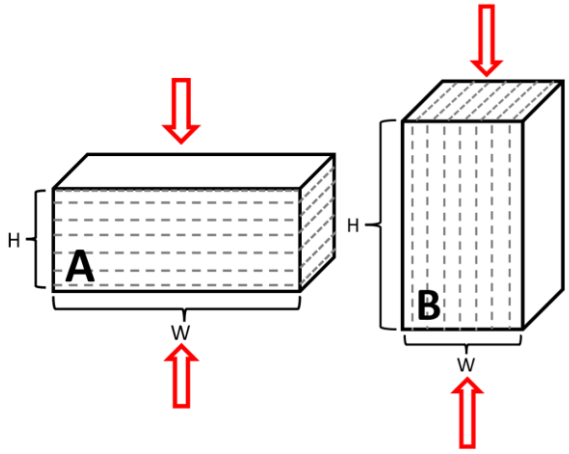

FIGURE 16: ILLUSTRATED IRREGULAR BLOCKS REPRESENTING SHAPE AND FOLIATION DIRECTIONS, FOR PLT USAGE. RED ARROW MARKS LOAD DIRECTION.

The sample is placed between cones within the apparatus, and a new measurement is taken of the height, ideally with a perpendicular platen-sample contact, as performed in figure 17. Load is applied from the bottom contact point by a piston controlled by a lever, increasing the pressure steadily to the point of failure or splitting. The test can only be counted if a failure occurs within the period 10-60s.

FIGURE 17: POINT LOAD TEST APPARATUS. PICTURE TAKEN AT NGI'S ROCK LAB [14.10.21].

Calculations of given parameters presents a Point Load Strength Index. The Index requests two measurements of average height and two for average diameter for irregular blocks. The uncorrected point load strength index (Is50) is a correlation factor for the Uniaxial Compressive Strength test (UCS), and the point load strength test (PLT) is given by failure load (P) divided by sample diameter. Water content can be used for more precise calculations, but our samples' moisture conditions were not preserved and cannot be accounted for. The point load strength index is considered to calculate a mean ratio for the axial and diametral plane of weakness (I_s).

2.5.3 The Uniaxial Compressive Strength test UCS

The UCS test is similar in concept to the point load, where pressure is applied to a sample along one axis until failure. It records the maximum stress intact rock can withstand before failing. Notably, the samples are uniform in cylinder shape and size, and pressure is distributed across the core surfaces. Therefore, the test is more representative of intact rock strength than the point load index.

The preparation process begins with the rock sample being cut into a cube (figure 18 A). Cores are drawn onto the cube to indicate where to drill. The cube is prepared to cylinders with a height of 52 +/- 2mm and core diameter to 25 mm to stay within the ASTM industry standard for UCS measurements (ASTM, 2014b) (figure 18 B). NGI uses the unofficial term p-plug when the cores height is parallel to foliation and s-plug for cores height perpendicular to foliation. Ideally, both p- and s-plug samples are needed for adequate results.

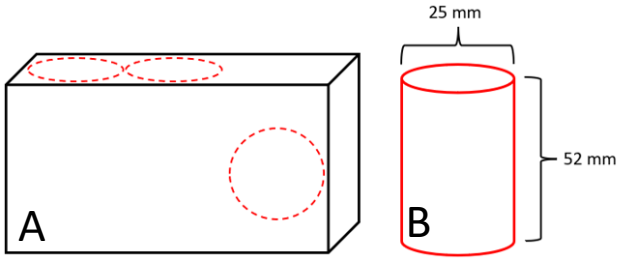

FIGURE 18: A: ILLUSTRATED STEP 1 WHEN THE SAMPLE IS CUT TO A CUBE. B: THE SHAPE OF THE CORE USED FOR USC TESTING. STANDARDIZED MEASUREMENTS MARKED IN.

The cube is placed in a container to keep it from moving during the drilling implementation. This procedure is done with great caution to prevent the cores from fracturing. The cores are adjusted with a grinder to standardize surface planes and equalize core height. This process is time-consuming and can take 4-8 hours, depending on the amount of grinding and asperities.

To get the exact mass of every test core, measurements of diameter, height, and weight are taken before the procedure starts. Pictures are also taken of every side of the test core (figure 19 A). For the UCS test to measure radial deformation, 4 knobs at two heights are glued to the test core in a measuring apparatus (figure 19 B). Before starting the UCS test, plastic is wrapped around the core to keep it intact after finished testing (figure 19 C).

The UCS test starts off by wiping the membrane platens clean from remains of previous material before aligning the platens with the specimen core (figure 19 D). The core sample is adjusted to the platens enough to keep the sample at place, with an axial load less than 100 N. The axial deformation components are checked and adjusted before additional load is applied. The stress rate should be selected to an amount that will produce failure within 2 – 15 min.

After the test starts, the axial load should be applied continuously until the load becomes constant, reduced, or achieves strain. Maximum load and deformation readings are to be measured and recorded. After testing, pictures are taken of each side of the test core.

Young's modulus, E, can be calculated, and in this case, it is convenient to know the material's elasticity. A measurement of the material's deformation is also considered valid, so Passion's ratio, μ, is calculated.

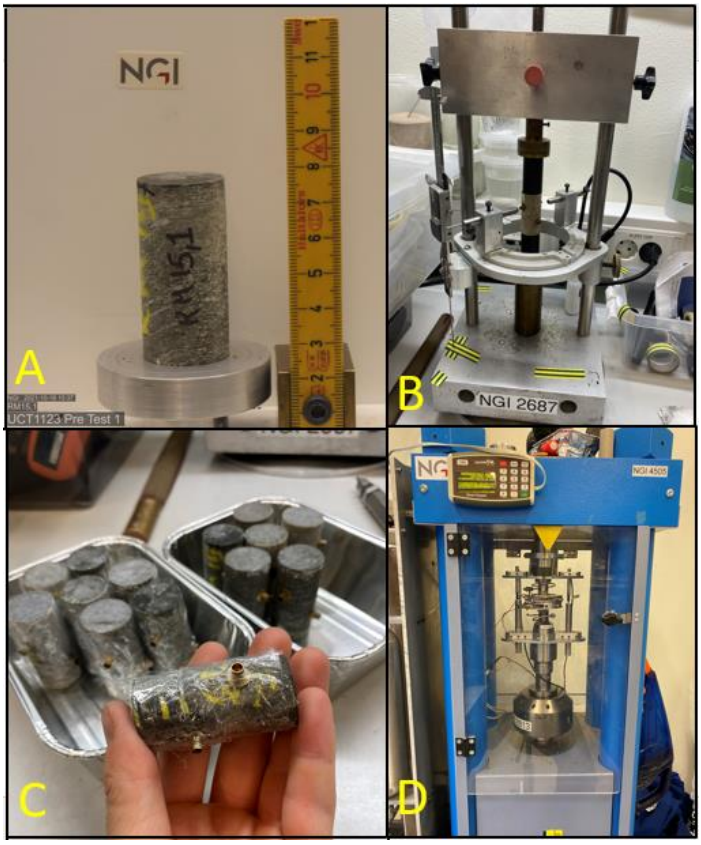

FIGURE 19: COLLAGE OF THE UCS PROCEDURE. A: PHOTOGRAPH OF A CORE BEFORE TESTING. B: THE SAME CORE PLACED IN THE APPARATEUS FOR ADJUSTING KNOBS. C: KNOBS PLACED AT THE CORE WITH STANDARIZED MEASUREMENTS. PLASTIC WRAPPED AROUND BEFORE TESTING. D: PHOTOGRAPH OF THE UCS APPARATEUS WITH THE PREPARED CORE SAMPLE. ALL PHOTOGRAPHS ARE TAKEN AT NGI'S ROCK LAB, OCTOBER 2021.

3 Results

This section will first present site overview observations of lithology, with a bedrock map presented with a petrological and structural description. Then a presentation of microscale structures from the sampled rocks at both sites. Lastly, the results of point load test (PLT) and uniaxial compression strength tests (UCS) are outlined.

3.1 Bedrock observations

Dusnjarga and Gámanjunni 3 are both underlain by metamorphosed bedrock of the Caledonides. Dusnjarga contains rocks of the Seiland Igneous Province (SIP), an intrusive complex within the Kalak Nappe Complex, and therefore contains magmatic rocks metamorphosed to various degrees, with some low-grade metamorphosed rocks being considered as gabbros. Gámanjunni 3 contains metasedimentary rocks of the Kåfjord Nappe. Consequently, the two URSs have very different bulk rock chemistries and, therefore, mineral assemblages. These also vary within the limits of the URSs, which is easily observed in the field.

The degree of anisotropy in the rocks should be established because anisotropic rock materials change their mechanical properties when loaded in different directions. Weak planes can be identified and the information about the anisotropic behavior can give information on possible points of failure.

3.1.1 Dusnjarga

The bedrocks at Dusnjarga are metagabbro and amphibolite, which are observed in and outside the URS. Metagabbro comprises a large part of the URS at Dusnjarga between 0 and 775 m asl. The Dusnjarga URS has a 1.2 km long backscarp, with a slope angle of 25° down to sea level.

3.1.1.1 Bedrock map

The bedrock at the Dusnjarga peninsula consists of meta igneous rocks. Investigations during fieldwork show a large part of the peninsula consists of metagabbro with magmatic layering. Within the metagabbro, the rock varies from gabbro to highly metamorphosed metagabbro with a well-foliated texture. Joint sets within the metagabbro vary, but foliation orientation is consistent throughout. The metagabbro transits to amphibolite at a higher elevation, with amphibole overgrows pyroxene as the bedrock becomes more metamorphic. Due to the graded transition, amphibolite is marked together with metagabbro in the bedrock map (figure 20).

At 750-800 m asl., a layer of the mafic and felsic mylonite is observed crosscutting the area. The layer is roughly 50 m thick and is central in the back scarp of the URS. Due to steep terrain, lack of exposure and weathered rocks at the outcrops, the extent of the mylonite layer was challenging to map and is therefore shown mostly with dashed lines in figure 20. The layer is oriented parallel to the foliation of metagabbro and likely follows this over the peninsula. It represents a large-scale shear zone in the metagabbro. Mylonite is also observed in thin layers below the central belt and represents smaller scale ductile shear zones within the metagabbro, oriented parallel to foliation.

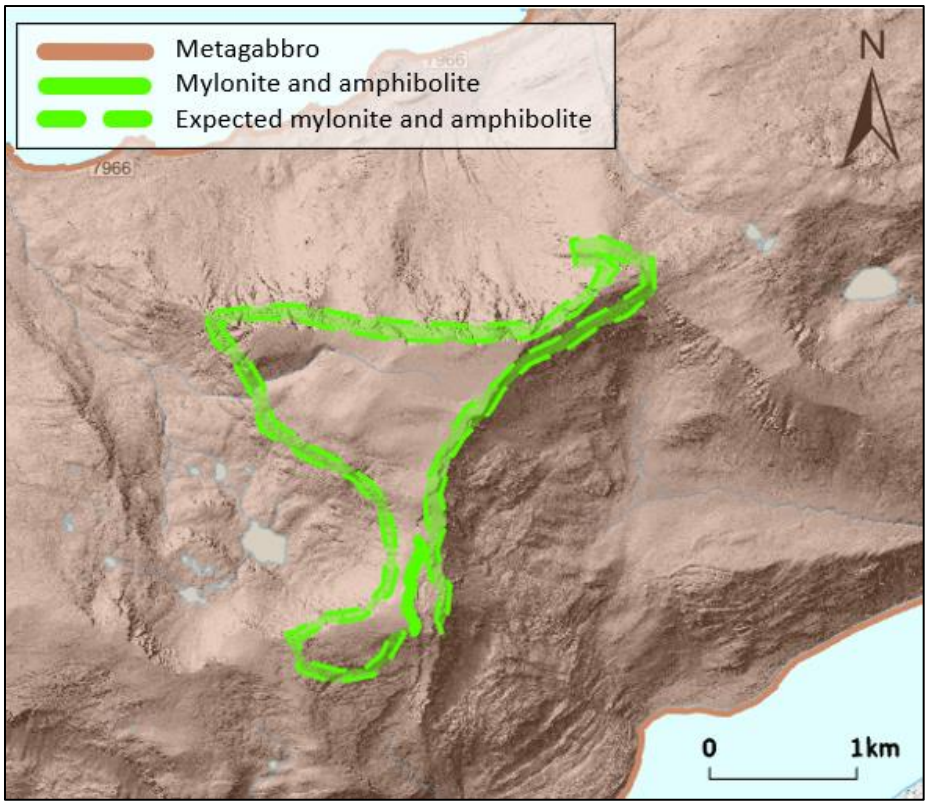

FIGURE 20: BEDROCK MAP OF DUSNJARGA PENINSULA, WITH A 0.5 M RESOLUTION DEM BASELAYER. POLYGONS ARE DEVELOPED IN ARCGIS PRO AND WITH AN A4 LAYOUT. DTM RETRIEVED FROM HOYDEDATA.NO.

3.1.1.2 Lithologies at Dusnjarga

In the upper section of Dusnjarga, metamorphic overprinting and tectonic (ductile) deformation are most substantial. Amphibolite and mylonite are observed at 775 m asl and to the top of the URS at 836 m asl. These rock types are only identified in the back scarp region on the plateau of the URS. The transition from metagabbro to amphibolite is progressive and cannot be easily mapped as a distinct boundary (figure 21).

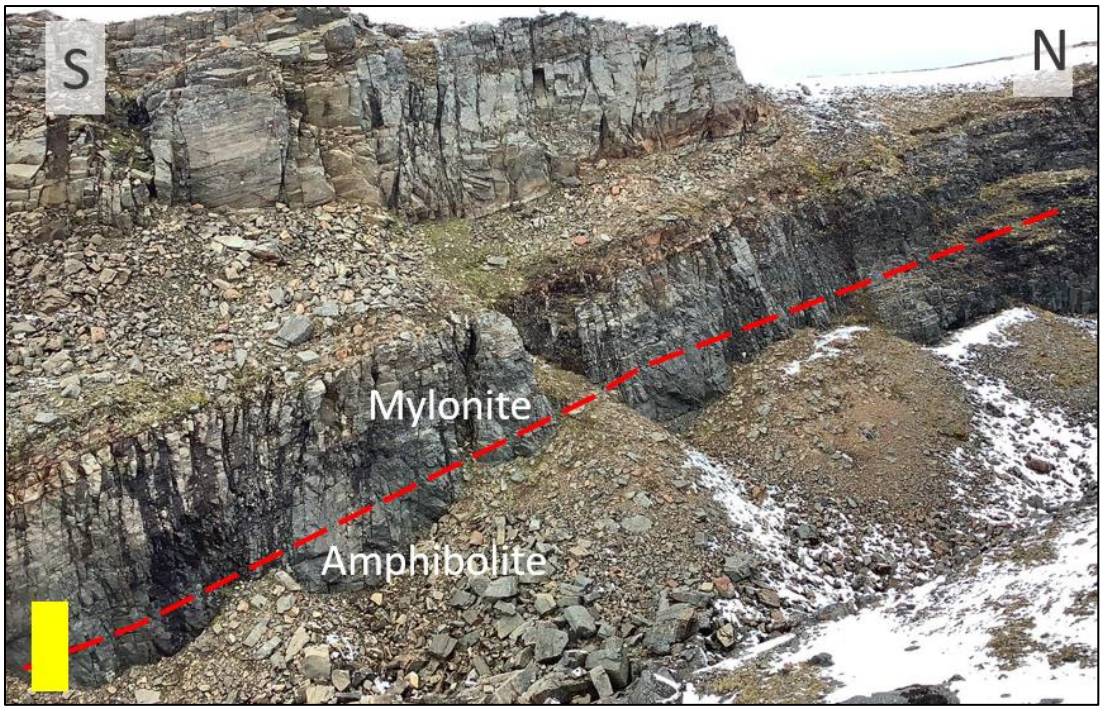

FIGURE 21: PHOTOGRAPH TAKEN AT THE BACK SCARP OF DUSNJARGA URS. THE YELLOW RECTANGLE REPRESENTS 2M AND RED LINE ILLUSTRATES LITHOLOGICAL BOUNDARY OF MYLONITE AND AMPHIBOLITE. PICTURE TAKEN IN SEPTEMBER 2021.

3.1.1.3 Metagabbro

Metagabbro is a rock type that has its origin from gabbro, but which has undergone metamorphism. Magmatic layering, a primary magmatic feature, is preserved within the metagabbro (figure 22). The scale of the layers varies from centimeter to meter thick, and the overall thickness of the layers generally increases with elevation. The layers vary from felsic to mafic and are easily divided by color: felsic presents as light grey and mafic metagabbro as dark grey. The felsic layers are dominated mainly by plagioclase (anorthositic composition) and display a weak to moderate foliation. Mafic layers have a varying mineral assemblage, with pyroxene, amphibole, quartz, and plagioclase dominating. The boundaries between magmatic layers are sharp, and the foliated fabric is oriented parallel to this magmatic layering.

The changing degree of metamorphic metagabbro is observed in changes in the mineral assemblage, grain size, and foliation (figure 22). Some lower sections at Dusnjarga are comprised of nearly unmetamorphosed phaneritic, equigranular gabbro without a foliation. In contrast, other areas at Dusnjarga have been overprinted by metamorphism, resulting in a continuous, penetrative foliation, recrystallized finer grains, and metamorphic mineral growth (e.g. amphibole).

The transition of gabbro to metagabbro is accompanied by new mineral growth, recrystallization, and foliation development. With increased deformation and metamorphism, amphibole replaces pyroxene, and plagioclase is recrystallized into finer grains.

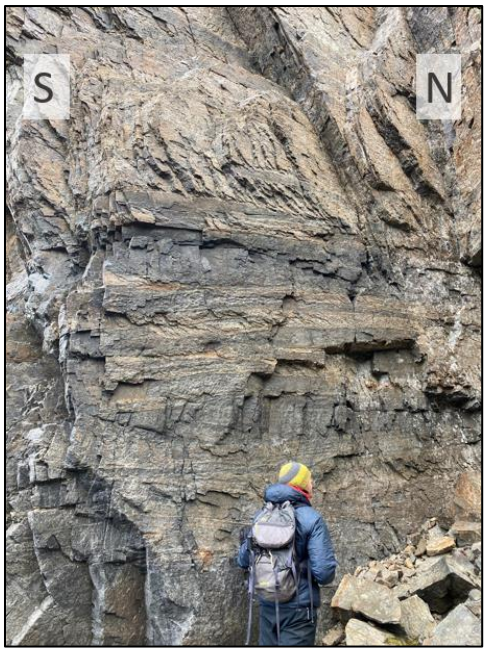

FIGURE 22: PHOTOGRAPH OF MAGMATIC LAYERING AT THE BACKSCARP OF DUSNJARGA URS. PICTURE TAKEN IN SEPTEMBER, 2021.

3.1.1.4 Amphibolite

In general, amphibolite is a metabasic rock, primarily composed of amphibole and plagioclase. Other minerals found at Dusnjarga are pyroxene, quartz, epidote, biotite, and garnet. Amphibolite is dark grey to greenish colored and significantly finer grained than the metagabbro.

The foliation is defined by plagioclase and aligned amphibole (figure 23). The plagioclase is fine-grained, and its grain shape is flattened. Amphibole is fine-grained and it is challenging to distinguish grains with the unaided eye.

FIGURE 23: PHOTOGRAPH OF THE AMPHIBOLITE AT THE BACKSCARP OF DUSNJARGA. PICTURE TAKEN IN SEPTEMBER, 2021.

3.1.2 Gámanjunni 3

Gámanjunni 3 is dominated by mica schist, with smaller sections of metapsammite and amphibolite (figure 24). These lithologies occur in layered bands, but the metapsammite and amphibolite are only repeated in the back scarp and top of the moving plateau (1050-1220 m asl). The URS has an angle on 35° from backscarp to toe, and a 42° from plateau to toe. The backscarp is 400 m long.

The muscovite and biotite schist constantly vary throughout the URS, sometimes on a cm-scale, and therefore mapping was challenging. Due to the rapid change in muscovite and biotite schist, mica schist is used as a collective term for both rock types.

FIGURE 24: PHOTOGRAPH OF THE BACKSCARP AT GÁMANJUNNI 3. YELLOW RECTANGLE MARKS 5 M FOR A SCALE AND RED POLYGONS REPRESENT LAYERS OF AMPHIBOLITE.

3.1.2.1 Mica schist

Mica schist is a metamorphic rock with a well-developed schistosity and is used as a general term for schist with a high content of phyllosilicate mica minerals. The texture is defined by oriented micas and is therefore lepidoblastic.

The biotite-dominant layers could easily be recognized in the field by a dark rusty surface color. Muscovite schist has a light grey color without the occurrence of rust. The different types of schist contain porphyroblastic garnet, with various grain sizes and densities within the bedrock.

At the URS, a grain size variation is observed in the field. The grains vary from fine to medium and can be easily identified with the unaided eye. Mica schist is the dominant rock type at Gámanjunni 3 (figure 25).

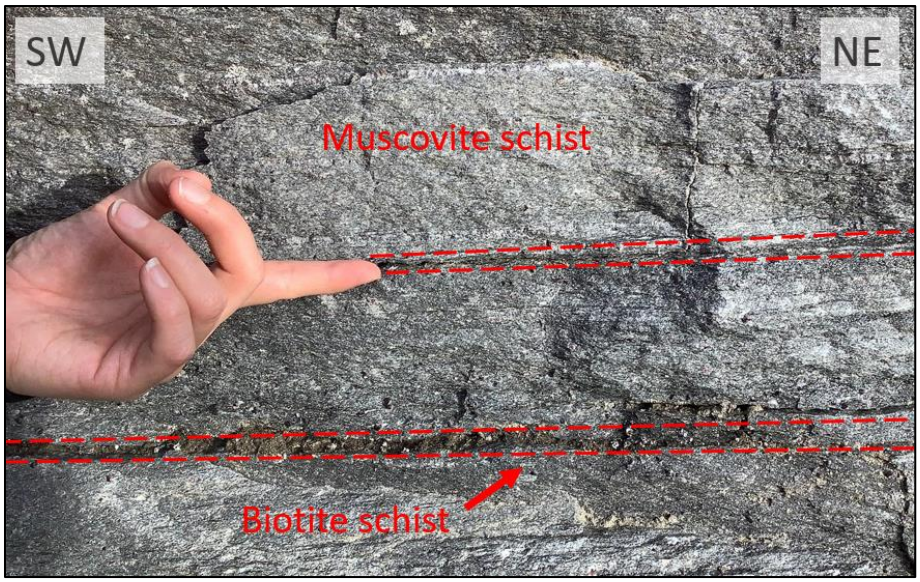

FIGURE 25: PHOTOGRAPH OF THE TWO DOMINANT BEDROCK TYPES AT GÁMANJUNNI 3: MUSCOVITE SCHIST (LIGHT GREY) AND BIOTITE SCHIST (DARK GREY), OR THE COLLECTIVE TERM: MICA SCHIST. BOTH LAYERS CONTAIN CRYSTALS OF GARNET. PICTURE TAKEN SEPTEMBER 2021.

3.1.2.2 Amphibolite

The amphibolite was found as layers and lenses in the upper section of the Gámanjunni 3 (1050-1200 m asl.) (e.g. backscarp in figure 24). The observed amphibolite layers vary from 10 cm and up to 3 m in thickness, and at some places with small folding (figure 26).

The grains are fine and difficult to distinguish with the naked eye. The color of the rock is dark grey to black. In some amphibolite layers and lenses, garnet porphyroblasts are observed with a size up to 0.5 cm in diameter.

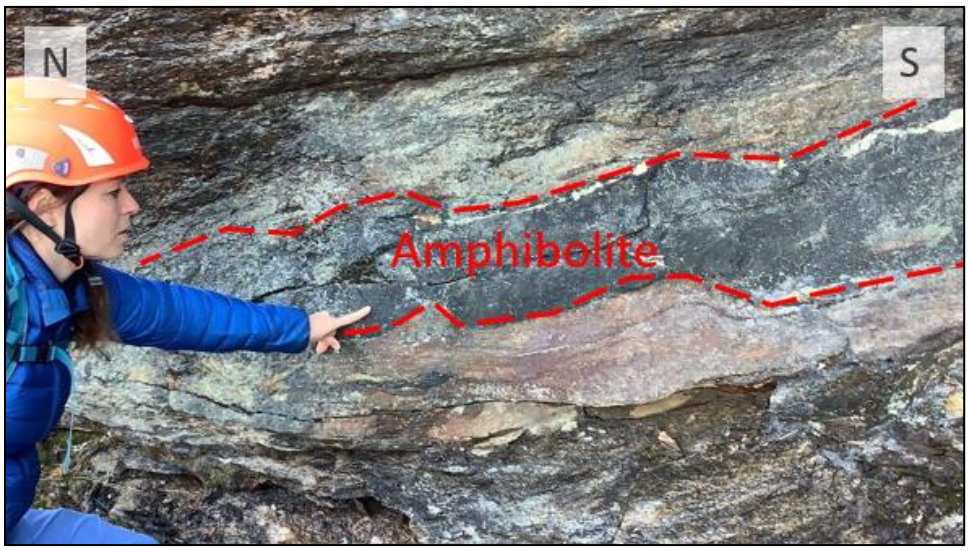

FIGURE 26: A PHOTOGRAPH OF THE AMPHIBOLITE LAYER AT THE BACKSCARP OF GÁMANJUNNI 3. PICTURE TAKEN SEPTEMBER, 2021.

3.1.2.3 Metapsammite

Metapsammite is sandstone or greywacke that has undergone metamorphism. The metapsammite is well-foliated with a lepidoblastic texture and a medium-fine grain size (figure 27). The metapsammite contains garnet porphyroblasts up to 0.5 cm in diameter. The color of the rock is light-medium grey with some grey-beige sections.

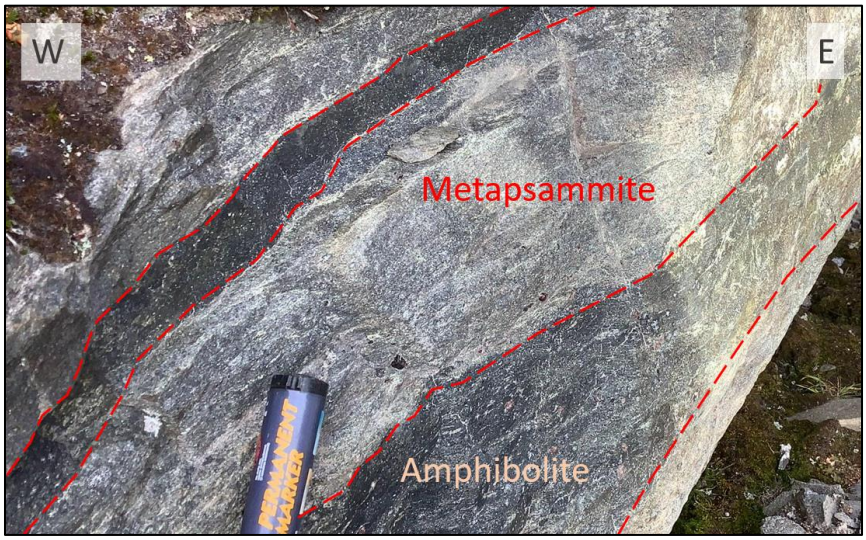

FIGURE 27: PHOTOGRAPH OF THE LAYERED METAPSAMMITE, FOUND AT THE PLATEAU OF THE MOVING BLOCK AT GÁMANJUNNI 3. PICTURE TAKEN SEPTEMBER, 2021.

3.1.3 Petrological description

This section includes descriptions of each rock type's mineral assemblage and texture. The main rock-forming minerals, general and specific textures, and dominating fabric and grain morphologies will be presented based on observations in the microscope.

The study of microstructures in thin sections will be used to understand how URS-related fractures might utilize pre-existing structures, metamorphic textures and mineralogies. Findings in the microscope will therefore be divided into petrology and microstructures.

3.1.3.1 Dusnjarga

Eleven thin sections were made of the samples collected from Dusnjarga. They are distributed throughout the URS (figure 28). The thin sections represent metagabbro, amphibolite, and mylonite. Metagabbro and amphibolite are rock types, and mylonite is a descriptive term for the lithology's fabric.

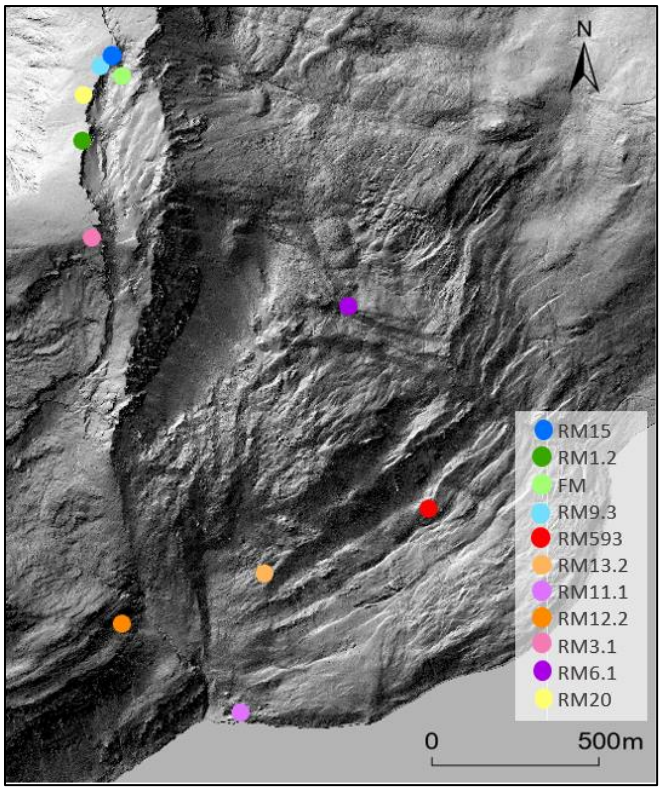

FIGURE 28: MAP REPRESENTING LOCATION OF THE THIN SECTIONS, RETRIEVED DURING FIELDWORK IN SEPTEMBER 2021. THE BASELAYER IS A DEM WITH RESOLUTION OF 0.5 M (HOYDEDATA.NO) AND DEVELOPED IN ARCGIS PRO.

Dominating minerals in the investigated samples are plagioclase, quartz, amphibole, and pyroxene. Mineral assemblage varies, but a high portion of plagioclase remains constant (table 1). Grain size and fabric are variable over the URS.

TABLE 1: A DIAGRAM FROM THE INVESTIGATED SAMPLE'S MINERAL ASSEMBLAGE. MINERAL DISTRIBUTION OBSERVED FROM STUDIES IN MICROSCOPY.

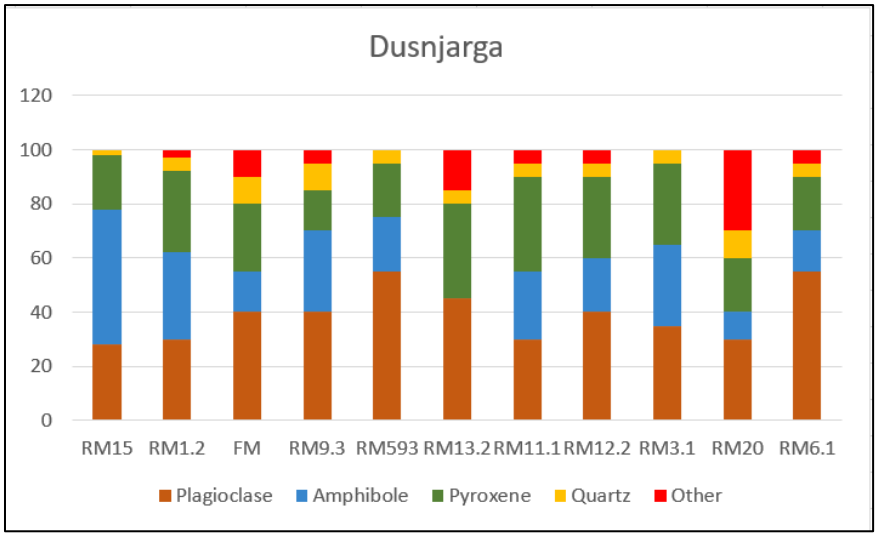

General findings and observations in the microscope are listed in table 2. Accessory minerals (minerals with less than 1 modal%) are considered unimportant for overall rock strength, and therefore not further described.

Magmatic layering is observed in the metagabbro and formed when the magma crystallized. This feature is recognized on a small scale. The layers vary from mafic (gabbro) to felsic (anorthosite), whereas the mafic layers are dominated by plagioclase, amphibole, clino- and orthopyroxene. The felsic layers contain a dominant portion of plagioclase and quartz. The occurrence of garnet crystals is observed in both layers.

Overall, metagabbro and amphibolite thin sections contains the following minerals; plagioclase varies between 28-55 modal%, quartz 5-10 modal%, amphibole 0-50 modal%, and pyroxene (clino- and ortho-) between 20-35 modal%. The presence of biotite and garnet varies from 0% to a maximum occurrence of 15 modal%. Amphibolite contains an assemblage of amphibole roughly at 50 modal% (figure 29). A high content of biotite is observed in relation to shear zones.

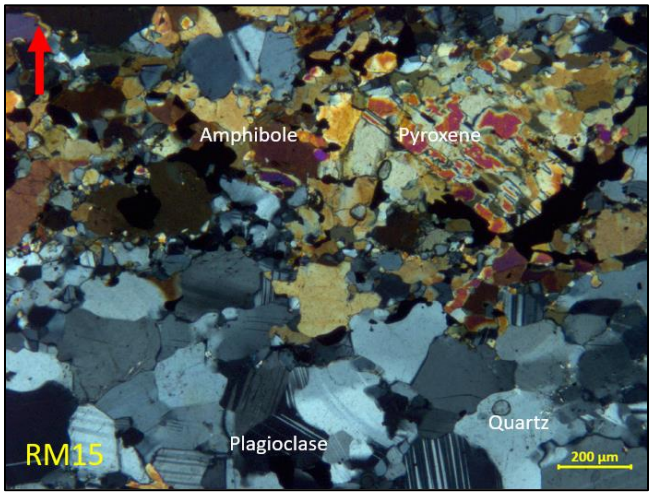

FIGURE 29: ANNOTATED PICTURE OF THE SAMPLED AMPHIBOLITE RM15 IN THE SCALE 1:200µM.

Grain size varies over the whole URS, visible in both macro- and microscope. The average grain size of mylonite is <0.1 mm, amphibolite is 0.1-1 mm, and metagabbro from 0.1-5 mm. Metagabbro shows a higher variation in grain size, but this is also the rock type with most data. There is also observed a larger average grain size in the felsic layer (i.e. plagioclase), than the mafic layer.

At Dusnjarga, the metagabbro has a variety of mineral assemblages and fabrics. The proportion of amphibole in metagabbro is found to be higher than expected from field observations. With mineral assemblage observed in thin section compared to elevation, the percentage of amphibole increases with height in the URS and replaces pyroxene. The amount of felsic minerals seems roughly constant in the sampled metagabbro throughout the URS.

The investigated amphibolite contains a significant proportion of pyroxene. The dominant minerals are, however, still amphibole and plagioclase, with a fine-grained texture.

Due to the mylonitic structure, the samples FM, RM9.3, and RM20 are named mylonite**.** The grain size varies from a very fine-grained matrix up to medium-sized porphyroblasts within a finer-grained matrix. The dominant minerals in the mylonite are amphibole, feldspar and pyroxene. Muscovite and biotite are also found in the mylonite samples. Variations in microstructure show that it includes areas similar to metagabbro, suggesting it is deformed metagabbro. This was observed in the microscope and field.

The thin sections indicate that the mineral composition of the mafic and felsic mylonite is more similar than first suggested from field observations. Thin sections reveal that all mylonite samples have a more intermediate mineral assemblage and therefore "mafic" mylonites are only darker in color than "felsic" mylonites, but their color is not indicative of mineral assemblage and may instead reflect grain size.

TABLE 2: PETROLOGY OF THE SAMPLES FOUND AT DUSNJARGA.

Thin section	Mineral assemblage (modal %)	Grain size (mm)	Comments
RM 15 Amphibolite	Plagioclase 28 Amphibole 50 Clinopyroxene 10 Orthopyroxene 10 Quartz 2	Fine – 0.1-1	Grain boundaries are lobate.
RM 1.2 Metagabbro	Amphibole 30 Plagioclase 32 Orthopyroxene 15 Clinopyroxene 15 Quartz 5 Biotite 3	Fine – 0.1-1	
FM Mylonite	Plagioclase 40 Quartz 10 Amphibole 15 Clinopyroxene 15 Orthopyroxene 10 Muscovite 10	Very fine – fine 0.01-1	Inclusions in grains, mostly in 1< large grains.
RM9.3 Mylonite	Quartz 10 Plagioclase 40 Amphibole 30 Clinopyroxene 5 Orthopyroxene 5 Accessory minerals > 5	Very fine- medium 0.01-1	Matrix of very fine grains, zoning, lobate boundaries, and no inclusions.
RM 593 Metagabbro	Plagioclase 55 Quartz 5 Amphibole 20 Clinopyroxene 10 Orthopyroxene 10	Fine – medium 0.1-5	

RM13.2 Metagabbro	Plagioclase 45 Orthopyroxene 20 Quartz 5 Clinopyroxene 15 Biotite 10 Garnet 5	Fine 0.1-1	Large shear zone/fault zone
RM11.1 Metagabbro	Amphibole 25 Plagioclase 30 Orthopyroxene 20 Clinopyroxene 15 Quartz 5 Biotite 5	Fine 0.1-1	
RM12.2 Metagabbro	Amphibole 20 Clinopyroxene 15 Orthopyroxene 15 Plagioclase 40 Quartz 5 Biotite 5	Very fine- medium 0,01-1	.
RM3.1 Metagabbro	Plagioclase 35 Amphibole 30 Clinopyroxene 15 Orthopyroxene 15 Biotite 5	Very fine – medium 0.01-5	
RM20 Mafic mylonite	Biotite/mica 30 Quartz 10 Plagioclase 30 Clinopyroxene 10 Orthopyroxene 10 Amphibole 10	Very fine 1-0.01	
RM6.1 Metagabbro	Plagioclase 55 Quartz 5 Orthopyroxene 10 Clinopyroxene 10 Garnet 5 Amphibole 15 Accessory minerals > 1	Large-very fine 5-0.1	Porfyroblastic texture.

3.1.3.2 Gámanjunni 3

The samples from Gámanjunni 3 are of biotite- and muscovite schist, metapsammite, and amphibolite, and collected from inside and outside the URS (figure 30). Ten samples were prepared as thin sections and studied using a petrographic microscope.

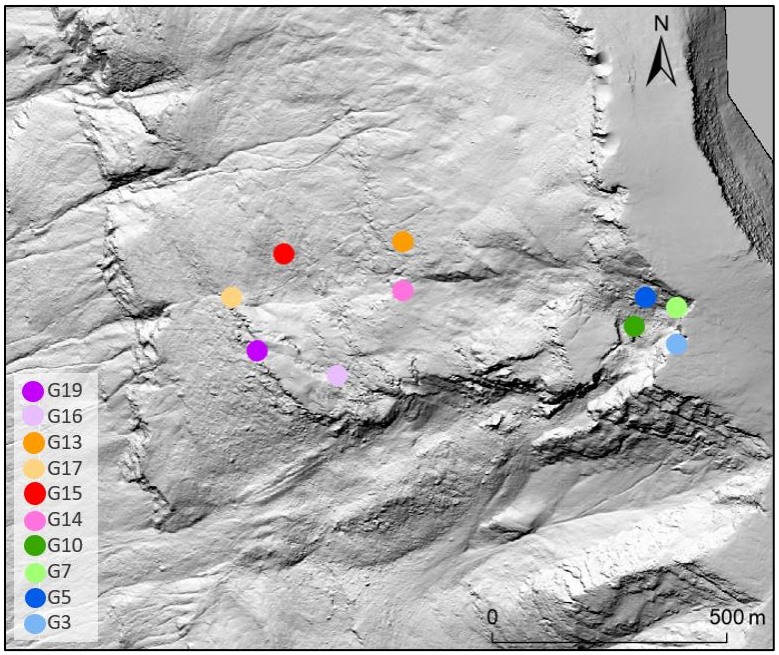

FIGURE 30: MAP REPRESENTING LOCATION OF THE THIN SECTIONS, RETRIEVED DURING FIELDWORK IN SEPTEMBER 2021. THE BASELAYER IS A DEM WITH RESOLUTION OF 0.5 M AND DEVELOPED IN ARCGIS PRO.

The dominant minerals at Gámanjunni 3 are biotite, muscovite, quartz, plagioclase and a minor proportion of garnet in all samples. The proportion of minerals in mineral assemblages and structures vary widely (table 3). Amphibole is only observed in the amphibolite.

TABLE 3: A DIAGRAM FROM THE INVESTIGATED SAMPLE'S MINERAL ASSEMBLAGE. MINERAL DISTRIBUTION OBSERVED FROM STUDIES IN MICROSCOPY.

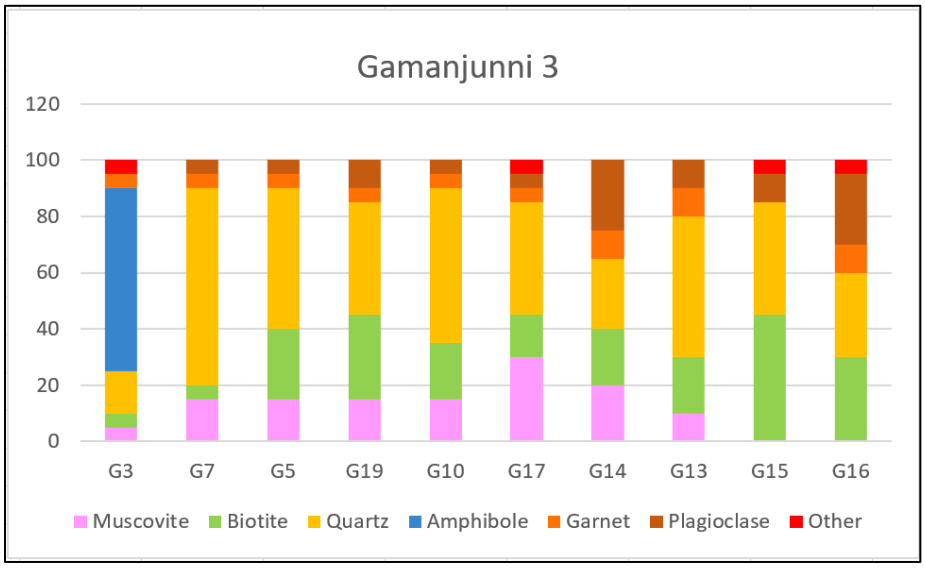

Muscovite, biotite, and quartz are minerals that remain constant throughout Gámanjunni 3. Plagioclase, garnet, and amphibole are other minerals with a high occurrence. Minerals with an occurrence of less than 5 % are grouped as "accessory minerals" and considered unimportant for overall rock. Staurolite, chlorite, calcite, and epidote are some of the minerals marked as accessory minerals.

The mica schist has an overall high content of mica minerals, muscovite and biotite, quartz, and plagioclase. In the mica schist the mineral assemblage varies from 10-45 % biotite, 15-30 % muscovite, 25-60 % quartz, 5-25 % plagioclase and a variation of 0-5 % garnet.

Biotite, plagioclase, and garnet are constant minerals in all investigated thin sections (table 4). The minerals in mica schist and metapsammite are roughly the same, only with a varying modal %. Amphibolite has a high percentage of ferromagnesian minerals, amphibole, pyroxene, and no observed muscovite. There is a <5-10% occurrence of minerals from the epidote group in some thin sections. For simplicity, these minerals are grouped together with other accessory minerals.

The grain size from the URS varies from fine grains that are difficult to identify, through medium-sized and up to 2-3 mm. The mica schist and metapsammite have roughly similar grain sizes, with muscovite and biotite as the largest average grains. The amphibolite has the same variation in grain size; only amphibole is the largest mineral in size.

The metapsammite and amphibolite appears more uniform, with a strong foliated fabric.
The fabric is considered strongly foliated in mica schist and metapsammite, where oriented micas define the foliation (i.e. lepidoblastic texture).

TABLE 4: PETROLOGY OF THE SAMPLES FOUND AT GÁMANJUNNI 3.

Thin section	Mineral assemblage (%)	Grain size (mm)	Comments
G3 Amphibolite	Amphibole 65 Quartz 15 Garnet 5 Muscovite 5 Biotite 5 Pyroxene 5?	3-0.5	
G7 Muscovite Schist	Quartz 60 Muscovite 15 Biotite 10 Plagioclase 10 Garnet 5	1-0.5	
G5 Breccia	Quartz 50 Biotite 25 Muscovite 15 Garnet 5	1.5-0.01	Lithological boundary separated by shear zone.

	Plagioclase 5		
G19 Biotite schist	Quartz 40 Biotite 30 Muscovite 15 Plagioclase 10 Garnet 5	1-0.1	
G10 Metapsammite	Quartz 55 Biotite 20 Muscovite 15 Plagioclase 5 Garnet 5	1-0.5	.
G17 Muscovite schist	Quartz 40 Muscovite 30 Biotite 15 Plagioclase 5 Garnet 5 Chlorite 5	2-0.1	S-c' fabric observed.
G14 Muscovite schist	Quartz 25 Plagioclase 25 Muscovite 20 Biotite 20 Garnet 10	2-0.1	Wavy schist texture.
G13 Muscovite/ biotite schist	Quartz 50 Muscovite 10 Biotite 20 Plagioclase 10 Garnet 10	1-0.1	
G15 Biotite schist	Biotite 45 Quartz 40 Plagioclase 5 Accessory minerals > 5	1-0.1	Wavy texture from schist minerals.
G16 Biotite schist	Biotite 35 Quartz 30 Feldspar 25 Garnet 5 Accessory minerals > 5	2-0.1	Quartz layers stops fracture propagation. Zoisite/clinozoisite

3.2 Morphology

The morphology at Dusnjarga and Gámanjunni 3 (figure 31 and 32) is irregular and complex to understand. Some of the most dominant morphological features at Dusnjarga and Gámanjunni 3 are back scarp, counterscarp, lateral boundary, fractured bedrock, ridges, and toe bulging. Large parts of the URS consist of disintegrated and disaggregated rock, resulting in a chaotic and disorganized morphology.

Dusnjarga faces SE and the slope has an average inclination of 23°, with an inclination up to 32° in the steeper, western sections of the URS. Gámanjunni 3 has an average inclination of 31° and faces directly west.

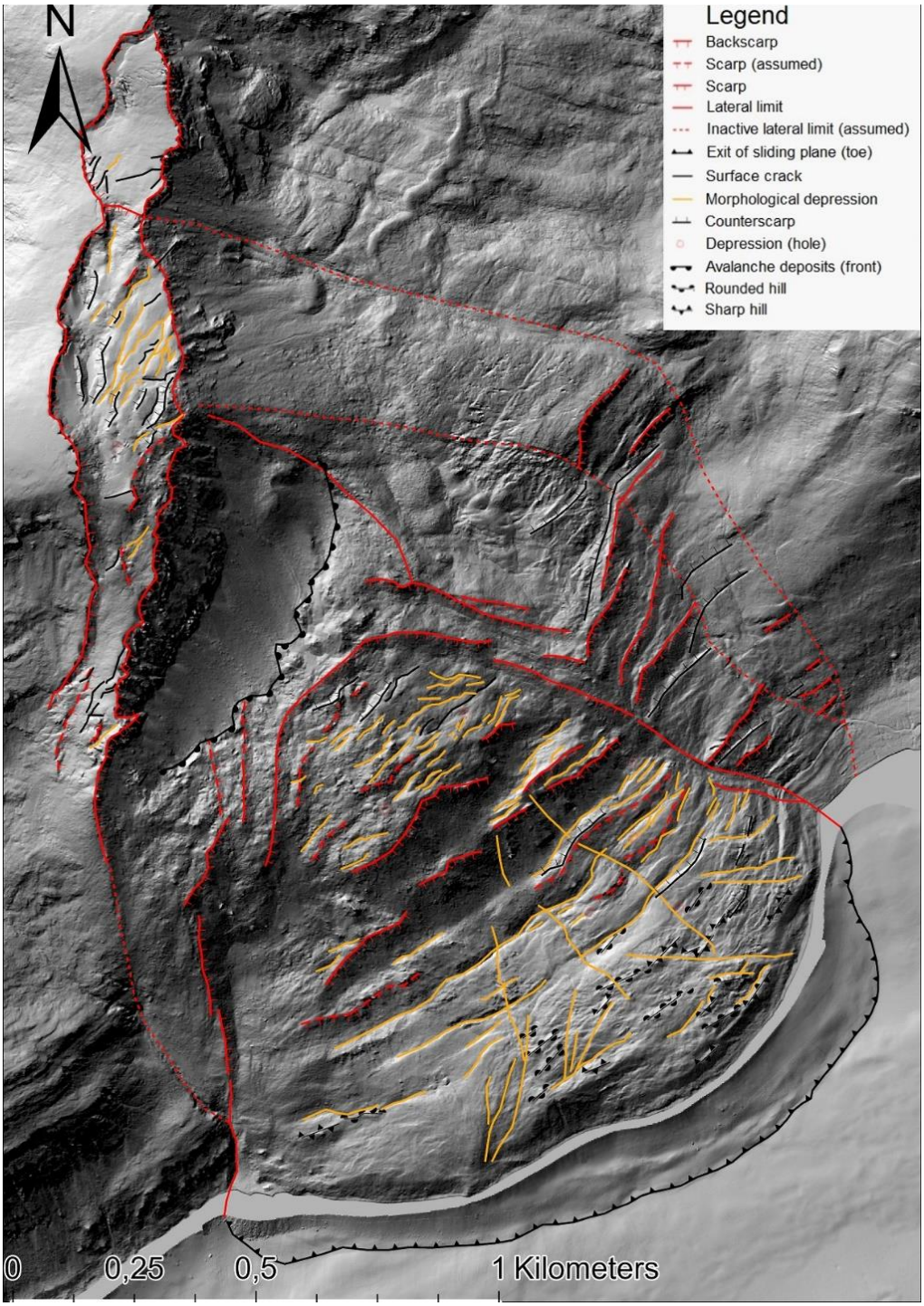

FIGURE 31: MORPHOLOGICAL MAP WITH A DEM BASELAYER, DEVELOPED IN ARCGIS PRO. FIGURE ADAPTED FROM SIMEN BEKKEVOLL, PERSONAL COMMUNICATION 22/4.22.

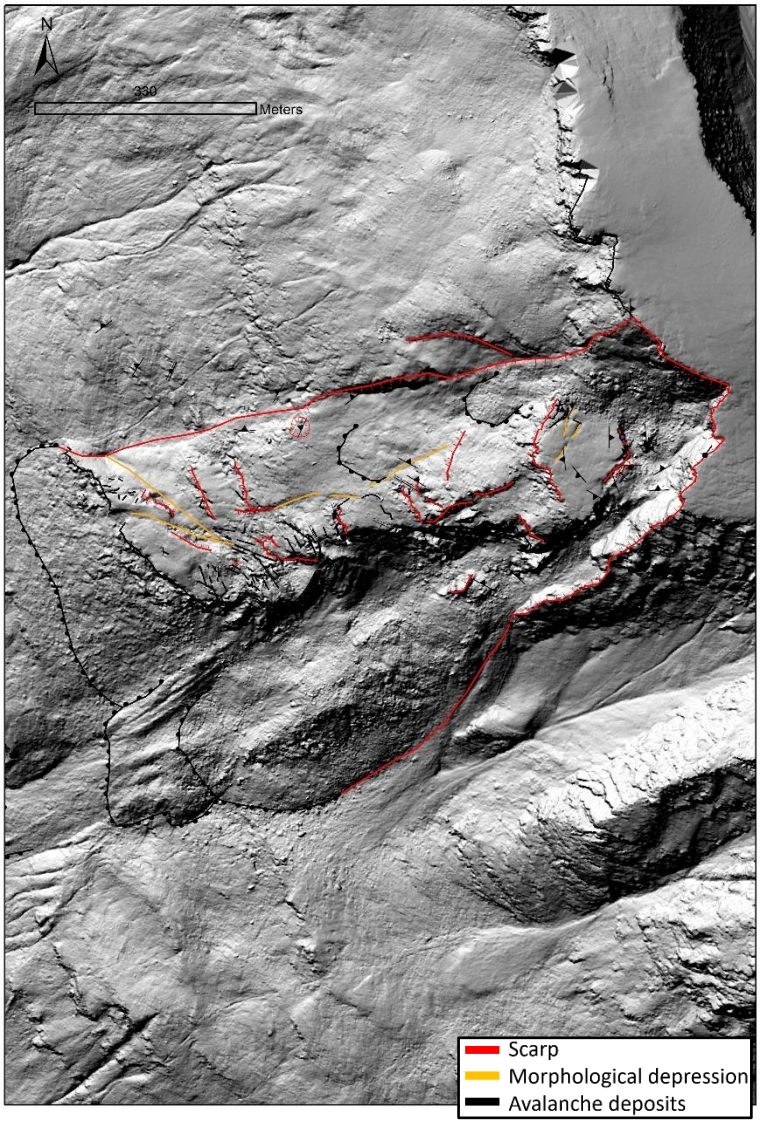

FIGURE 32: MORPHOLOGICAL MAP FROM NVE, 2019 – RETRIEVED FROM STEFFEN BERGH. BASELAYER IS A HIGH-RESOLUTION DEM.

3.2.1 Structural description

This section will present data describing the discontinuities (foliation, lenses, folds, shear zones, brittle faults and joint sets) observed from fieldwork at Dusnjarga and Gámanjunni 3. The mapping of discontinuities is believed to be of importance due to the physical properties resulting in weakness planes and lowering the overall rock mass strength. Pre-existing discontinuities as folds, lenses, magmatic layering, brittle and ductile deformation zones cause a mountain side to become unstable (Saintot et al., 2011). Rupture initiation often follows pre-existing structural discontinuities, so the understanding and mapping of the relevant discontinuities helps understand the rock mass and potential hazards (Vick et al., 2020).

All structural measurements presented in Dips are used with the following settings: upper hemisphere, equal area for projection and pole vectors as plot mode.

3.2.1.1 Dusnjarga

A total of 3063 structural measurements were taken at Dusnjarga. The data is combined from fieldwork completed with Simen Bekkevoll and Andreas Grumstad. Observed and measured structures include a ductile foliation, ductile shear zones, brittle faults, and joints.

3.2.1.1.1 Foliation

The foliation in the metagabbro is oriented 183/20 and defined by the shape-preferred orientation of plagioclase grains. The shape preferred orientation of grains at Dusnjarga varies from weak (figure 33 A) to strong (figure 33 B) depending on the degree of metamorphism and accompanying deformation. Section 33 A is representative of nearly unmetamorphosed gabbro with a mineral composition dominated by plagioclase and pyroxene and little to no amphibole. The grain size is medium to coarse-grained. Section 33 B is a highly metamorphic metagabbro with strong, pervasive foliation. The mineral composition is dominated by plagioclase, pyroxene, and amphibole. The mineral grains are finer-grained with plate-shaped minerals and a stronger preferred orientation. The variation varies locally and changes with lithology, and amphibolite is considered to have a moderately to poorly foliated fabric.

The zones that are more intensely metamorphosed and deformed, plagioclase appears to be recrystallized, leaving platy, white foliation parallel bands in a mafic, less foliated texture. The degree of foliation and thickness of magmatic layering appears to increase upwards with elevation, causing the planar plagioclase bands to appear around the higher elevations at Dusnjarga (e.g. fig. 33 B).

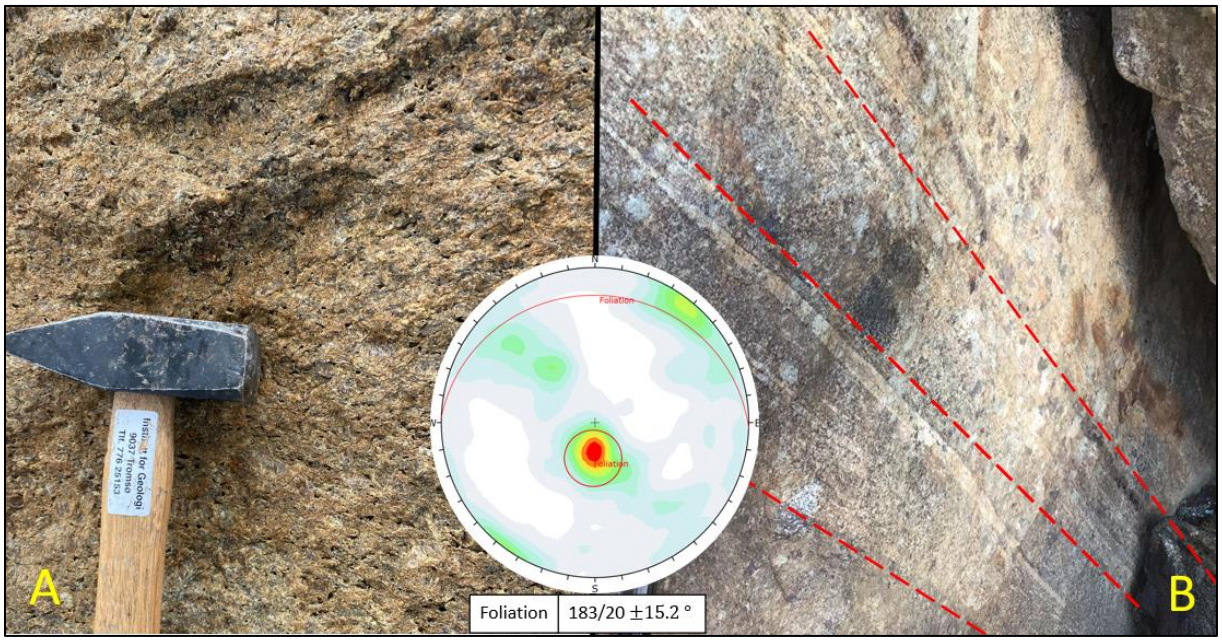

FIGURE 33: COLLAGE OF DIFFERENT DEGREE OF FOLIATED FABRIC IN THE METAGABBRO AT DUSNJARGA. STRUCTURAL MEASUREMENTS OF FOLIATION REPRESENTED IN THE MID-SECTION, DEVELOPED IN THE APPLICATION DIPS. A: NEARLY METAMORPHOSED METAGABBRO. B: HIGHLY METAMORPHOSED METAGABBRO, WITH A STRONG FOLIATION. PICTURES TAKEN DURING FIELDWORK IN SEPTEMER, 2021.

3.2.1.1.2 Structures

Lenses are observed at the upper section of Dusnjarga, within the back scarp and transition zone. The identified bedrock within the lenses is undeformed gabbro surrounded by foliated metagabbro (figure 34 A). Gabbro is the only rock type found in the lenses at Dusnjarga. The lenses are found in varying sizes but mostly within the interval 0.5 m to 5 m of length.

At Dusnjarga, folding of magmatic layers is observed in the upper section of the URS, in the vicinity of the mylonite. However, folding was not observed much elsewhere in the URS and is not considered a dominant structure. Figure 34 B shows a tight S-fold from near the mylonite zone at the top of the URS.

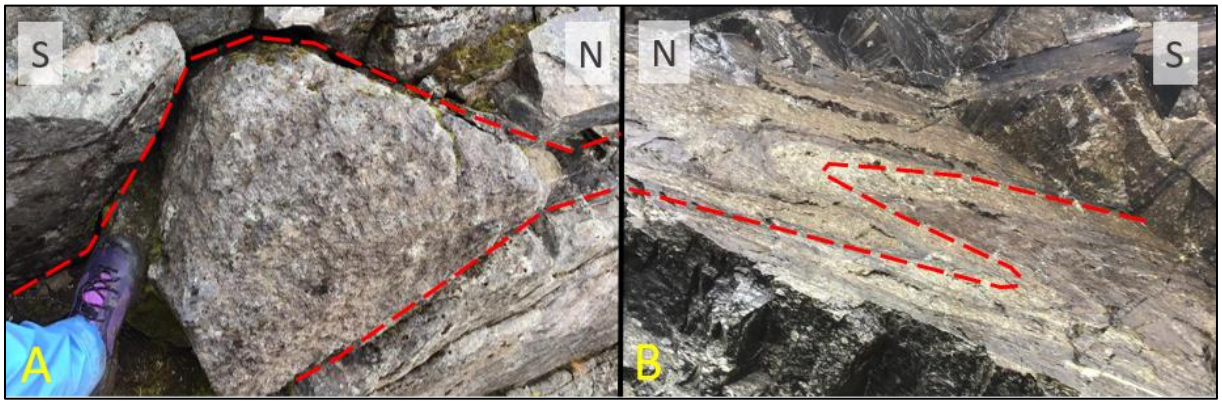

FIGURE 34: COLLAGE OF GEOLOGICAL STRUCTURES AT THE BACKSCARP REGION AT DUSNJARGA. A: LENSE OF GABBRO SURROUNDED WITH METAGABBRO. B: S-FOLD FOUND THE MOVING PLATEAU. PICTURES TAKEN DURING FIELDWORK IN SEPTEMBER, 2021.

3.2.1.1.3 Shear zones and brittle faults

A ductile shear zone is characterized by a zone of high deformation and levels of dynamic recrystallization. The innermost zone in the affected rock is a highly deformed, recrystallized zone named the mylonite zone (Marulanda et al., 2013).

Ductile shear zones are much older structures than the brittle faults at Dusnjarga. Figure 35 represents the observed location and orientation of the ductile shear zones and brittle faults at the URS.

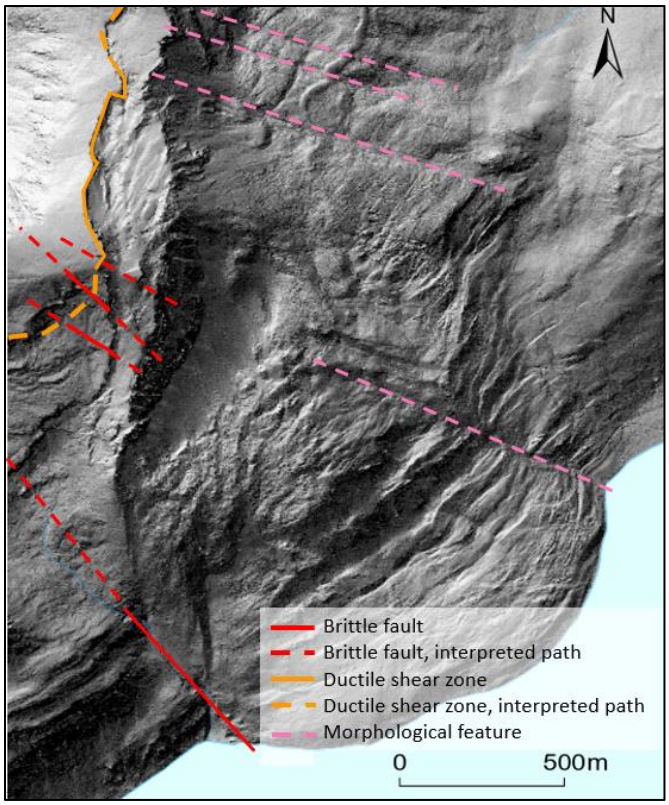

FIGURE 35: ILLUSTRATED ORIENTATION AND LOCATION OF OBSERVED DUCTILE SHEAR ZONES AND BRITTLE FAULTS. MAP IS USED WITH A 0.5 M HIGH RESOLUTION DEM DEVELOPED IN ARCGIS PRO.

The innermost deformed section in a ductile shear zone can be called a mylonite zone. The name mylonite describes a certain fabric and does not give any information about the mineral composition. Mylonite is a zone/rock formed by high degrees of recrystallization due to high strain ductile deformation.

The ductile shear zones can vary from 50 m (mylonite) to 5 cm and faces southwest with a 13-degree dip. The observed several ductile shear zones at different elevation throughout the URS, whereas figure 36 A is from 136 m asl. and figure 36 B marks a thick shear zone at 800 m asl. At the backscarp the thick shear zone is observed as a 50 m thick mylonite zone oriented 207. The mylonite zone is layered in a felsic and mafic appearance (e.g felsic layer represented in fig. 36 A). The felsic mylonite has a light beige-grey color with no rust and the mafic mylonite has a dark and rusty color.

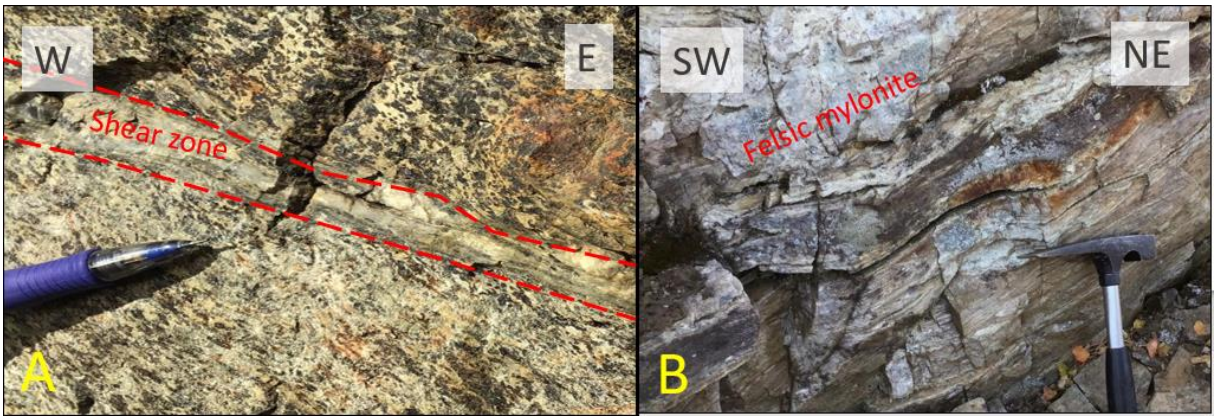

FIGURE 36: A: DUCTILE SHEAR ZONE OBSERVED IN THE METAGABBRO AT DUSNJARGA URS. B: FELSIC MYLONITE FROM THE BACKSCARP AT DUSNJARGA. PICTURES TAKEN DURING FIELDWORK IN SEPTEMBER, 2021.

Brittle faults are defined by curved brittle P-planes bound by usually straight Y-/fault planes, and often contain slickensides (Mukherjee, 2015). Brittle faults are a result of brittle behavior at low temperatures and low confining pressure.

Several brittle faults are observed at Dusnjarga with roughly the same orientation striking NW-SE (e.g. interpreted in figure 35), and therefore interpreted as a brittle fault system. The fault system is 1-5 m. thick with a steep inclination. The brittle faults are observed best at the backscarp region (figure 37)

FIGURE 37: BRITTLE FAULT FROM THE BACKSCARP OF DUSNJARGA URS. PICTURE TAKEN DURING FIELD DAYS IN SEPTEMBER, 2021.

Slickenlines were found in a brittle fault in the back scarp region and are a result of shear movement, either from fault or URS. The slickenline is more smooth downward in figure 38, indicating that the

missing block moved downwards with respect to the remaining block. The fault is likely a subsidiary of the Langfjord fault. Slickenlines are also observed at the western lateral boundary of the URS.

FIGURE 38: SLICKENLINES OBSERVED FROM A BRITTLE FAULT AT THE BACKSCARP REGION OF DUSNJARGA URS. DIRECTION OF MOST SMOOTH IS DOWNWARDS. PICTURE TAKEN DURING FIELDWORK IN SEPTEMBER, 2021.

3.2.1.1.4 Joint sets

Three consistent joint sets are observed at Dusnjarga. The most consistent joint set dips shallowly to the south and parallel to foliation (figure 39 A), which dips 20° towards the south (figure 39 B). This joint set is named JN F. The two other joint sets are conjugate, roughly 90° to one another. JN1 dips towards NW at 52° and is parallel to the back scarp of the URS. JN2 dips towards NE and dips 86° towards NW. JN2 is considered parallel to the lateral boundary of the URS. JN 1 and 2 are recognized in the field as consistent joint sets.

In the structural analysis another joint set is identified close to JN 2, the data set of this joint set is not big and therefore tagged "JN 2 (displaced).

The identified joint sets dominant in different magmatic layers, where JN1 is seen most frequently in the felsic layers and JN F in the mafic layers. There is only where the joint sets occur with a higher frequency, all joint sets are observed in felsic and mafic layers.

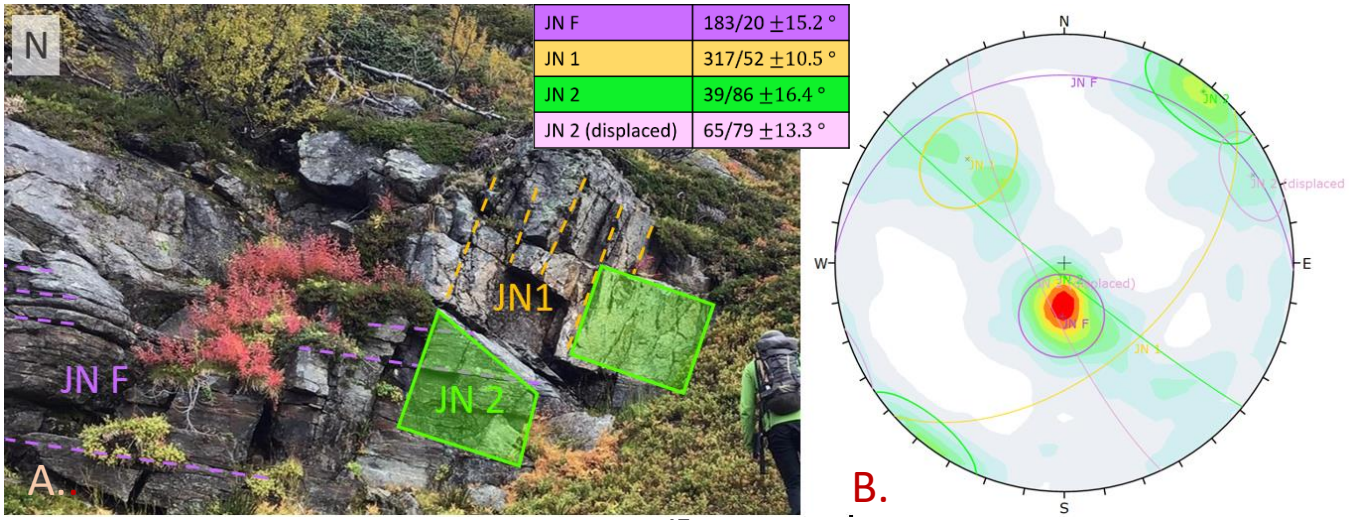

FIGURE 39: A: DIFFERENT JOINT SETS ANNOTATED IN THE METAGABBRO AT DUSNJARGA. B: STRUCTURAL MEASUREMENTS OF JOINT SETS RECOGNIZED FROM FIELDWORK AND DEVELOPED IN THE APPLICATION DIPS.

3.2.1.2 Gámanjunni 3

Due to limited time at Gámanjunni 3, structural measurements are borrowed from Martina Böhme (NGU) to improve the data set. The data set from Gámanjunni 3 consists of 419 structural measurements, including NGU data. The structural data will be presented together with the corresponding structures.

3.2.1.2.1 Foliation

Gámanjunni 3 is dominated by a well-foliated schistose fabric in the muscovite- and biotite schist. The foliation orientation is considered continuous in and outside the URS, with a shallow dip of 10 degrees towards NW. The foliation is more pervasive in sections with higher muscovite content. The metapsammite presents a well-developed foliation oriented parallel to the rest of the URS (figure 40).

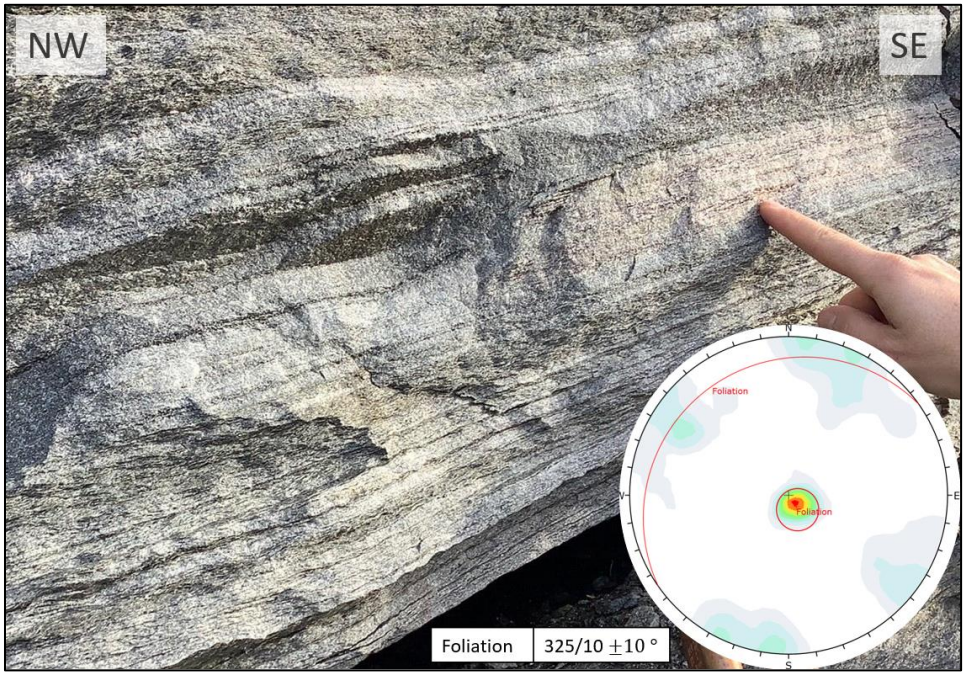

FIGURE 40: PHOTOGRAPH OF FOLIATION IN THE MICA SCHIST. STRUCTURAL MEASUREMENTS IS PRESENTED IN THE LOWER RIGHT ELLIPSOID, DEVELOPED IN DIPS.

3.2.1.2.2 Structures

At Gámanjunni 3, lenses of quartzite, biotite- and muscovite schist are all observed within the upper 1000-1200 m asl. Figure 41 A shows a lense in the back scarp of the URS, oriented within the foliation. The lense is a large sigma-clast of amphibolite with surrounding biotite schist. Both the biotite schist and the amphibolite contain crystals of garnet.

Folding at Gámanjunni 3 is observed at several locations, mainly within the upper half section of the URS. Figure 41 B shows chevron folds in muscovite- and biotite schist layers. The morphology of large-scale folds also varies from open (120-180°) to closed (30-70°) with most fold axes dipping towards W-NW. Small-scale folding is also observed the more pervasive mica schist with larger grains, but orientation were not possible to identify from field investigations

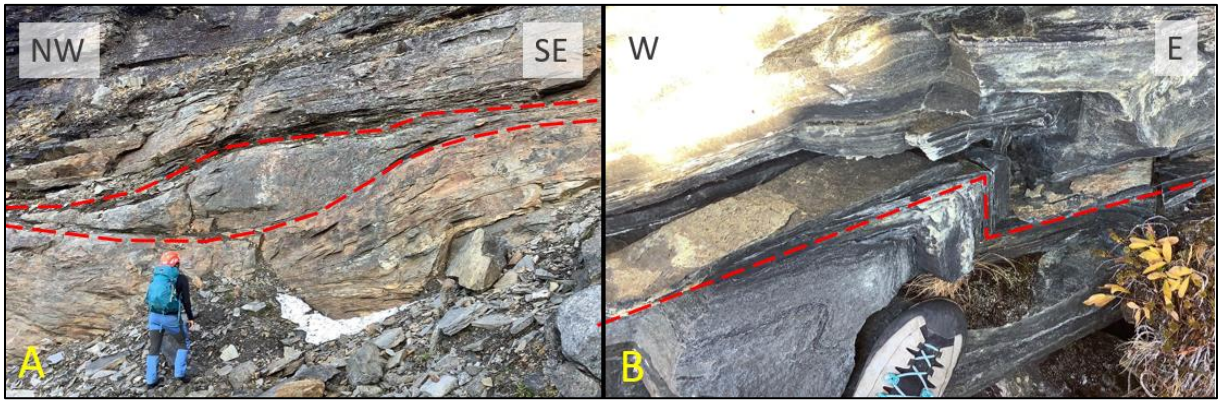

FIGURE 41: PHOTOGRAPHS OF DUCTILE STRUCTURES AT THE BACKSCARP OF GÁMANJUNNI 3. A: A SIGMA-CLAST OF AMPHIBOLITE SURROUNDED BY RUST-COLORED BIOTITE SCHIST. PICTURE A AND B TAKEN DURING FIELD DAYS IN SEPTEMBER, 2021.

3.2.1.2.3 Brittle faults

Brittle faults are observed within the toe section of the URS. Figure 42 A shows a 15 cm thick fault gauge resulting from brittle deformation. The gauge is loose, fine-graine, and easily separated with little force. The thickness of the brittle fault varies from 5-50 cm and is recognized by the fine-grained gauge material. The brittle faults appear to be parallel to foliation and occurs at some places with less than a meter spaced to each other (figure 42 B).

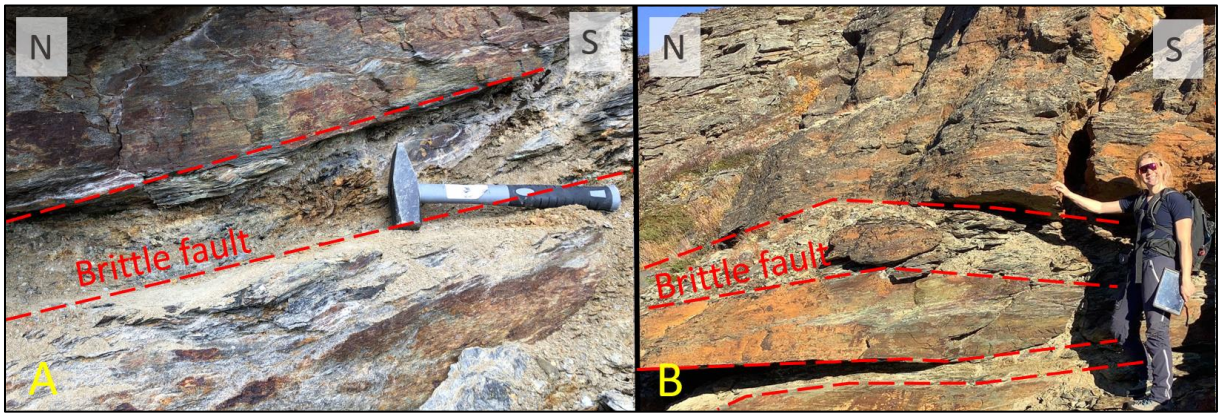

FIGURE 42: A: PHOTOGRAPHS TAKEN FROM RUST-COLORED BIOTITE SCHIST AT THE TOE SECTION AT GÁMANJUNNI 3. A: 15 CM THICK BRITTLE FAULT. PICTURE ADAPTED FROM NVE, DURING FIELDWORK IN AUGUST 2019. B: SEVERAL BRITTLE FAULTS PARALLEL ORIENTED. PICTURE TAKEN DURING FIELD DAYS IN SEPTEMBER.

Slickenlines were observed at the back scarp face of Gámanjunni 3. A displacement direction could not be determined from the slickenlines in figure 43, but they are most likely a result from slope failure related movement in the back scarp. Therefore, an interpretation done in the field is that the missing block has moved downwards.

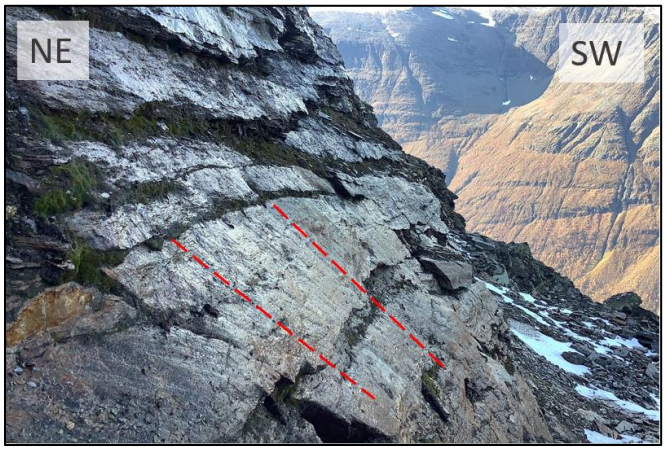

FIGURE 43: SLICKENLINES WITH ANNOTATED IN THE NW-FACING BACKSCARP AT GÁMANJUNNI 3. PICTURE TAKEN DURING FIELD WORK IN SEPTEMBER, 2021.

3.2.1.2.4 Joint sets

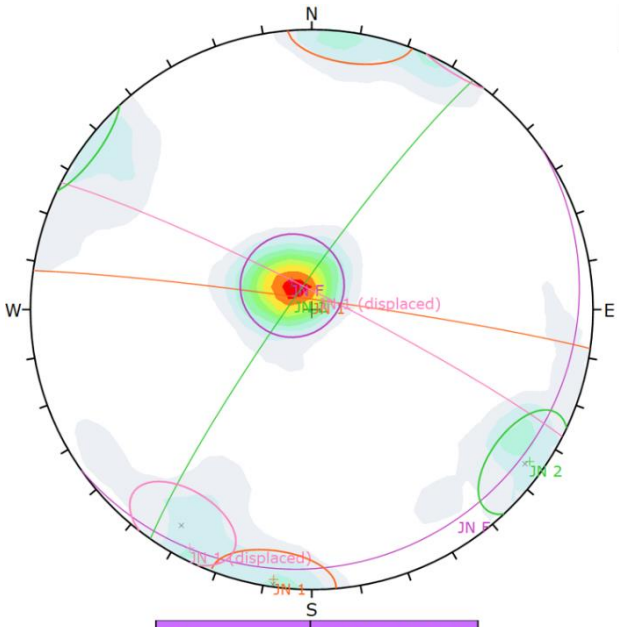

JN F	325/10 ±13.9.2 °
JN 1	188/87 ±13.4 °
JN 2	125/84 ±13.24 °
JN 2 (displaced)	65/79 ±13 °

FIGURE 44: ELLIPSOID REPRESENTING STRUCTURAL MEASUREMENTS FROM JOINT SETS RECOGNIZED DURING SEPTEMBER 2021. MEASUREMENTS ARE ADAPTED FROM NGU. FIGURE DEVELOPED IN DIPS.

There are three conjugate joint sets observed at Gámanjunni 3 in the field, and 4 identified joint sets from structural analysis (figure 44). JN F is the most common join set and parallel to foliation. JN f is oriented NW and dips shallowly 10° (figure 45 A).

The two consistent joint sets are parallel to the orientation of the back scarp, giving both joint sets a near-vertical inclination (figure 45 B). JN1 is oriented to the south and JN2 is oriented towards SE. JN 1 and 2 are recognized in field.

Close to JN 1 in the structural analysis a fourth joint set is identified. Due to the little data set, and properties similar to JN 1, the data set is tagged as "JN 1 (displaced)". This joint set is not recognized in field.

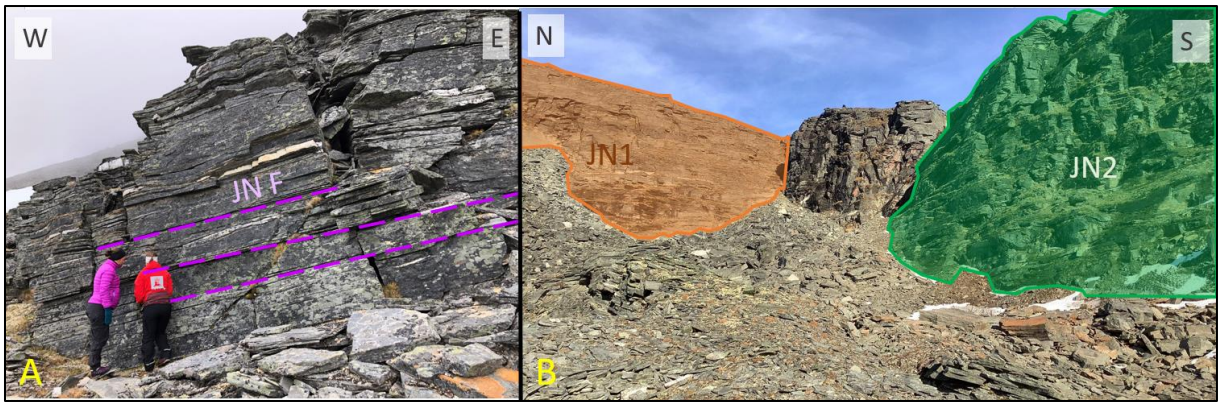

FIGURE 45: AN OUTCROP REPRESENTING THE JOINT SET PARALLEL TO FOLIATION: JN F. B: BACKSCARP WITH ANNOTATED JOINT SET 1 AND 2 PARALLEL FACES. BOTH PICTURES WERE BORROWED FROM FIELDWORK COMPLETED IN JUNE 2019 BY ANNE-MARTE HANSEN ACCOMPANIED BY NVE.

3.3 Microstructures from thin sections

The goal of microstructural description was to establish how brittle fracturing, which is likely related to URS deformation, exploits pre-existing weaknesses in the rock at a microscale and to define what those pre-existing weaknesses are. The thin sections from Dusnjarga and Gámanjunni 3 are taken inside and outside of the URS with a focus on representative sampling. Some of the rock samples fractured during selection or preparation and were therefore not able to use. As a result, the thin sections represent some of the more intact samples collected from fieldwork.

Table 6 is used to describe the degree of fracturing in each sample. The table is a scheme for evaluation of fracture patterns considering rock stability. Fracture grade gives a simplified overview of small-scale structure analysis from thin sections.

Microcracks has been subdivided into more detailed terms (Kranz, 1989):

- Intergranular: microcracks coincide with grain boundaries.
- Intragranular: microcracks confined to the interior of a single grain.
- Transgranular: microcracks cross more than one grain.

TABLE 5: FRACTURE GRADE WITH DESCRIPTION, DEVELOPED FROM A THIN SECTION STUDY OF SAMPLES FROM DUSNJARGA AND GÁMANJUNNI 3.

Fracture grade:	Texture:	Number:
1	• Fractures do not cross sample. • Does not display a specific joint set	1-3, depending on fracture direction and size.
2	• Continuous fracturing • A joint set can be established	2-8, depending on fracture length
3	• Some microfractures are dilated and continuous • Joint set is clear • Fractures favor specific minerals or structures. • Shear zone is observed	5+, depending on fracture length
4	• Fractures are transgranular and continuous through the thin section with some dilation • 1 or more joint sets • Fractures favor minerals or structures • Shear zone with fractures • Overall body strength is presented as weak	6 +, depending on fracture length

3.3.1 Dusnjarga

Table 7 focuses on describing fractures, fracture path, and shear zones from Dusnjarga thin sections. The row comments are used for other observations from microscope work that may be relevant for the sample.

For simplicity, felsic and mafic minerals are grouped in some rows in table 7. “Felsic minerals” represent feldspar and quartz, and “ferromagnesian minerals” amphibole and clino- and orthopyroxene. Individual fracture grade for each sample with location is marked in figure 46.

TABLE 6: SUMMARY OF FINDINGS IN THE THIN SECTION FROM DUSNJARGA. THE OVERVIEW OF THE THIN SECTION LOCATION IS IN FIGURE 46.

Thin section	Mineral assemblage (modal %)	Fractures Shear zone	Fractures favoring	Fracture grade	Comments
RM 15 Amphibolite	Plagioclase 28 Amphibole 50 Clinopyroxene 10 Orthopyroxene 10 Quartz 2	3 fractures, 2 perpendicular and 1 parallel to foliation.	Not favoring any specific mineral	**2** – few fractures and not well developed.	Not a well-developed fracture system. Grain boundaries are lobate and transgranular.
RM 1.2 Metagabbro	Amphibole 30 Plagioclase 32 Orthopyroxene 15 Clinopyroxene 15 Quartz 5 Biotite 3	8 + fractures, 1 shear zone. Fractures are parallel to the foliation but not consistent.	Felsic minerals. Fractures are isolated and linked; some are dilated.	**3** – Several microfractures, some dilated.	Mostly intergranular microfractures.
FM Mylonite	Plagioclase 40 Quartz 10 Amphibole 15 Clinopyroxene 15 Orthopyroxene 10 Muscovite 10	4 + fractures and 1 shear zone.	Fractures are not favoring minerals, transgranular.	**3** – Fractures are not very consistent and do not favor any minerals.	Inclusions in grains, mostly in 1< large grains. The color is light beige-grey.
RM9.3 Mylonite	Quartz 10 Plagioclase 40 Amphibole 30 Clinopyroxene 5 Orthopyroxene 5 Accessory minerals > 5	8 + fractures.	Mainly randomly oriented, two fractures favor fine-grained ferromagnesian minerals.	**5** – Many small and large fractures dominate the thin section	Most fractures are 45’ to foliation. Matrix of very fine grains, zoning, lobate boundaries, and no inclusions. Microcracks are inter- and transgranular.
RM593 Metagabbro	Plagioclase 55 Quartz 5 Amphibole 20 Clinopyroxene 10 Orthopyroxene 10	7 + fractures, 1 shear zone. Many partly isolated microfractures. Perpendicular to foliation	Not favoring any specific minerals, sometimes feldspar	**4** – high density of microfractures	Microcracks crossing most grains unaffected. Some grains have intergranular microfractures.
RM13.2 Metagabbro	Plagioclase 45 Orthopyroxene 20 Quartz 5 Clinopyroxene 15 Biotite 10 Garnet 5	6 + fractures. Fractures and shear zone parallel to foliation. 1 fault zone with 12 connected fractures	Fractures favor biotite (shear zone) and plagioclase. Some dilated fractures.	**4** – Fractured zone and parallel to foliation	Large ductile shear zone/fault zone, with transgranular dilated microcracks.
RM11.1 Metagabbro	Amphibole 25 Plagioclase 30	6 + fractures. 1 thin shear zone.	Felsic minerals and some biotite	**2** – Few fractures	Transgranular microcrack is neither

	Orthopyroxene 20 Clinopyroxene 15 Quartz 5 Biotite 5	Several linked and isolated micro cracks.	are also boundaries to ferromagnesian minerals	and not very consistent.	parallel nor perpendicular to foliation.
RM12.2 Metagabbro	Amphibole 20 Clinopyroxene 15 Orthopyroxene 15 Plagioclase 40 Quartz 5 Biotite 5	8 + fractures, Shear zones. Fractures are dilated.	Fractures favor feldspar, and shear zone favor biotite. Mostly parallel to foliation	**5** – Many wells developed fractures, dilated and shear zones	High density of ductile shear zones with and linked and isolated transgranular microcracks.
RM3.1 Metagabbro	Plagioclase 35 Amphibole 30 Clinopyroxene 15 Orthopyroxene 15 Biotite 5	4 + fractures, 1 small shear zone. Following foliation	Felsic minerals. Some fractures are dilated.	**2** – Few and not consistent fractures.	Mostly intergranular microcracks.
RM20 Mylonite	Biotite/mica 30 Quartz 10 Plagioclase 30 Clinopyroxene 10 Orthopyroxene 10 Amphibole 10	6 fractures, 1 shear zone	Not favoring any minerals, moves at the grain boundary	**4 –** isolated microfractures, not very continuous	Microcracks intra-, inter, and transgranular. Color is light beige to grey.
RM6.1 Metagabbro	Plagioclase 55 Quartz 5 Orthopyroxene 10 Clinopyroxene 10 Garnet 5 Amphibole 15 Accessory minerals > 1	5 fractures, no shear zone	Favor felsic significant minerals and cleavage in grains.	**4 –** fractures are perpendicular to foliation with a high frequency of intragranular microfractures**.**	Most of the grains have intragranular microfractures that are perpendicular to foliation. Porphyroblastic texture.

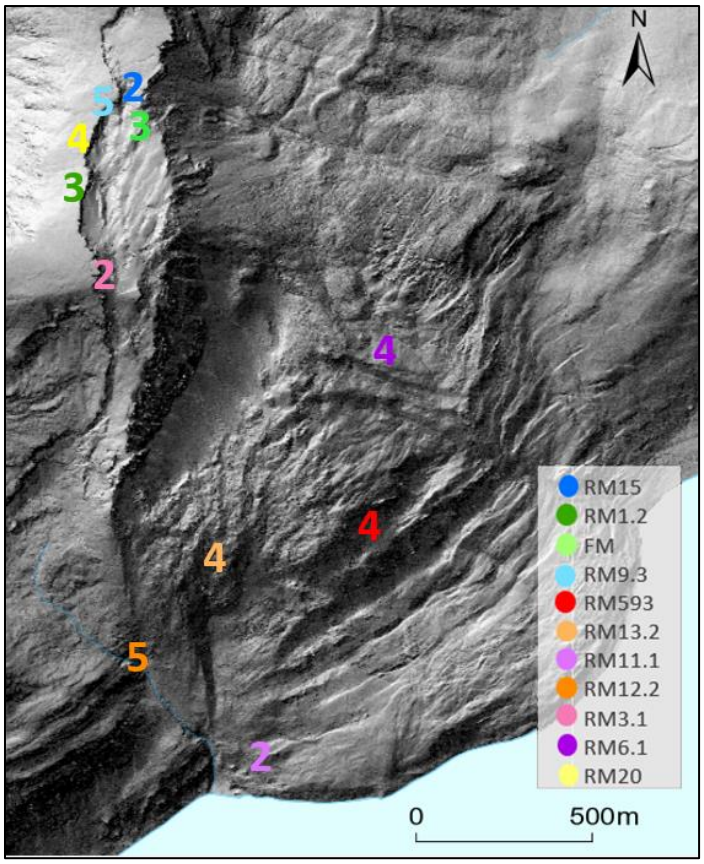

FIGURE 46: LOCATIONAL MAP OF THIN SECTION, COMBINED WITH FRACTURE GRADE NUMBER FROM SAMPLES AT DUSNJARGA. THE BASELAYER OF THE MAP IS A HIGH-RESOLUTION 0.5 M DEM, DEVELOPED IN ARCGIS PRO.

The samples of mylonite contain lenses of less deformed material, where a more gabbroic texture is visible. There are signs of ductile deformation with a mylonitic texture and monoclinic shape symmetry in the more mylonitic sections. The linear shape fabric in the mylonite shows a poor shape preferred grain orientation in microscope. The samples present a high grain size variation in the mylonite due to porphyoblastic grains in a fine-grained matrix (figure 47). The matrix consists of minerals mainly too fine to be recognized in the microscope. Microcracks are mainly transgranular and randomly oriented, with a fracture grade varying from 3-5. The mylonite is graded high due to a well-developed fracture system, but the joints are more randomly oriented than presenting as an obvious, consistent joint set.

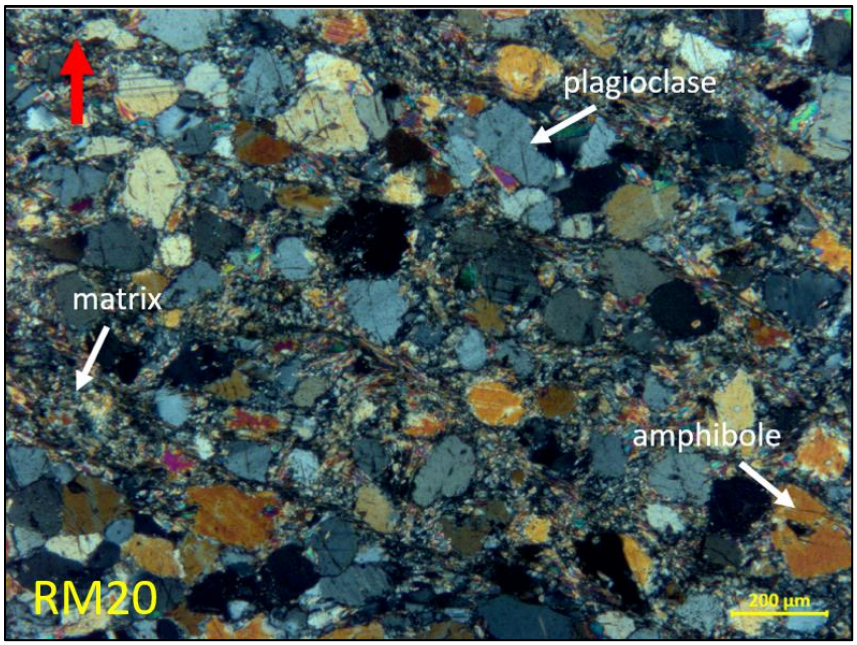

FIGURE 47: SAMPLE RM20, FELSIC MYLONITE - A THIN SECTION PICTURE WITH A SCALE OF 1:200µM. ANNOTATED WITH DOMINATED MINERALS.

The degree of fractures in each sample is highly variable. The sampled rock types vary from 2 to 5 in fracture grade, with metagabbro being the rock type with the highest variation in fracture grade. The amphibolite sample is given a fracture grade of 2, and the three mylonite samples vary from 3 to 5.

Several small-scale ductile shea zones are observed in thin sections (figure 48 A) and defined by oriented biotite grains (figure 48 B). The shear zones are only observed in the metagabbro's and oriented parallel to the foliation. Most of the shear zones contains microcracks, indicating that small-scale fractures favor shear zones. These microcracks also tend to dilate when fractured (e.g. figure 48 B).

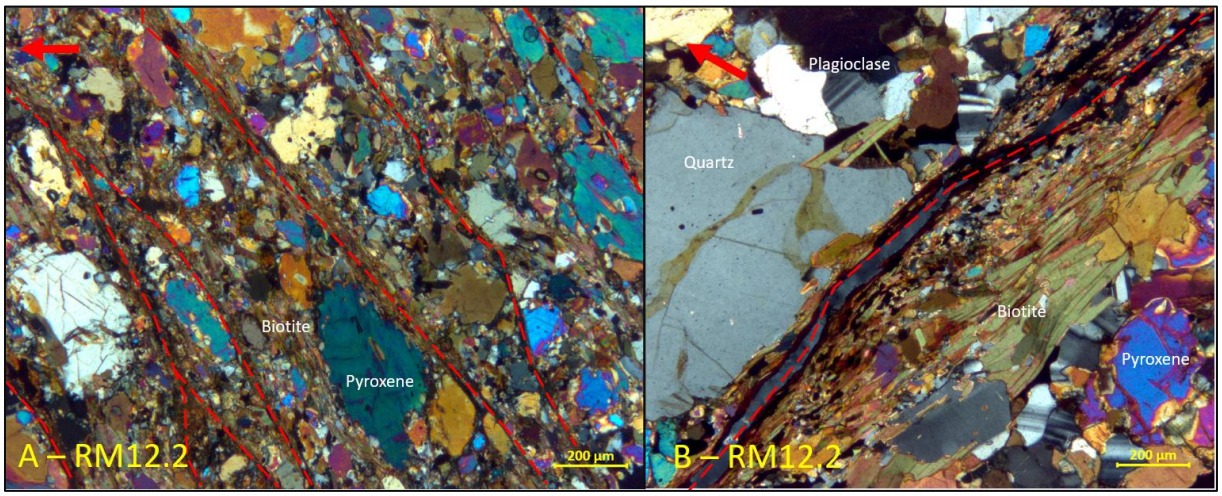

FIGURE 48: THIN SECTION PICTURES. A: METAGABBRO SAMPLE RM12.2 WITH ANNOTATED SHEAR ZONES AND MINERALS. B: METAGABBRO SAMPLE RM12.2 WITH ANNOTATED DILATED SHEAR ZONE. BOTH PICTURES ARE TAKEN WITH A 5X MAGNIFICATION WITH CROSS-POLARIZED LIGHT IN A 1:200µM SCALE. RED ARROW INDICATED UP DIRECTION.

In the metagabbro there are two compatible common sets, parallel and normal to the foliation that can be identified easily. In samples with shear zones, fractures favor the weakness plane of the shear zone and result in a higher fracture frequency (RM12.2, RM13.2, and RM593) (figure 49 A). The degree of deformation caused by fractures varies from 2 – 5 . The fractures in the metagabbro appear to favor plagioclase and fractures are more continuous in bands of plagioclase parallel to foliation (figure 49 A). Fractures favor plagioclase in all 7 metagabbro, out of 11 thin sections. In samples with a smaller amount of plagioclase, the fractures tend to follow cleavage in ferromagnesian minerals, resulting in transgranular microcracks (e.g. pyroxene; fig. 49 B). Some microfractures are also observed at a smaller scale, where the grains are intragranular fractured with identical orientation as the two identified joint sets, as presented in figure 49 B (e.g. RM6.1). Linked and isolated microfractures give a wider fracture zone. Metagabbro with a high percentage of amphibole has several fracture zones, with a high frequency of linked and isolated microfractures.

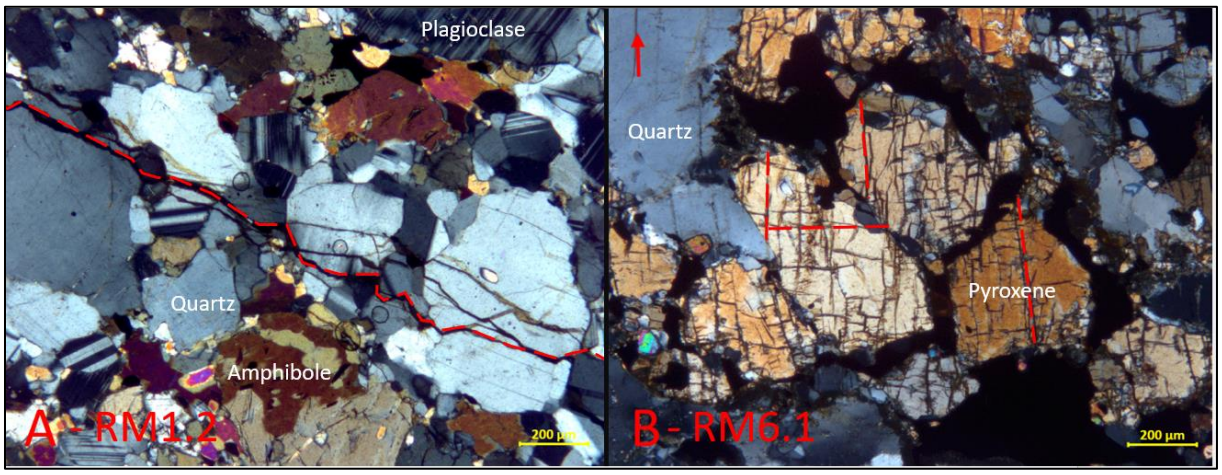

FIGURE 49: THIN SECTION PICTURES FROM DUSNJARGA. A: METAGABBRO SAMPLE RM1.2 FROM THE BACKSCARP, SHOWING MICROFRACTURES FAVORING PLAGIOCLASE. B: METAGABBRO SAMPLE RM6.1 FROM NW OUTER BOUNDARY OF URS. SHOWING INTRAGRANULAR MICROCRACKS IN PYROXENE. BOTH PICTURES ARE TAKEN WITH A 5X MAGNIFICATION WITH CROSS-POLARIZED LIGHT IN A 1:200µM SCALE. RED ARROW INDICATED UP DIRECTION.

The amphibolite samples favor both plagioclase and amphibole cleavage. Fractures favoring plagioclase tend to be oriented parallel to foliation, and fractures linking up in intragranular microfractures in amphibole cleavage tend to be oriented normal to the foliation (figure 50). Fractures in the plagioclase also have a wider fracture zone. The fracture grade in the amphibolite sample is 2, so the sample is not heavily affected by fractures (i.e. RM15).

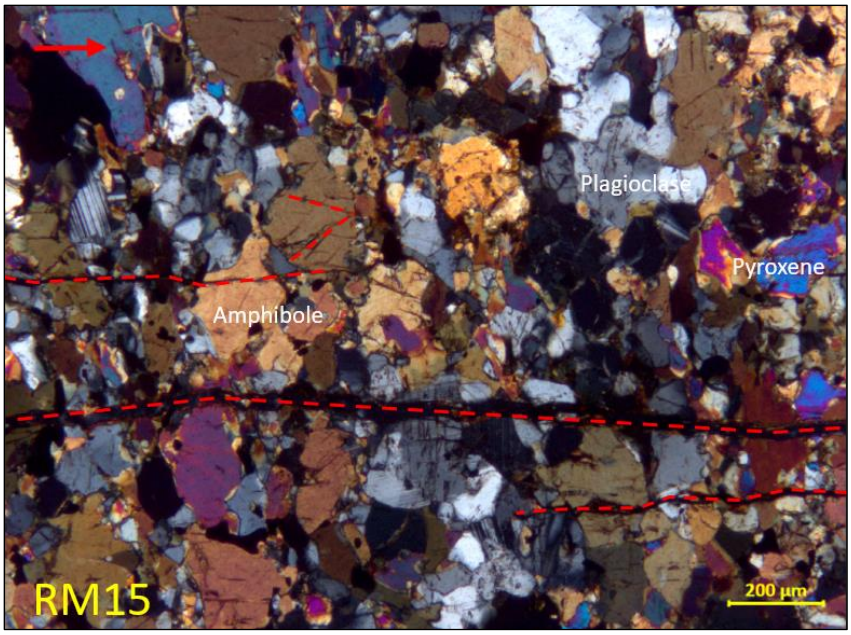

FIGURE 50: THIN SECTION PICTURE OF THE AMPHIBOLITE, SAMPLE RM15. PICTURE MARKS INTRAGRANULAR MICROCRACK IN AMPHIBOLE CLEAVAGE, AND LARGER TRANSGRANULAR FRACTURES PERPENDICULAR TO FOLIATION. PICTURE IS TAKEN WITH A 5X MAGNIFICATION WITH CROSS-POLARIZED LIGHT IN A 1:200µM SCALE. RED ARROW INDICATED UP DIRECTION.

3.3.2 Gámanjunni 3

Samples from Gámanjunni 3 are investigated in a petrographic microscope, and the findings are listed in Table 8.

In needs to be noted that due to challenging weather, the field work was completed just in time to send the samples from Gámanjunni 3 to Oslo. As a result, the PLT tests were performed before thin section was prepared. This could affect the degree of fracture in some thin sections.

Individual fracture grade for each sample with location is marked in figure 51.

TABLE 7: SUMMARY OF FINDINGS IN THE THIN SECTION FROM GÁMANJUNNI 3. OVERVIEW OF THIN SECTION LOCATION IS PLACED IN FIGURE 51.

Thin section	Mineral assemblage (%)	Grain size (mm)	Fractures Shear zone	Fractures favoring	Fracture grade	Comments
G3 Amphibolite	Amphibole 65 Quartz 15 Garnet 5 Muscovite 5 Biotite 5 Pyroxene 5?	3-0.5	8 + fractures and a small shear zone. 5 quartz intrusions	Favor cleavage in amphibole.	2 – many microfractures, but they are not continuous.	Transgranular microcracks and quartz intrusions are normal to foliation.
G7 Muscovite Schist	Quartz 70 Muscovite 15 Biotite 5 Plagioclase 5 Garnet 5	1-0.5	4 + fractures	Following mica minerals.	2 – not many fractures	Intra- and transgranular microcracks parallel and normal to foliation.

G5 Breccia	Quartz 50 Biotite 25 Muscovite 15 Garnet 5 Plagioclase 5	1.5-0.01	4 + and 3 shear zones.	Fractures follow schist and shear zones.	3, not many fractures. Some are dilated.	Lithological boundary separated by shear zone. Mostly intergranular microcracks.
G19 Biotite schist	Quartz 40 Biotite 30 Muscovite 15 Plagioclase 10 Garnet 5	1-0.1	0 – no fractures.		1 – wavy texture defined by schist.	Intergranular microcracks
G10 Metapsammite	Quartz 55 Biotite 20 Muscovite 15 Plagioclase 5 Garnet 5	1-0.5	1 fracture	Linear fractures in quartz grains, zigzag in micas.	1 – not many fractures.	Transgranular microcracks normal to foliation.
G17 Muscovite schist	Quartz 40 Muscovite 30 Biotite 15 Plagioclase 5 Garnet 5 Chlorite 5	2-0.1	No fractures		1 – no fractures.	
G14 Muscovite schist	Quartz 25 Plagioclase 25 Muscovite 20 Biotite 20 Garnet 10	2-0.1	No fractures		1 – no fractures.	Wavy schist texture.
G13 Muscovite/ biotite schist	Quartz 50 Biotite 20 Muscovite 10 Plagioclase 10 Garnet 10	1-0.1	2 + fractures	Does not favor any minerals.	1 – two fractures but not continuous	Transgranular microcracks with linked and isolated microfractures.
G15 Biotite schist	Biotite 45 Quartz 40 Plagioclase 10 Accessory minerals < 5	1-0.1	No fractures		1 – no fractures	Wavy texture from schist minerals.
G16 Biotite schist	Quartz 30 Biotite 30 Feldspar 25 Garnet 10 Accessory minerals < 5	2-0.1	2 + fractures	1 intergranular microcrack follows biotite	1 – not very continuous fractures	Quartz intrusion stops fracture propagation.

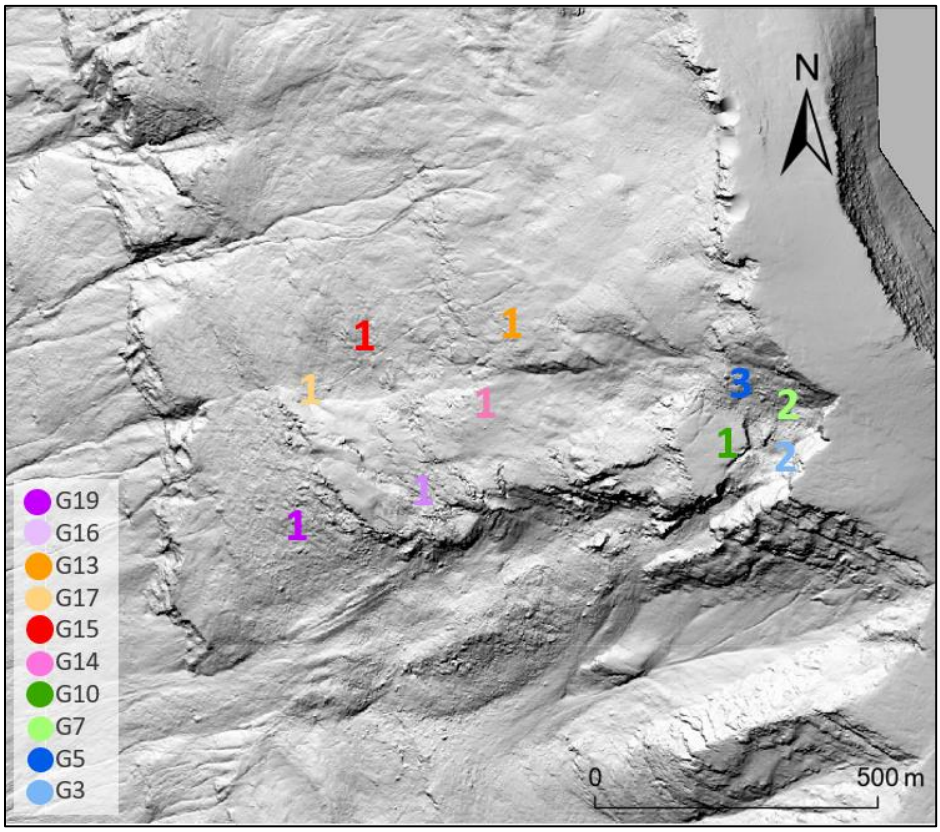

FIGURE 51: LOCATIONAL MAP OF THIN SECTION, COMBINED WITH FRACTURE GRADE NUMBER FROM SAMPLES AT GÁMANJUNNI 3. THE BASELAYER OF THE MAP IS A HIGH-RESOLUTION 0.5 M DEM, DEVELOPED IN ARCGIS PRO.

Due to few observed fractures, 9 out of 10 samples vary with a fracturing grade from 1 to 2. A fracturing grade of 1-2 represents a poorly developed fracture system and does not define the samples. Fractures are observed in 6 out of 10 samples and observed in all rock types. The observed fractures are either parallel or normal to the foliation, giving two consistent joint sets with mostly inter- and transgranular microcracks. These joint sets are not observed in samples with a high assemblage of mica minerals.

In thin sections, the sampled mica schist shows a wavy, small-scale folding in areas where muscovite and biotite are more developed. This is an s-c' fabric observed in the samples with a high assemblage of mica minerals. An s-c' fabric is a result of intersection of shear surfaces from dynamic metamorphism, whereas S is foliation and C shear bands. The muscovite schist samples G14 and G17 display a high assemblage of mica minerals and present a partially developed s-c' fabric (figure 52 A and B). The s-c' fabric is not interpreted to be completely developed, as a second foliation is not recognized. This fabric is not observed in samples with a lower assemblage of mica minerals.

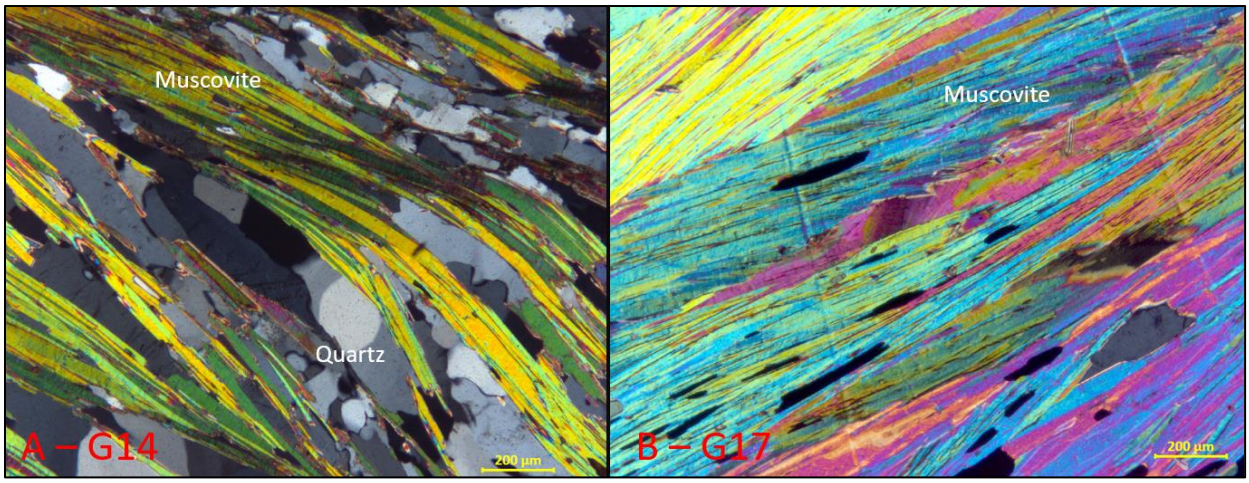

FIGURE 52: PICTURES OF THIN SECTION. A: MUSCOVITE SCHIST SAMPLE G14, SHOWING S-C' FABRIC OF MICA GRAINS WITH QUARTZ GRAINS IN BETWEEN. B: MUSCOVITE SCHIST SAMPLE G17. BOTH PICTURES ARE TAKEN WITH A 5X MAGNIFICATION WITH CROSS-POLARIZED LIGHT IN A 1:200µM SCALE.

The foliation parallel join set favors mica minerals in between quartz grains (figure 53 A). When these conditions are fulfilled the microfractures tend to dilate. A breccia is identified in the backscarp region (i.e sample G5, figure 53 B), and the sample represents the boundaries of muscovite- and biotite schist with the shear zone not completely parallel to foliation. Fractures is observed to favor mica minerals in all observed thin sections.

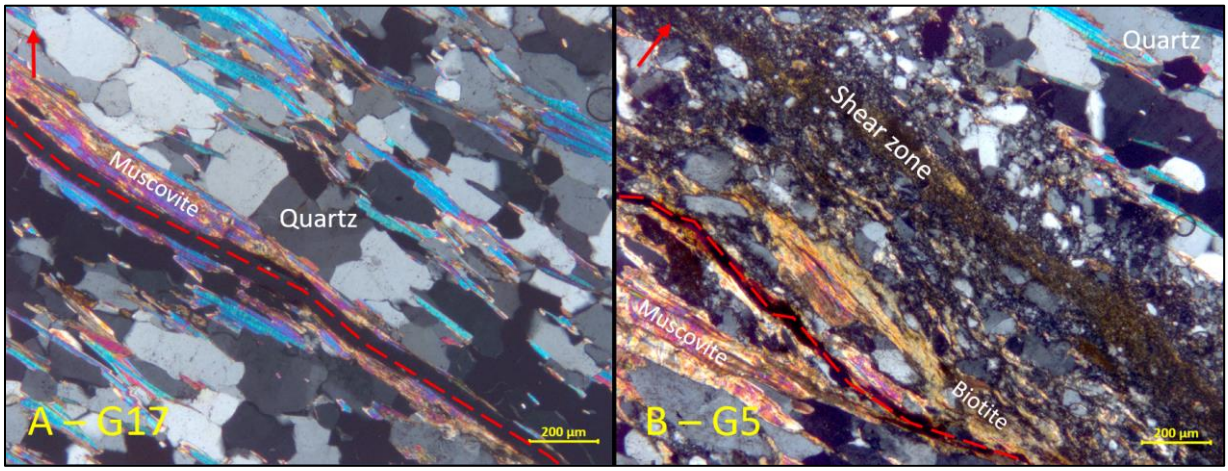

FIGURE 53: PICTURES OF THIN SECTIONS. A: MUSCOVITE SCHIST SAMPLE G17, WITH A DILATED FRACTURE IN A THIN MUSCOVITE LAYER. B: BRECCIA SAMPLE G5. SHEAR ZONE MARKS A BOUNDARY BETWEEN MUSCOVITE- AND BIOTITE SCHIST. MICROFRACTURE ANNOTATED IN THE MUSCOVITE SCHIST. SAMPLE FOUND AT BACKSCARP OF GÁMANJUNNI 3. BOTH PICTURES ARE TAKEN WITH A 5X MAGNIFICATION WITH CROSS-POLARIZED LIGHT IN A 1:200µM SCALE. RED ARROW INDICATED UP DIRECTION.

The amphibolite presents intragranular microfractures in the amphibole cleavage. The microfractures appears to link up and form a more consistent fracture, resulting in a decrease of microfractures but increase in fracture length (e.g figure 54 A). The fracture zone becomes wider, as most amphibole grains appears to be affected by intragranular fracturing.

Figure 54 B shows a zig-zag pattern in the fractured metapsammite. The fractures progress straight through the quartz and move plastically with a change of orientation through the mica grains (i.e., micas bend). This fracture mechanism is only in the fractures normal to foliation and consists of linked microfractures that displays a broader fracture zone.

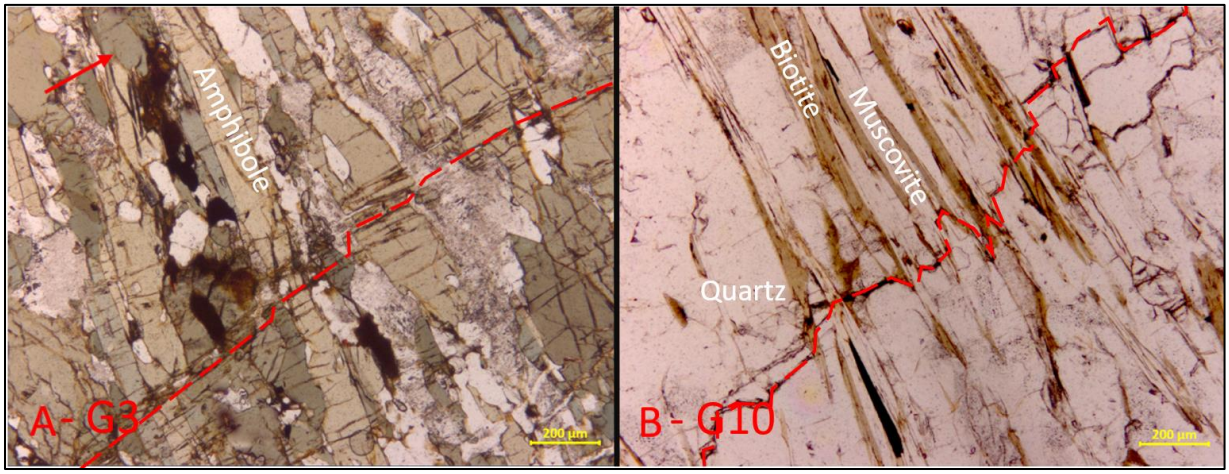

FIGURE 54: PICTURE OF THIN SECTION. A: AMPHIBOLITE SAMPLE G3 WITH INTRAGRANULAR MICROCRACKS IN AMPHIBOLE CLEAVAGE PERPENDICULAR TO FOLIATION. B: METAPSAMMITE SAMPLE G10 WITH MICROFRACTURES PERPENDICULAR TO FOLIATION. BOTH PICTURES ARE TAKEN WITH A 5X MAGNIFICATION WITH PLANE-POLARIZED LIGHT IN A 1:200µM SCALE. RED ARROW INDICATED UP DIRECTION.

3.4 Laboratory tests

The goal of laboratory tests was to identify the mechanical properties of the sampled rocks. This section presents results from point load and uniaxial compressive strength tests. All tests have been completed in NGI's lab in Oslo. The time dispositioned at the lab was two weeks in total; 263 tests with PLT and 20 tests with UCS.

3.4.1 The Point Load test PLT

The samples used for point load tests were irregularly shaped rock samples from both outside and inside the URS of Dusnjarga and Gámanjunni 3 (figure 55 A and B). In total, 43 samples were tested, divided into 263 experiments. 23 of the experiments were considered invalid due to improper fracture paths.

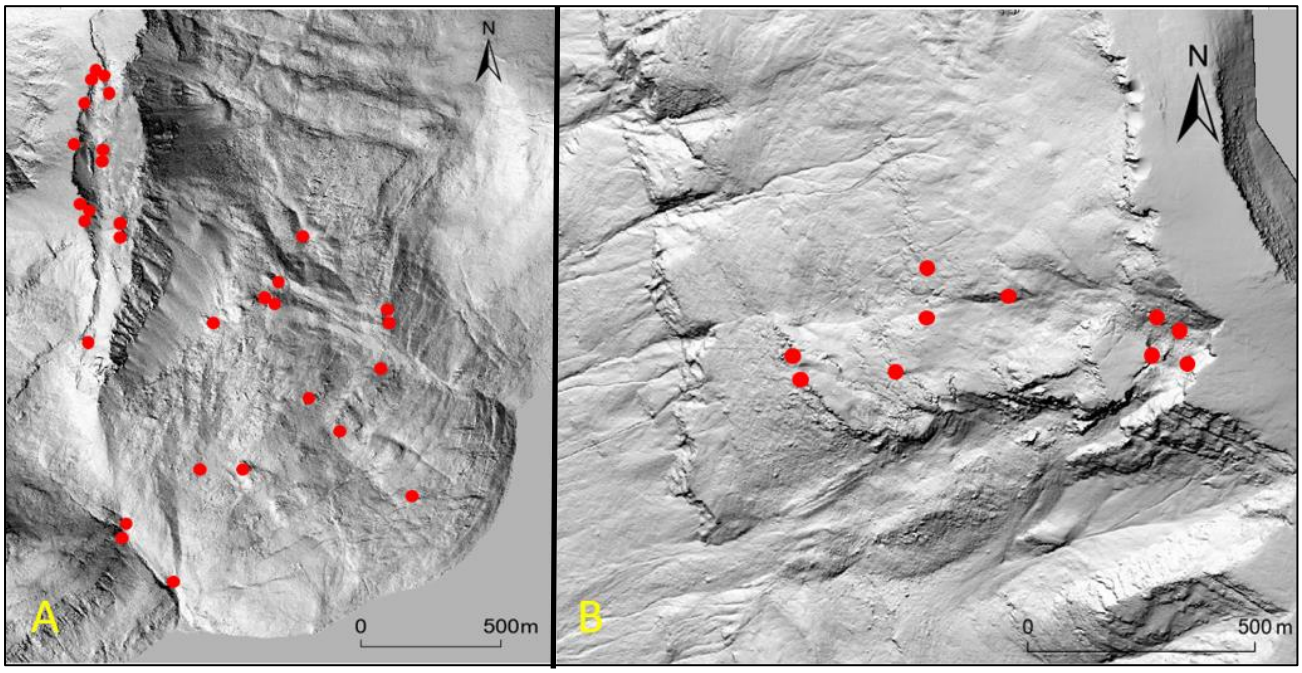

FIGURE 55: LOCATION OF PLT SAMPLES AT EACH URS A: DUSNJARGA WITH RED MARKS FOR SAMPLE LOCATION. B: GÁMANJUNNI 3 WITH RED MARKS FOR SAMPLE LOCATION. THE BASELAYER OF BOTH MAPS IS A HIGH-RESOLUTION 0.5 M DEM, DEVELOPED IN ARCGIS PRO.

The invalid tests mainly consisted of biotite and muscovite schist from Gámanjunni 3. The invalid testing is caused by the anisotropic properties of the schist, resulting in a very weak rock with diametral loading parallel to foliation (figure 56 A). The mica schist presents a high resistance with loading normal to the foliation, but fractures tend to favor foliation in most load directions. In the samples from Dusnjarga, the failed PLT tests were mostly mylonite samples.

Many of the experiments, especially from Dusnjarga, fractured at preexisting joints, and the true strength of the rock was not considered accomplished (figure 56 B). This was determined by identifying fracture systems and rust-formation in fractures. These tests were considered valid; however, they represent the rock strength found at the two URSs. The higher values in the box diagrams are considered the rock strength unaffected by internal fracturing (figure 57).

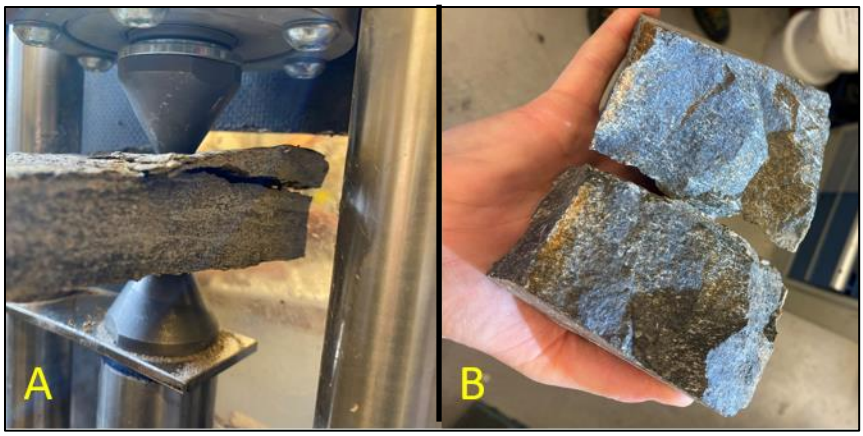

FIGURE 56: A – AN INVALID FRACTURE IN A MUSCOVITE SCHIST SAMPLE FROM GÁMANJUNNI 3. B – PREEXISTING JOINTS IN A METAGABBRO SAMPLE FROM DUSNJARGA.

The test results are systematized in a box diagram divided into rock types and test directions (figure 57). Dusnjarga has a more extensive data set than Gámanjunni 3, but both indicate that load normal to foliation is more resistant to failure than load parallel to foliation. The data set from Dusnjarga displays the largest degree in strength variation, but this is also the largest data set. Also, the average strength of the Dusnjarga samples is higher than Gámanjunni 3-samples. However, the difference in strength parallel and normal to foliation is higher at Gámanjunni 3 (i.e high degree of anisotropy).

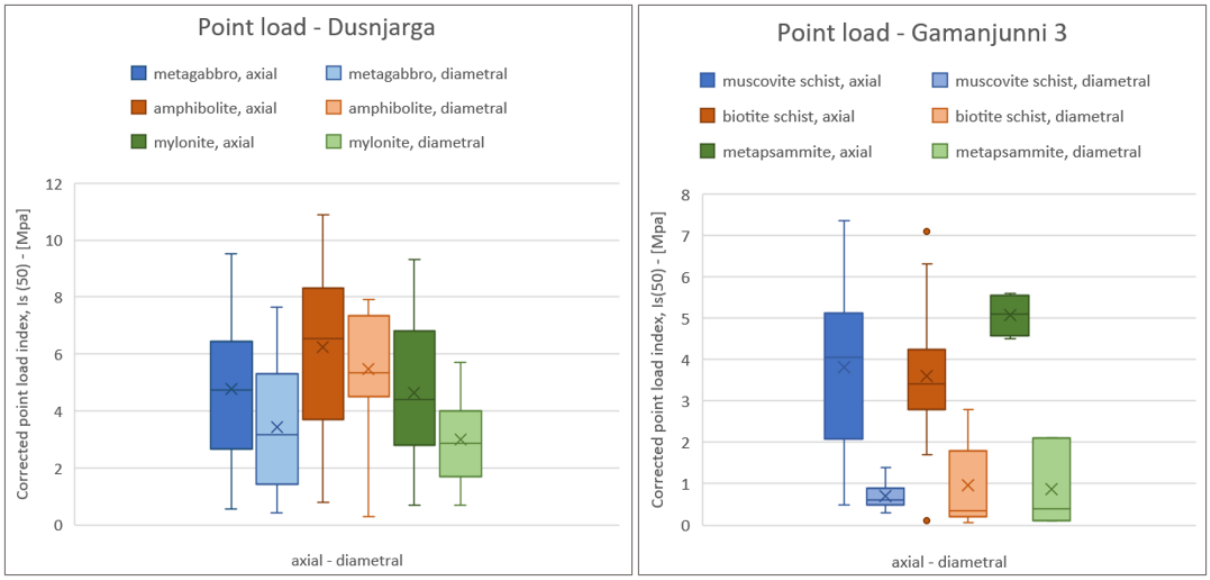

FIGURE 57: BOX-DIAGRAMS OF PLT DONE FROM SAMPLES AT DUSNJARGA (LEFT) AND GÁMANJUNNI 3 (RIGHT). DARK COLORS REPRESENTS TESTS IN AXIAL DIRECTION AND LIGHT COLORS IN DIAMETRAL DIRECTION.

3.4.2 The Uniaxial Compressive Strength test UCS

The preparation for UCS testing presented some problems due to a high frequency of pre-existing fracturing within the samples, from either slope deformation or pre-existing geological structures. The high frequency of internal fracturing made sample preparation time-consuming, whereas many samples failed during drilling. This resulted in a poorer lithological and locational sample range from the two URSs.

For simplicity, the term s-plug is used for cores with the y-axis normal to foliation, and p-plug is used for cores with the y-axis parallel to foliation. S-plug became the easiest direction to prepare for the samples at Dusnjarga and p-plugs easiest for Gámanjunni 3 (figure 58).

FIGURE 58: PICTURE TAKEN OF ROCK SAMPLES WHERE FAILURE OCCURRED DURING SAMPLE PREPARATION. PICTURE TAKEN AT NGI'S ROCK LAB 18/09.2021.

The test results from UCS show a variation in both Youngs' modulus (E_{50}) and Poisson ratio (μ_{50}). They are described in table 8, and 10. Youngs' modulus describes the materials stiffness, meaning a material's ability to resist deformation and degree of elasticity. Poisson's ratio describes a materials' degree of deformation. Poisson's ratios has some numbers marked in red because the values are non-theoretical and evaluated as invalid.

The UCS cores are also graded based on the fracturing grade system in table 6. Fractures parallel to load direction are longitudinal and lateral directions perpendicular to load direction.

3.4.2.1 Dusnjarga

In table 8 from Dusnjarga, the amphibolite displays a higher Young modulus, indicating a more resistant material to deformation. The Poisson ratio has only one valid value, indicating that the amphibolite does not deform much during loading. These numbers suggest that amphibolite is a resistant and strong bedrock when loaded perpendicular to foliation. Before failure, the maximum load varies greatly between amphibolite samples RM15_1 & _3 and RM15_2.

Observations from a varying metagabbro texture during field investigations corresponds with observations in microscope. The UCS confirms this with a wide range of values for Young's modulus and Poisson ratio. The metagabbro's elasticity varies somewhat, but amphibolite is overall more elastic and resistant to deform. The material's ability to deform is presented as poor in s-plug and better in p-plug, if one assumes that the one valid p-plug test is representative.

Metagabbro sample RM12_24 is missing data due to complications during logging.

TABLE 8: RESULTS OF UCS TESTS WITH SAMPLES FROM DUSNJARGA. TABLE SHOWS DATA OF BULK DENSITY, AREA, MAXIMAL LOAD, SAMPLE LOCATION, YOUNGS MODULUS (E_{50}), POISSON RATIO (μ_{50}) AND DIRECTION OF FOLIATION IN CORE (P/S-PLUG).

Test ID:	Rock type:	Bulk density: (g/cm^3)	Area: (cm^2)	$\sigma_v$max: (MPa)	Height: (m asl)	E_{50}: (GPa)	μ_{50}:	P/S-plug:
RM15.1	Amphibolite	3.08	4.84	227.68	783	63.75	-0.11	s
RM15.2	Amphibolite	3.07	4.88	138.75	783	65.29	0.03	s
RM15.3	Amphibolite	3.09	4.85	255.92	783	67.68	-0.09	s
RM13.21	Metagabbro	3.13	4.95	173.68	245	50.33	-0.02	s
RM13.22	Metagabbro	3.13	4.94	164.67	245	42.09	0.01	s
RM12.21	Metagabbro	3.11	4.84	129.95	229	38.41	0	s
RM12.22	Metagabbro	3.09	4.86	116.29	229	39.07	0.07	s
RM12.23	Metagabbro	3.14	4.86	110.87	229	58.85	0.14	p
RM12.24	Metagabbro	3.13	4.86	87.43	229	-	-	p
RM11.1	Metagabbro	2.99	4.88	134.71	43	39.51	0.33	p

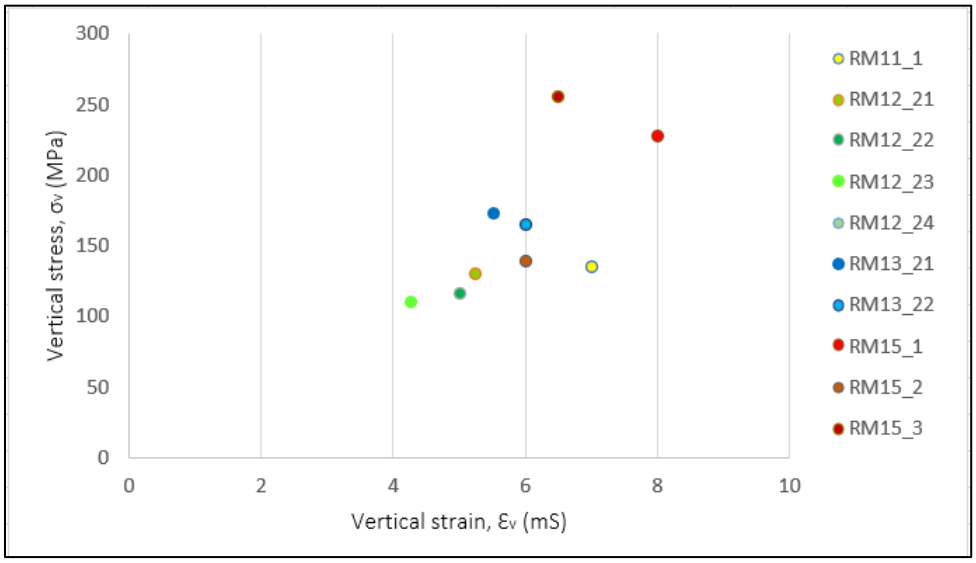

FIGURE 59: STRESS-STRAIN DIAGRAM OF ALL UCS TESTS RESULTS FROM THE DUSNJARGA SAMPLES. THE MODEL MARKS DIFFERENT SAMPLING STRENGTH.

The fracturing grade from the residual UCS cores are graded in the interval 1-3. Most of the cores are graded 1, due to clean fractures resulting in less fragments after testing (table 9).

TABLE 9: POST UCS CORES WITH A GIVEN FRACTURE GRADE. TABLE INCLUDES A REVIEW OF THE CORE FRACTURING, DIRECTION TO FOLIATION AND DESCRIPTIVE COMMENTS.

Test ID:	Fracture grade:	P/S-plug:	Comment:
RM15.1 Amphibolite	2	s	2 continuous fractures, several smaller. The continuous fractures are longitudinal. One small lateral fracture. Sample in 7 parts. Tested 25° to foliation.
RM15.2 Amphibolite	1	s	1 continuous fracture, several smaller. The largest fracture is longitudinal, and some smaller are lateral. Sample in 4 parts. Tested 25° to foliation.
RM15.3 Amphibolite	1-2	s	1-2 continuous fractures, several smaller. Fractures do not follow any joint systems but are mostly longitudinal to load direction. Sample in 6 parts. Tested 20° to foliation.
RM13.21 Metagabbro	3	s	2 partly continuous longitudinal fractures. Several smaller joints are both longitudinal and lateral fractures. Sample in 8 parts + several parts in grain size.
RM13.22 Metagabbro	1	s	2 continuous fractures. No fractures follow joint systems. Sample in 4 parts.
RM12.21 Metagabbro	1	s	1 continuous fracture. Fracture is zig-zag with longitudinal fractures and previous lateral fractures. Sample in 2 parts.
RM12.22 Metagabbro	1	s	1 longitudinal fracture that is being cut off by a previous, rusty, lateral joint. The sample is in 3 parts.
RM12.23 Metagabbro	1-2	p	1 continuous longitudinal fracture. 2 other fractures following previous, rusty joints. Sample in 4 parts.
RM12.24 Metagabbro	3	p	3 continuous longitudinal fractures that are partly pre-existing with rusty color. Several smaller lateral and longitudinal. The sample is in ~10 parts.
RM11.1 Metagabbro	3	p	2 continuous fractures, 1 rusty longitudinal fracture, and the other are fractured in several parts. Sample in 8 parts.

Metagabbro RM12.24 and RM12.23 represents some of the samples with lowest internal strength. Both samples have a well-foliated fabric and fractures developing parallel to the foliation (figure 60 A and B). The metagabbro sample RM12.23 fractured along a rusty zone in the core, possibly a pre-existing fracture. The amphibolite represents the strongest rock mass tested with UCS. The amphibolite sample RM15.3 is the absolute strongest core measured, but split into several pieces (i.e. plastic at picture in figure 60 C). The amphibolite sample RM15.2 is the second strongest and represents an s-plug with a fracture near to normal to foliation (figure 60 D).

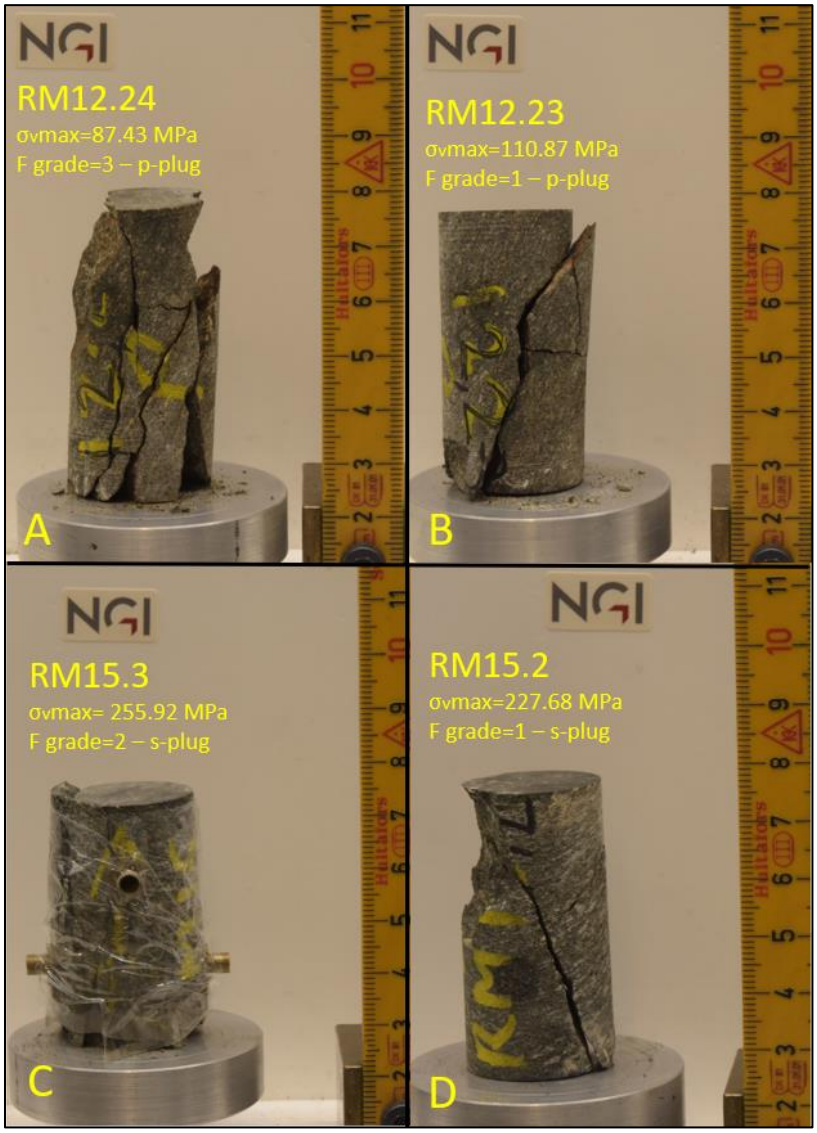

FIGURE 60: DUSNJARGA POST-CORES AFTER UCS TESTING AT NGI'S ROCK LAB. A: METAGABBRO SAMPLE RM12.2 AND MARKS THE WEAKEST CORE AT DUSNJARGA. B: METAGABBRO SAMPLE RM12.23 AND MARKS ONE OF FEW TESTED SAMPLES IN P-DIRECTION. FRACTURED ALONG PRE-EXISTING FOLIATION PARALLEL PLANE. C: AMPHIBOLITE SAMPLE RM15.3 AND REPRESENTS THE STRONGEST SAMPLE, LOCATED AT THE URS BACKSCARP. D: AMPHIBOLITE SAMPLE RM15.2 WITH A STRAIGHT FRACTURE PERPENDICULAR TO FOLIATION.

3.4.2.2 Gámanjunni 3

The three rock types tested for UCS are muscovite schist, biotite schist, and metapsammite, and divided into 10 sample cores. Muscovite- and biotite schist have approximately equal strength properties, but table 9 suggests that muscovite can sustain more load before failure occurs in p-plug. In the sample G19, the biotite schist presents the load differentiation between s- and p-plug. Given the test results, metapsammite is presumed to have the same internal strength as muscovite- and biotite schist.

The overall ability to deform under loading in p-plug is good in the mica schist and metapsammite, indicating that it deforms easily. Poisson ratio in both muscovite- and biotite schist samples are high. The elasticity is not very high in the schist but indicates that the muscovite schist is more resistant to deformation than the biotite schist.

Sample G13, the muscovite schist appears to be the rock mass able to withstand highest vertical stress. The muscovite schist G7 and metapsammite G10 are roughly equal on strength of rock mass (table 10).

TABLE 10: RESULTS OF UCS TESTS WITH SAMPLES FROM GÁMANJUNNI 3. TABLE SHOWS DATA OF BULK DENSITY, AREA, MAXIMAL LOAD, SAMPLE LOCATION, YOUNGS MODULUS (E_{50}), POISSON'S RATIO (μ_{50}) AND DIRECTION OF FOLIATION IN CORE (P/S-PLUG).

Test ID:	Rock type:	Bulk density: (g/cm^3)	Area: (cm^2)	$\sigma_v$max: (MPa)	Height: (m asl)	E_{50}: (GPa)	μ_{50}:	p/s-plug:
G7.1	Muscovite schist	2.67	4.88	72.01	1165	40.14	0.34	p
G7.2	Muscovite schist	2.66	4.92	77.96	1165	38.03	0.16	p
G7.3	Muscovite schist	2.63	4.92	81.35	1165	37.35	0.42	p
G10.1	Metapsammite	2.68	4.83	75.44	1074	34.11	0.12	p
G10.2	Metapsammite	2.68	4.83	78.54	1074	33.48	0.26	P
G13.1	Muscovite schist	2.66	4.80	128.23	891	41.99	0.07	s
G13.2	Muscovite schist	2.66	4.80	167.90	891	52.47	-0.00	p
G19.1	Biotite schist	2.73	4.97	106.53	678	19.29	0.18	s
G19.2	Biotite schist	2.73	4.94	46.39	678	17.54	0.45	p
G19.3	Biotite schist	2.75	4.94	36.68	678	18.92	0.26	p

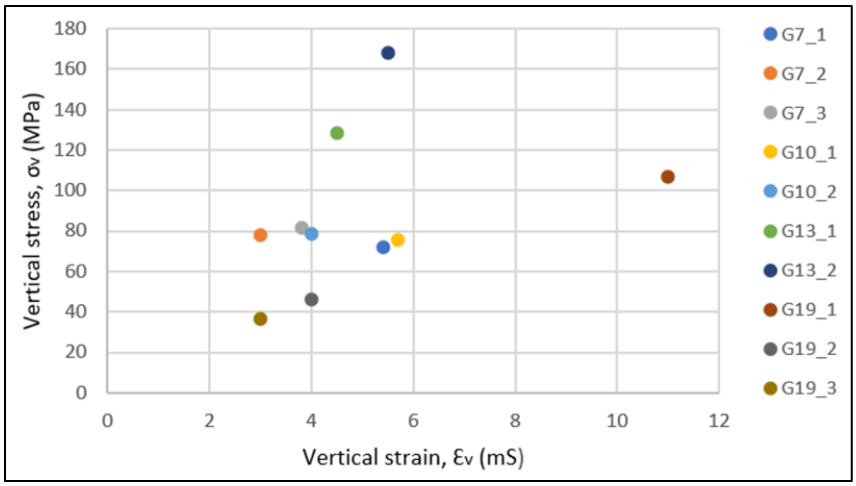

FIGURE 61: STRESS-STRAIN DIAGRAM OF ALL UCS TESTS RESULTS FROM THE GÁMANJUNNI 3 SAMPLES. THE MODEL MARKS DIFFERENT SAMPLES IN COLOR-CODES, WITH EACH CORE REPRESENTING A MARK.

The fracturing grade of the tested UCS rock mass from Gámanjunni 3 varies from 2 to 4. Meaning that most of the residual UCS cores fractured in several pieces, most in 10 or more pieces (table 11).

TABLE 11: POST UCS CORES WITH A GIVEN FRACTURE GRADE. TABLE INCLUDES A REVIEW OF THE CORE FRACTURING, DIRECTION TO FOLIATION AND DESCRIPTIVE COMMENTS.

Test ID:	Fracture grade:	P/S-plug:	Comment:
G7.1 Muscovite schist	3	p	1 continuous fracture 70° angle and several smaller foliation parallel fractures. Sample in ~10 parts.
G7.2 Muscovite schist	4	p	4 continuous fractures parallel to foliation. The sample is in ~10 parts.
G7.3 Muscovite schist	4	p	2 continuous and several smaller fractures parallel to foliation. Sample in ~10 parts.
G10.1 Metapsammite	2	p	1 continuous fracture partly parallel to foliation.2 fractures 70° angle to foliation.
G10.2 Metapsammite	3-4	p	3 continuous fractures parallel with foliation. Several smaller foliation parallel fractures. The sample is in 7 parts.
G13.1 Muscovite schist	3	s	No continuous fractures and following any joint systems. Sample in 7 parts.
G13.2 Muscovite schist	4	p	2 continuous fractures and several smaller fractures. All fractures follow foliation. The sample is in ~10 parts.
G19.1	2	s	No continuous fractures. 3 fractures parallel to

Biotite schist			foliation and 1 perpendicular. Sample in 4 parts.
G19.2 Biotite schist	2	p	No continuous fractures. 1 fracture is cutting foliation with 50 angles and 1 foliation parallel fracture. Sample in 4 parts.
G19.3 Biotite schist	3	p	3 continuous fractures partly following foliation. 1 fracture with an angle on 70°. Sample in 4 parts.

The biotite schist sample G19.3 represents the sample with lowest internal strength, and the muscovite schist sample G13.2 the strongest. Both samples are muscovite schist and p-plug (figure 62 A and B). The muscovite schist sample G13.1 is also a muscovite schist but tested in s-plug. The sample show a decreased internal strength when tested normal to foliation (figure 62 C). Sample G7.2 represents a highly fractured muscovite schist with fractures parallel to foliation (figure 62 D).

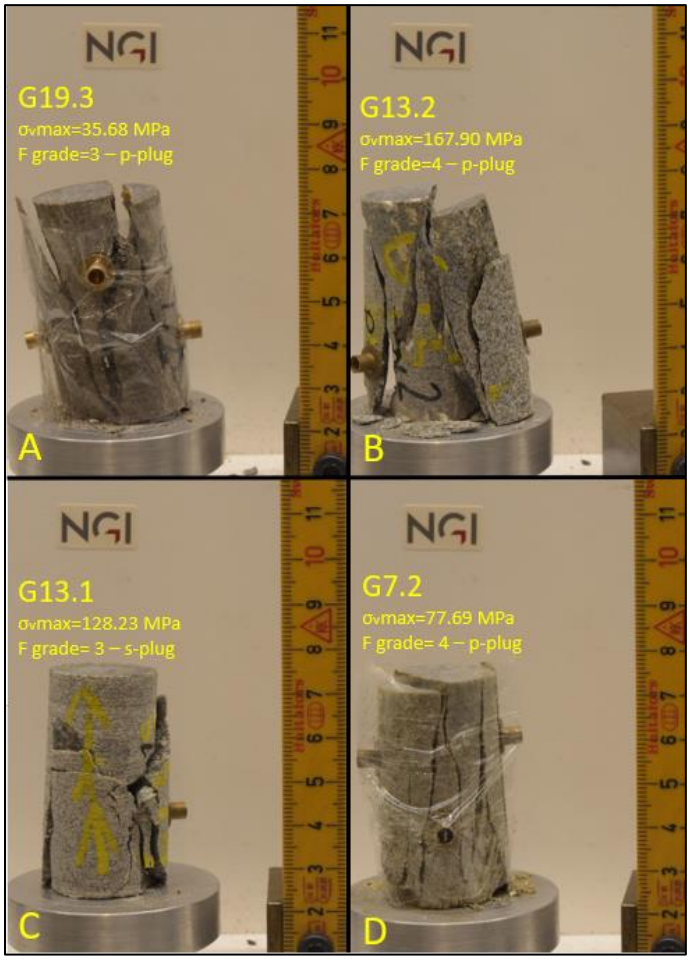

FIGURE 62: GÁMANJUNNI 3 POST-CORES AFTER UCS TESTING AT NGI'S ROCK LAB. A: BIOTITE SCHIST SAMPLE G19.3 REPRESENTING THE LOWEST UCS TESTED SAMPLE IN TERMS OF UNIAXIAL STRENGTH. B: MUSCOVITE SCHIST SAMPLE G13.2 MARKS THE STRONGEST TESTED SAMPLE. C: MUSCOVITE SCHIST SAMPLE G13.1 AND REPRESENTS ONE OF FEW SAMPLES TESTED NORMAL TO FOLIATION. D: MUSCOVITE SCHIST SAMPLE G7.2 IN SEVERAL PIECES.

3.5 Comparison of microfractures and joint sets

This section compares joint sets identified from structural analysis and micro-joint sets identified using microscopy. Large-scale joint sets and small-scale joint sets (microfractures) are plotted on rose diagrams for comparison with one another.

Figure 63 represents the observed small-scale joint sets in a rose diagram at Dusnjarga, combined with the three large-scale joint sets. In this figure there is a correlation between orientations of field-scale joint sets and microscale joint sets. JN F 183/20, foliation-parallel, and JN 1 317/52, backscarp-parallel, in particular, are recognized to be oriented closely to the small-scale joint sets. Some joint sets from thin sections are, however, randomly oriented. The cause of this could be challenges related to translating 2D joints from thin sections to 3D structures.

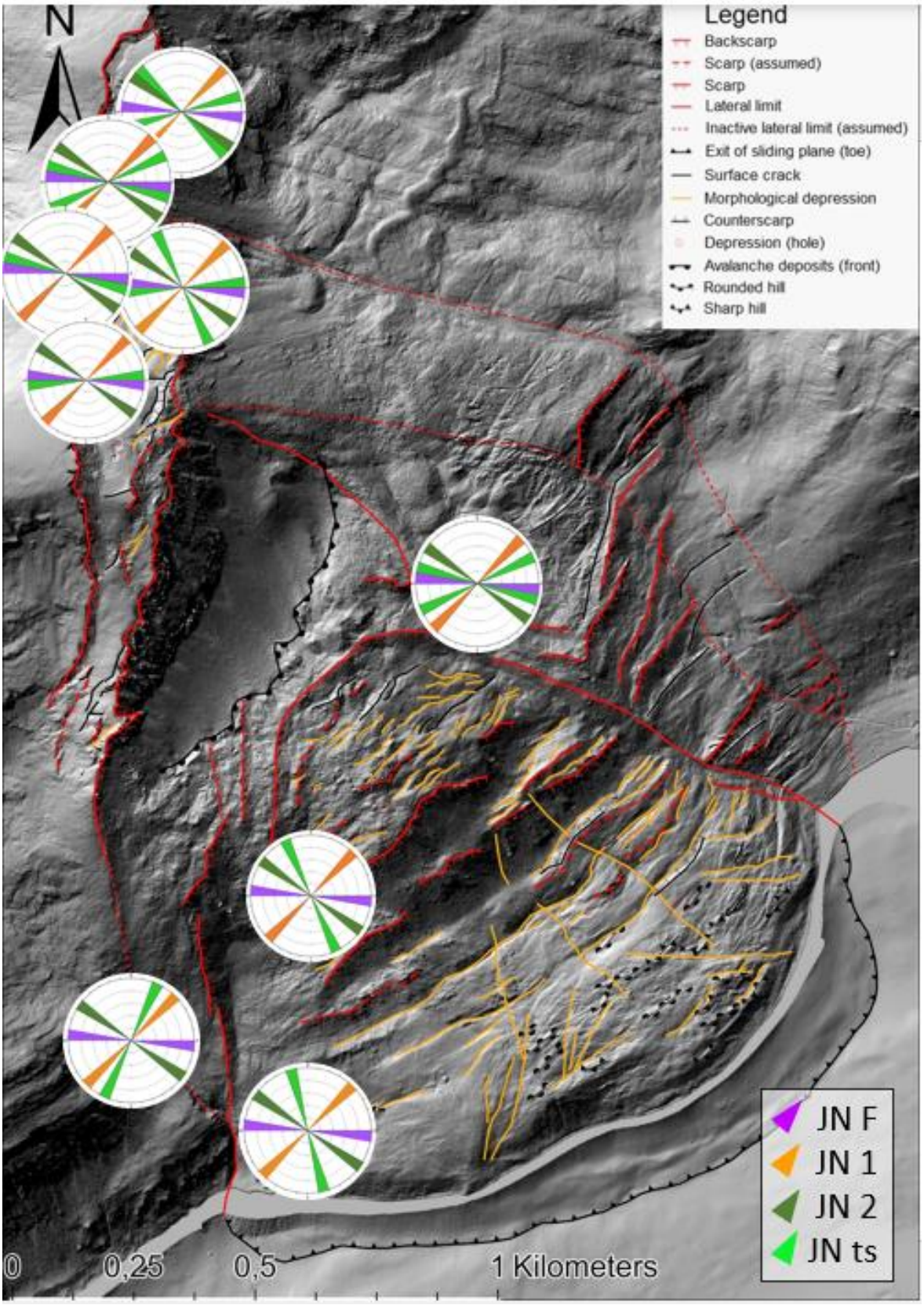

FIGURE 63: MORPHOLOGICAL MAP OVER DUSNJARGA URS, ADAPTED FROM SIMEN BEKKEVOLL (2022). ROSE DIAGRAM REPRESENTS DIFFERENT JOINT SETS. PURPLE, DARK GREEN AND ORANGE MARKS LARGE SCALE JOINT SETS OBSERVED FROM FIELD WORK/STRUCTURAL ANALYSIS. LIGHT GREEN MARKS JOINT SETS OBSERVED IN THIN SECTION THROUGH MICROSCOPY.

Figure 64 displays joint set recognized in thin section and compares it to consistent joint sets from structural measurements at Gámanjunni 3. JN F, the foliation parallel joint set 325/10, and JN 1, parallel to backscarp 188/87, are recognized in thin sections. JN 2, also backscarp parallel 125/84, is recognized in some samples.

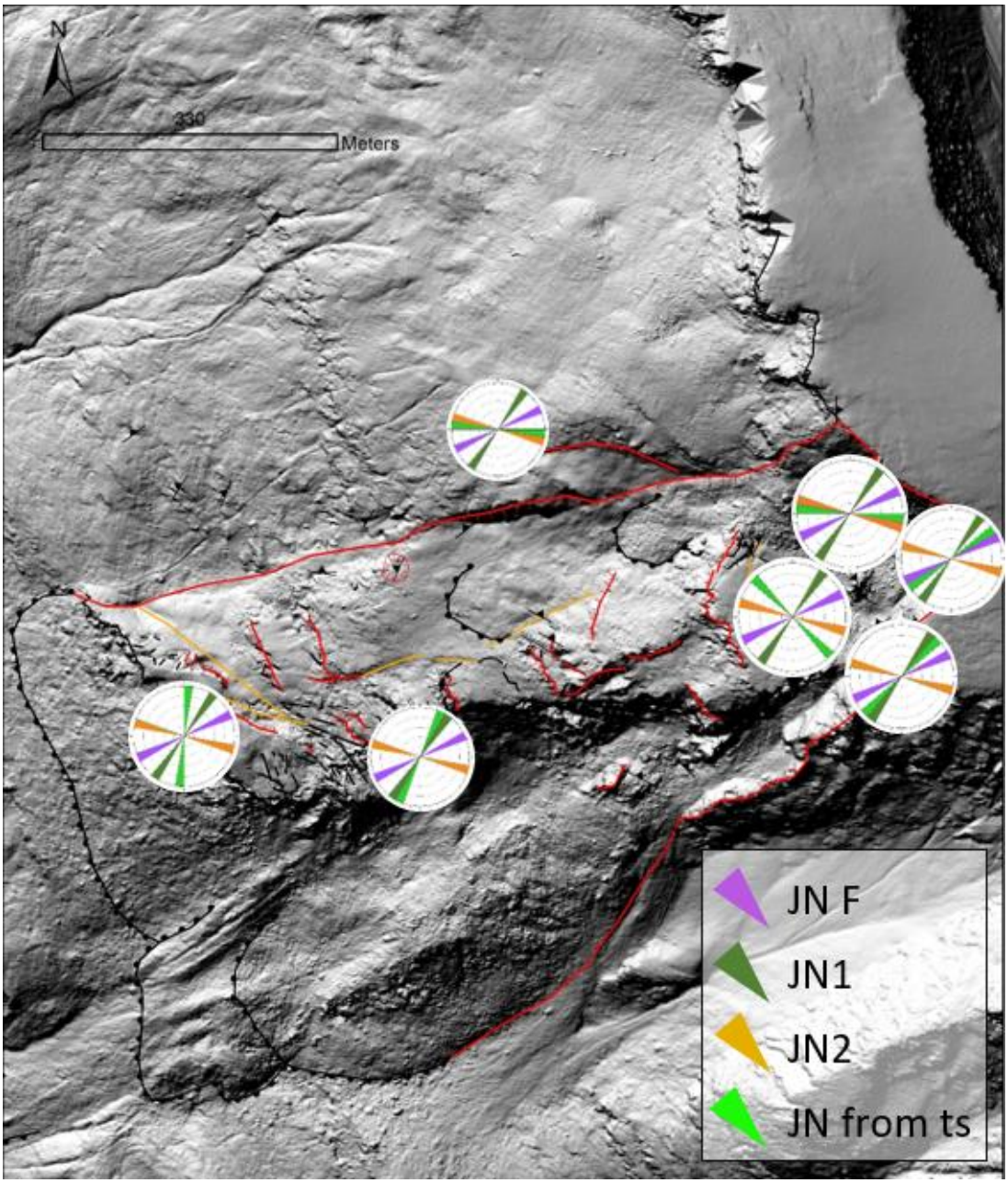

FIGURE 64: MORPHOLOGICAL MAP AT GÁMANJUNNI 3 URS ADAPTED FROM STEFFEN BERG. ROSE DIAGRAM REPRESENTS DIFFERENT JOINT SETS. PURPLE, DARK GREEN AND ORANGE MARKS LARGE SCALE JOINT SETS OBSERVED FROM FIELD WORK/STRUCTURAL ANALYSIS. LIGHT GREEN MARKS JOINT SETS OBSERVED IN THIN SECTION THROUGH MICROSCOPY.

4 Discussion

The two URSs, Dusnjarga and Gámanjunni 3, are both underlain by metamorphosed bedrock of the Caledonides. However, the two investigated sites are underlain by different lithologies and affected by different pre-existing structures, each with their own potential to affect how a rock slope may deform and fail. The bedrock at Dusnjarga consists of magmatic rock from the Kalak Nappe Complex, which has been metamorphosed to various degrees. The URS consists of nearly undeformed gabbro to highly metamorphosed and deformed amphibolite and mylonites. Gámanjunni 3, on the other hand, consists of metasedimentary rocks from the Kåfjord Nappe. Highly schistose mica-schist dominates the URS, with layers of amphibolite and metapsammite. Both localities have a significant variation in the mineral assemblage throughout the URS, visible in field and microscopy.

Both localities are heavily affected by the varied geology and the presence of dominating discontinuities. The main research question, therefore, poses to what degree geology and discontinuities impacts the deformation processes in an unstable rock slope. To simplify the magnitude of this question, the discussion will be divided into sub-discussions each addressing different aspects of the main research question.

4.1 Small scale structures affect large scale structures

It is theorized that discontinuities (e.g., faults, joints, foliation planes) can be a controlling factor in soil and rock slope failure. Pre-existing influential structures are required for the development of instabilities and have been proven to contribute a significant role in the formation of instabilities (Einstein et al., 1983; Saintot et al., 2011; Yanuardian et al., 2020). The outcrop-scale discontinuities will be separated from internal smaller-scale rock- and brittle structures and discussed separately for each locality.

Most rock failures in steep slopes have brittle behavior (Paronuzzi et al., 2015). Structural features that are oriented favorably to the rock slope weaken the slope stability dramatically (Saintot et al., 2011).

4.1.1 Internal rock structures

The rock-forming structures identified in this study are foliation, folds, lenses, and ductile shear zones. These can be identified as discontinuities that promote directional weaknesses in the rocks. They are therefore important to map and understand in relation to URS. These internal structures also reveal important information about the rock's geological history. The influence of the pre-existing ductile folds and fabrics can likely be a significant controlling factor in URS geometry and development and is therefore discussed below.

4.1.1.1 Foliation

Foliation is considered to be a discontinuity and is an important factor in slope stability (Panazzolo & da Silva, 2017). The foliation at both sites was developed by ductile deformation of the rock during tectonic deformation and is considered a pre-existing geologic structure. Foliations are usually defined by aligned minerals or elements in a rock. Hence, foliation have an anisotropic effect on the bedrock strength and combined with certain valley orientations, they can cause mass instability (Vick et al., 2020). The degree and style of anisotropy is therefore important to identify and describe when investigating instabilities.

4.1.1.1.1 Dusnjarga

The foliation at Dusnjarga is defined by plagioclase, meaning that the plagioclase is oriented with the longest axis parallel to foliation. Plagioclase appears to be the mineral best ordered, giving the fabric a pronounced foliation, especially in the more deformed regions (i.e. stronger foliation). The crystal size of plagioclase gradually decreases as a result of increased ductile deformation with elevation.

Microscopy supports the observation that plagioclase defines foliation. This appears to be the case in all rock types at Dusnjarga, with variable foliation development in different samples. Compositional layers, or small-scale magmatic layering, are parallel to foliation and are found in the metagabbro and amphibolite. The overprinting of pyroxene by amphibole appears to also be foliation forming, whereby amphibole crystals form parallel to the foliation, which supports the field observation of increased strength in foliation with elevation. The increased content of amphibole also increases the frequency of intergranular microcracking along foliation.

From field observations, the mylonite appears to be strongly foliated on the macroscale, but in the thin section, it has a more random fabric. Favorable orientation of individual grains can be identified, but it is very weak and parallel to the rest of the foliation in the area.

Overall, foliation provides consistent weakness planes and microfractures favor the same mineral plagioclase. The increased degree of metamorphism with elevation presents a fabric more prone to layering of plagioclase higher up at the URS, suggesting increased weakness at the microscale higher up in the URS. The presence of consistent weakness planes (i.e. discontinuity) combined with a favorable orientation of dip direction can in theory work as a basal rupture surface (Vick et al., 2020). In this case the foliation is considered to dip too shallow for it to be a factor to initiate the instability. However, a dip of 20° is still a substantial slope inclination and suggested to affect the slope geometry, and more precisely a plane of failure controlled by foliation.

4.1.1.1.2 Gámanjunni 3

The lepidoblastic fabric at Gámanjunni 3 is found in the mica schist and the metapsammite, and the amphibolite has an amphibole-defining foliation. As a result of the different foliation formed minerals, the foliation will also behave accordingly with respect to development of weaknesses.

The mica schist and metapsammite have a well-developed foliation with planar foliation planes dipping shallowly down the slope. The foliation is clear and easily identified on a micro- and macro scale. However, the possibility of a second foliation is presented from the observed s-c' fabric. In microscopy the development of the s-c' fabric is observed to only be partial, resulting in small-scale folds with a less planar main foliation and no development of a second foliation. This fabric is suggested to work in a stabilizing manner for the URS, as small-scale folding in the foliation can improve shear strength and have a preventative effect for sliding. This is supported by microscopy observations, presenting an overall lessened grain preferred orientation, thereby less grains parallel to the actual foliation. In this case the degree of anisotropy would likely decrease.

Observations from microscopy suggest that the mica rich sections behave in a more plastic manner, and fractures behave brittlely. The plastic behavior is interpreted from the absence of microfractures in mica rich thin sections. Increased content of quartz in the mineral assemblage is therefore observed to be advantageous for fracture propagation along foliation. These observations suggests that the sections at Gámanjunni 3 with strongest foliation are also the sections with a lower frequency of microfractures along foliation. The rock mass implies the need for stiffer properties, i.e. a quartz rich assemblage, for large-scale fractures to propagate and initiate a joint separation of the block in motion.

The amphibolite, on the other hand, behaves completely differently due to its amphibole-defined foliation. The orientation of the amphibole grains is strongly developed along foliation, suggesting the direction of foliation to be the direction most prone for failure. To the contrary, only intragranular microcracks favoring amphibole cleavage are observed, suggesting the amphibolite foliation to have a stabilizing effect on the URS in comparison to the mica schist foliation.

4.1.1.2 Ductile structures and shear zones

A ductile shear zone is characterized by the deformation of rock and the presence of dynamic recrystallization of the affected rock, generally resulting in mylonite (Marulanda et al., 2013). In the shear zone, the mylonitic fabric is characteristic and can be recognized at all scales. In this section, the ductile shear zones from Dusnjarga and Gámanjunni will be discussed, together with some other ductile structures.

4.1.1.2.1 Dusnjarga

Ductile shear zones are present at all scales at Dusnjarga, from the 50 m-thick mylonite zone at the top of the URS to thin shear zones only seen in microscopy. The shear zones are approximately parallel to foliation and found at all heights. Due to the orientation of the shear zones and foliation, they are likely of Caledonian age, however, it cannot be ruled out that they are older.

Microfractures consequently favor small-scale ductile shear zones in the investigated metagabbro (e.g. fig. 65). The fractures appear to easily move through the shear zones and often with dilation. This indicates that the displacement vectors are sub-simple translational shear components. Shear zones have been known to have a positive association to URS and display a zone of markedly lower strength than the surrounding host rock (Braathen et al., 2004; Brideau et al, 2005; Neuhäuser et al.2012, Andresen, 2018; Vick et al., 2020; Vick et al., 2020b). With this in mind, ductile shear zones are suggested to act as planes of weakness, facilitating failure, and controlling the geometry of the URS. In addition, the strategic location of the thick mylonite zone at the backscarp implies ductile shear zones may act as point of rupture initiation for the URS.

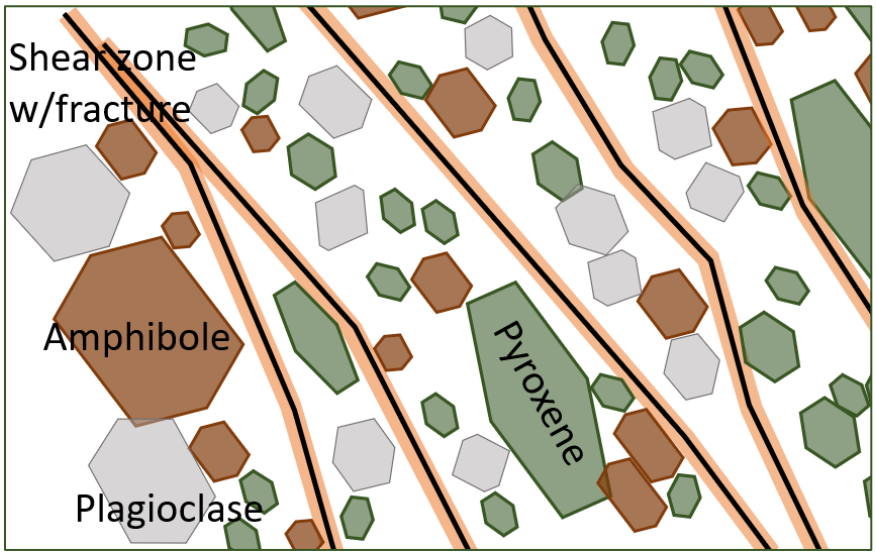

FIGURE 65: SKETCH OF A METAGABBRO WITH THE SCALE ROUGHLY AT 1.200µM. SKETCH ILLUSTRATES THE HIGH FREQUENCY OF DUCTILE SHEAR ZONES AT A MICROSCALE.

Other ductile structures at Dusnjarga are not as pronounced as the ductile shear zones, but lenses and folds are observed in the backscarp region. Observations from microscopy suggest that microcracks favor changes in texture (i.e. discontinuities). Since lenses and folds provide such textural changes, they may contribute to the facilitation of fracture propagation.

4.1.1.2.2 Gámanjunni 3

At Gámanjunni 3 there are no ductile shear zones observed from field work, but ductile features such as folds and lenses are found frequently in the back scarp region. However, a small-scale ductile

shear zone is identified from the NW-facing back scarp (e.g. sample G5), confirming the presence of ductile shear zones at Gámanjunni 3. The observed shear zone in microscopy is not completely parallel to foliation and acts as a boundary between muscovite- and biotite schist.

The proximity of the Cappis thrust to the URS may indicate that the toe of the URS is part of a large-scale shear system, or in fact, that the mechanical strength of the rock mass has been weakened due to proximity to the thrust. The URS is located 350 m higher than the nappe thrust boundary, so the destabilizing effect on the URS is unclear. Nevertheless, the Caledonian orogeny is known to be responsible for all the ductile features (Bredal, 2016). The presence of these discontinuities is very relevant to the initiation and development of the URS.

Ductile structures such as folds and lenses (i.e. discontinuities) are observed during field work but are not found at the microscopic scale. However, observations in the microscope show that fractures favor changes in texture, suggesting that fractures would also likely favor folds or lenses on the macroscale, as a change of grain size and texture commonly occurs in relation to these structures. The presence of these discontinuities is strategically located in the backscarp region, implying changes in texture on a macro scale has a point of rupture initiation effect on the URS.

4.1.1.3 Joint sets

Joint sets are another set of brittle discontinuities. Hence, it is important to identify them to understand the slip/failure processes in a URS. The physical properties and brittle behavior remain crucial in the formation of large instabilities.

4.1.1.3.1 Dusnjarga

There are three consistent joint sets at Dusnjarga, with JN F parallel to foliation, JN 1 parallel to the backscarp and JN 2 parallel to the lateral boundary. During field work the joint sets are easily recognized, but from structural analysis the structural data are scattered. The data may include rotated or dislocated parts of the URS and cannot be considered completely reliable. Studies show that large instabilities can be internally partitioned as a result of varying movement direction and deformation velocity (Dahle et al., 2008; Blikra et al., 2009). This could result in large discrepancies in the join set data. Large-scale folding can affect the data set in the way of changing the fabric properties and the orientation on fracture preferred structures.

Microcracks in plagioclase crystals are often parallel to the mineral cleavage planes, or even coincide with them, implying that these crystallographic preferred orientations act as planes of weakness, resulting in controlling the fracture path (Rigopoulos et al., 2012). Plagioclase is favored in all observed metagabbros, suggesting that the presence of plagioclase remains central in the formation of a foliation-parallel joint set.

The metagabbros fracture with a different style in comparison to the amphibolite. They display fracture zones consisting of linked and isolated microcracks, resulting in overall more chaotic and wider fracture zones. The degree of metamorphism and the resulting change in mechanical properties therefore appears to affect the amount of isolated and linked microfractures. Kranz's theory (1983) suggests that fractures under compressive loading is a result of fracture growth, coalescence and interacting of many microcracks, not the growth of a single crack. This mean that some of the pre-existing isolated intragranular and intergranular microcracks may propagate and then link together during the compressional loading, which would result in a reduction in the number of microcracks, but an increased fracture length (Rigopoulus et al., 2012). With this in mind, the difference in fracture style between amphibolite and metagabbro may simply indicate the difference in exposed stress as a result of different mechanical properties caused by variation in mineralogy from varying degrees of metamorphic overprint. In this way the pre-existing metamorphic history of the rocks dictates how fractures form and propagate from the microscale, and therefore has the potential to control the evolution of the URS.

The amphibolite is observed to have a narrow fracture zone, with transgranular grain boundaries and only small-scale microfractures observed normal to the foliation. The degree of metamorphism and ordered grain fabric in the amphibolite appear to be advantageous for fracture propagation. It differs from the gabbro and metagabbro being finer-grained, has more uniform mineralogy (i.e. mostly amphibole), and often a stronger foliation. The amphibole grains also display a well-developed mineral cleavage. The role of cleavage planes in the mechanical behavior of rocks can be explained by cleavage being the preferential plane with the lowest fracture resistance within the crystals (Watana & Tsurekawa, 1999; Rigopoulos et al., 2011; Lotfolahpour & Zaeem, 2021). With this in mind, increased proportions of amphibole, driven by a higher degree of metamorphic overprinting of the gabbros, appear to have an ordering effect on the mineral texture, resulting in an oriented cleavage path and a rock that is favorable for fracturing (however not parallel to the foliation).

The mylonite does not have any clear large-scale consistent joint set observed from field investigations. Challenges in PLT tests, sample preparation and preparation for thin sections, suggest a highly fractured mylonite mass, but with a random orientation of the fractures. Investigations in microscopy suggests a possible small-scale joint set with 45° angle to foliation, this is only the preferred orientation of selected microfractures. Despite the lack of data for the mylonites, field and lab observations clearly indicate that it is extremely weak with respect to brittle deformation and provides a significant weak zone in the URS.

As the degree of metamorphism in the metagabbro increases with elevation, so does the controlling small-scale joint geometry in the two recognized joint sets. The favored plagioclase (e.g. fig. 66 A)

and cleavage in amphibole (e.g. fig. 66 B) appear more frequent and the microfractures responds with a more consistent, transgranular fracture behavior. Even with the different mechanical properties that metagabbro and amphibolite display, the pre-existing discontinuities that a metamorphic fabric presents remains as the controlling factor in the formation of joint sets and is central in the URS geometry. This is most pronounced in the foliation, whereas the degree of foliation affects development of the joint set parallel to foliation.

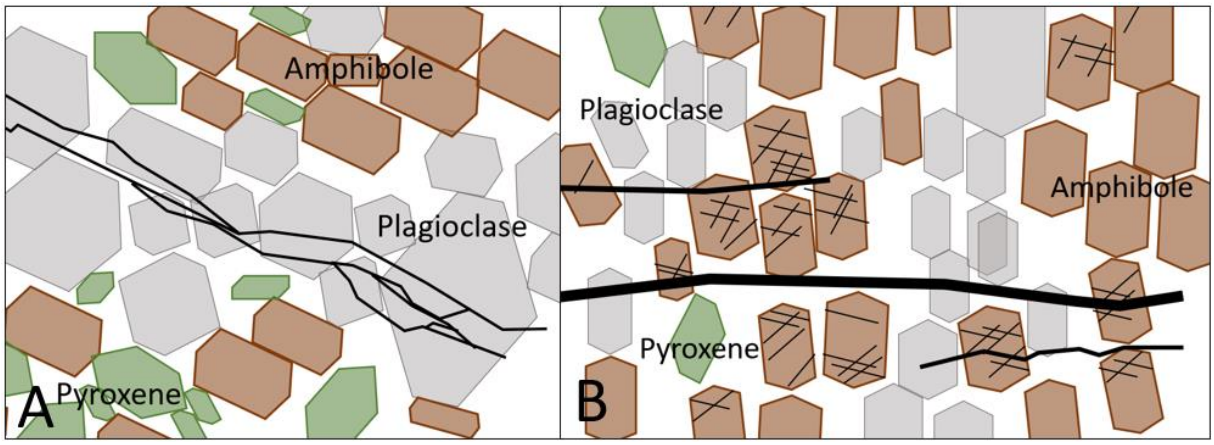

FIGURE 66 SKETCH OF THIN SECTION SAMPLES, SCALE IS ROUGHLY AT 1:200µM. A: ILLUSTRATES A METAGABBRO WITH MICROFRACTURES FAVORING LAYERED PLAGIOCLASE. B: ILLUSTRATES THE FABRIC IN A AMPHIBOLITE – INTRAGRANULAR MICROCRACKS IN AMPHIBOLE CLEAVAGE AND LARGER FRACTURES USING THE INTRAGRANULAR FRACTURES TO PROPAGATE.

4.1.1.3.2 Gámanjunni 3

The three large-scale joint sets observed from field investigations are: JN F parallel to foliation, and the two backscarp-parallel: JN 1 and JN 2. These joint sets are consistent and do not seem to vary much between the different lithologies. The amphibolite has an overall more massive texture, but the observed layer in the back scarp is oriented parallel to the same joint sets as the rest of the URS.

From field observations, the fracture frequency of JN F, parallel to foliation, is high and appears to be consistent throughout the investigated area. JN F is less frequent in the metapsammite and difficult to identify in the amphibolite. The lepidoblastic fabric in the mica schists remains central and is interpreted to be directly related to the frequency of JN F. With this in mind, the presence of mica minerals is also observed to prevent small-scale development of JN F in mica rich sections. Thin sections with a high content of mica minerals are completely without microcracks, even where the mica minerals are perfectly oriented to foliation. Fractures are observed to mostly form and propagate where the non-mica minerals touch. In more competent minerals, such as quartz or amphibole, the strength is high enough such that when a fracture propagates through, the stress radiates out and continues to fracture the grain in contact. The stress impingements a grain of higher strength and the stress decreases significantly when in contact with a weaker mica grain. This can be

identified as critical differential stress that reaches a fracture tip, and the potential energy needs to be equal or greater than the increase in surface energy if creating new surface planes – propagating continues (Griffith theory, Zehnder, 2013). A theory is that high bulk differential stress in a grain boundary causes the stress to dissolve, as would be the case in the mica schist with quartz-mica grain contact. This appears to be the case when the fracture and mica grain are oriented parallel, as the stress dissolves along the mica grain boundary. In other words, the released potential energy of a propagating fracture in mica minerals is less than the development of forming new surfaces. If the mica content is reduced and only a thin mica layer surrounded by quartz grains occurs, microfractures will develop further as the body per unit fracture area is greater than or equal to the reduction in potential energy, and often results in dilation. This suggests that the contact between the mica and the quartz is weaker than the mica mineral cleavage, and the mica mineral cleavage itself is, in fact, not be the weakest structure in the mica schist (e.g. fig 67 A).

When in case the fracture is oriented normal to the platy mica grain, the fracture moves more plastically through the grain, resulting in a zigzag fracture path and the fracture continues in the quartz. The fracture behavior appears to be brittle in the quartz grains and plastic in the mica grains (e.g. fig 67 B).

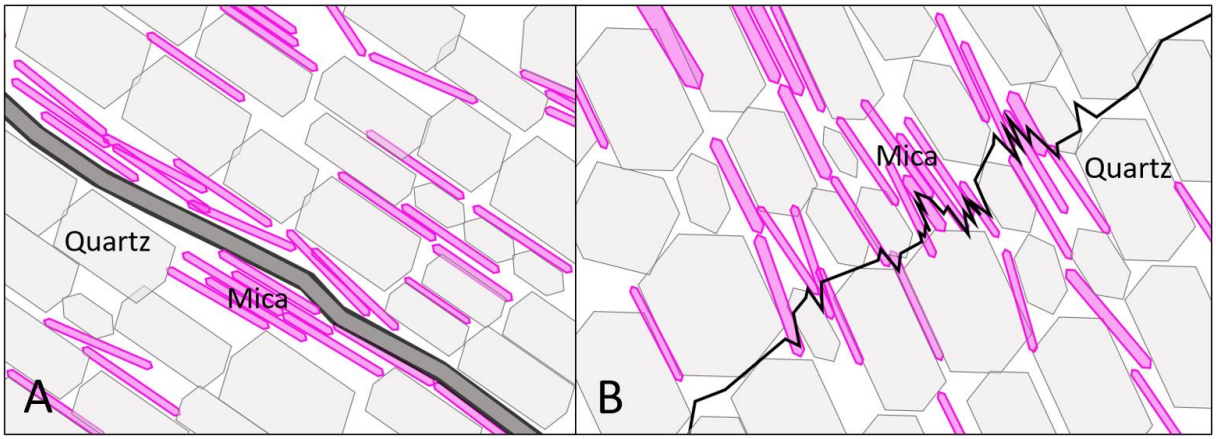

FIGURE 67: SKETCH OF MICA SCHIST IN MICRO SCALE OF 1:200µM. A: MICA SCHIST WITH DILATED FRACTURE FOLLOWING MICA GRAINS ORIENTED PARALLEL TO FOLIATION. B: ILLUSTRATED OF OBSERVATIONS BY A METAPSAMMITE FROM GÁMANJUNNI 3. SKETCH REPRESENTS MICROFRACTURES NORMAL TO FOLIATION WITH A DIFFERENT FRACTURE PATTERN THROUGH DIFFERENT MINERAL GRAINS. SKETCH IS PRESENTED WITH A CROSS-POLARIZED LIGHT, HENCE THE PINK MICA COLOR.

The amphibolite at Gámanjunni 3 appears to have a massive fabric at macroscale, but a well-developed amphibole foliation is visible at the microscale. The amphibole has many intergranular microcracks along the amphibole cleavage, with some development of microcracks, forming a joint set normal to foliation (e.g. fig. 68). This small-scale joint system appears to match the observed large-scale joint sets, see figure 64.

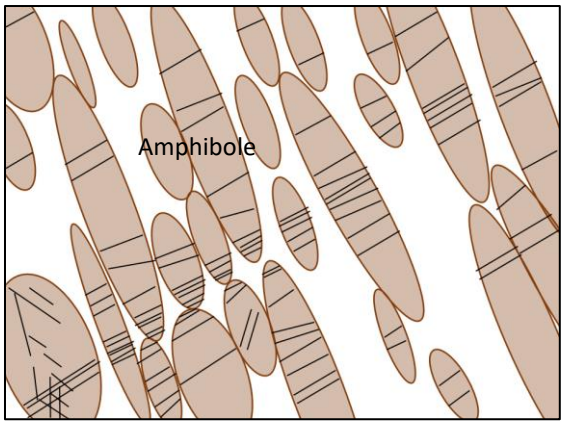

FIGURE 68: SKETCH DIAGRAM OF INTRAGRANULAR MICROCRACKS IN AMPHIBOLE CLEAVAGE FACILITATING A CONSISTENT JOINT SETS TO DEVELOP IN A MACROSCALE IN AN AMPHIBOLITE.

4.1.1.4. Brittle faults

Both Dusnjarga and Gámanjunni 3 have been exposed to brittle deformation at low temperature and confining pressure, resulting in brittle faulting in the rock mass. In this section the brittle fault formation from each locality will be discussed.

4.1.1.4.1 Dusnjarga

The observed brittle faults in the backscarp region are parallel to JN 1 and the lateral boundary of the URS. JN 1 may therefore be associated with the earlier brittle faulting. The observed brittle faults are linked together with possible brittle faults from morphological features seen from the DEM (e.g. fig. 35). In the western lateral boundary, a 5 m thick brittle fault is observed with slickenlines, this suggests that the eastern lateral boundary of the URS has utilized a pre-existing brittle fault. The slickenlines indicate a downwards movement towards the URS-block, making the initiation of the URS movement a possible reactivation of the brittle fault system.

No small-scale brittle faults were observed in microscopy in the metagabbro or amphibolite, however this does not preclude their existence. Fault gouge was not investigated at the microscale due to material being non-coherent and therefore presenting challenges with sampling and sample preparation. However, brittle faulting has been shown to control the geometry of URS at other sites all over the world (Ambrosi & Crista, 2006; Bois et al, 2008). It is found that the proneness of a given instability increases with its density to brittle structures, and faults with associated gauge have been known to reactivate other rockslides (El Bedoui et a., 2011; Saintot et al., 2011). A brittle fault gouge has lower shear strength than foliation and joint sets, suggesting the presence of brittle faults is likely to be favored by failure, and possibly control the geometry at Dusnjarga URS. Brittle faults can also affect the surrounding area by tectonic damage, and thereby a lower rock mass strength (Brideau et al., 2009; Stead & Wolter, 2005). At Dusnjarga JN 1 is oriented parallel to the extensive Langjord fault

(Roberts & Lippard, 2005), suggesting that tectonic damage can have affected the URS and lowered the strength of the entire area.

4.1.1.4.2 Gámanjunni 3

Schist is a highly anisotropic rock, and the strength of the rock is positively correlated with the ability of the weak plane to resist shear failure (Yin et al., 2019). Therefore, mica schist is considered a bedrock prone to URS shear deformation along foliation. In the toe section there is also a well-developed brittle fault system parallel to the foliation (e.g. fig. 42 B) and easily recognized with a loose gouge zone. It is unclear if the fault system is a result of pre-existing brittle faults that the URS utilizes as sliding zones, or the brittle fault system is a result of shear movement from the weight of the moving block. Either way, the presence of the brittle faults in the toe section makes the area more prone for further movement.

4.1.1.5. Combined evaluation of discontinuities

Dusnjarga and Gámanjunni 3 both display a high frequency of large-scale discontinuities in the backscarp region, which strongly indicates a causal link to point of rupture initiation of the instability. Furthermore, the anisotropic rock combined with numerous ductile shear zones at Dusnjarga, and a highly anisotropic mica schist at Gámanjunni 3, makes the bedrock prone to brittle deformation during URS evolution controlled by the anisotropies. In addition, both localities have consistent joint sets identified at all scales. The joint sets control the orientation of the back scarp in both cases and can also be recognized at microscopic scale. This indicates that small-scale discontinuities (i.e. foliation and mineral cleavage) are a significant controlling factor for the development of large-scale consistent joint sets, which again affects the geometry and initiation of an URS. In addition, the brittle fault system at each URS is suggested to work as an overall controlling factor for the URS geometry.

4.2. Factors that influence the rock strength

In this section the strength of each rock type will be discussed together with the location in and outside the URS. The process of measuring sample strength spread out in an URS presented some difficulties, whereas the weakest samples failed in preparation, and the strongest samples represent the results.

4.2.1. Strength of rocks at Dusnjarga

The strength of metagabbro, amphibolite and mylonite are highly variable and difficult to measure. Several thin sections of the metagabbro are similar to amphibolite (i.e. have a relatively high amphibole content), indicating that they are metamorphosed to various degrees, but only a small portion of the samples were defined as proper amphibolite.

The overall weakest metagabbros from Dusnjarga have amphibole as one of the dominating minerals (e.g. sample RM12.2). The overgrowing amphibole (i.e. replacing pyroxene) is part of the increased metamorphism at Dunsjarga, and UCS tests suggests that increased amphibole assemblage can have a weakening effect on rock strength, as intragranular microcracks in amphibole cleavage facilitate for large-scale fractures to develop. This suggests that amphibolite with a well-developed foliation is weakest normal to foliation, as amphibole cleavage is presented as weaker than, or equally weak as foliation.

At Dusnjarga, the presence of pyroxene is related to a less metamorphosed metagabbro. Increased content of pyroxene suggests a decrease in ordered texture, which results in less continuous weakness planes for microfractures to follow. In other words, when a metagabbro low on amphibole is tested with axial loading, the high strength values indicate a lack of weakness planes and no favorable structures for the microfracture to easily propagate along (e.g. metagabbro sample RM13.2).

However, the strongest overall sample tested is amphibolite. The tested amphibolite from Dusnjarga is tested with a 20-25° to foliation. In UCS testing amphibolite's are weakest when the foliation plane angle is 30° and strongest angle is perpendicular to foliation (Ali et al., 2014). This suggests that the amphibolite is tested at its weakest angle. The rock mass with such high strength properties will likely have less microfractures, but when the stress is high enough for fracture propagation to occur, it fractures straight and not affected by structures, as the mass is so strong and impenetrable (e.g. fig 50).

The high frequency of ductile shear zones is considered one of the main factors when reviewing the rock mass strength, and the density of these zones is observed to change rapidly. Mineral assemblage remains an important factor in terms of fracture propagation, as fractures favor plagioclase parallel to foliation and amphibole cleavage normal to foliation, but shear zones are favored above mineralogy. These conditions develop best in the more metamorphosed sections, which increase with elevation.

Conditions that facilitate a rock being strong with respect to URS deformation are therefore infrequent weakness planes with a disordered fabric, i.e. a low grade metamorphic rock.

4.2.2 Strength of rocks at Gámanjunni -3

At Gámanjunni 3 the mechanically tested rock types are metapsammite and muscovite- and biotite schist. Mica schist is the dominating bedrock, so most of the sampled and tested rock consists of muscovite- and biotite schist.

As a result of unfortunate weather during the field period, the samples from Gámanjunni 3 were sent to the mechanical lab in Oslo before prepared for thin sections. The samples first underwent PLT, which opens the possibility for none-representative fractures to develop during loading from the apparatus. With regards to the little fracture frequency Gámanjunni 3-samples presented in thin section, this is not suggested to affect the observations in a large degree.

The idea of stronger rock mass outside the URS could be supported by the values of the biotite schist sample G13, being the strongest sample and located outside of the lateral boundary (e.g. table 9). Sample G7, muscovite schist from the backscarp, has average medium-low strength values. Sample G19, biotite schist from the toe section, shows below average values and indicates a weak rock mass. Anyhow, with only four samples tested on 10 cores, the data set is not enough to conclude or reject any hypotheses related to the location within the URS at this point in the study.

The observation of no small-scale microfractures in mica rich rocks contradicts observations in field, indicating a high frequency of large-scale fractures in the mica rich schist. The high grade of anisotropy causes a weak shear strength in the schist, and as the foliation is mica forming, the mica minerals cause the rock to be weak along the foliation and the rock becomes weaker in mica-rich sections. Mica minerals are therefore suggested to have a weakening effect on the rock mass strength.

Muscovite and biotite schist have approximately equal properties in Poisson's ratio, but muscovite schist has a higher in Young's modulus. This indicates that muscovite schist appears stiffer and more resistant when exposed to loading, while the sampled biotite schist appears to be of a more elastic material. Muscovite schist has been observed from field investigations to have a better foliated fabric, than the biotite schist (Hansen, 2020). The UCS experiments consist of two sampled muscovite schists (samples G7 and G13) and one biotite schist (sample G19). Sample G19 presents a higher mica content with 45%, compared to 20% for sample G7 and 30% for sample G13. Muscovite and biotite are considered minerals with similar mechanical properties as they have the same crystal structure (Dietrich et al., 2021). Hence, it is possible that sample G19, biotite schist, is more elastic due to the high content of mica minerals. Some of the sampled mica schists and metapsammites have a high content of quartz, this can also indicate that quartz has a stiffening effect on a rock mass and makes the rock mass perform more brittle. This is supported by strength implications from PLT and microscopy.

The amphibolite from Gámanjunni 3 was not mechanically tested. The mineral assemblage from microscopy, and lack of mica minerals, implies a strong rock mass. Observations in thin section suggests mineral cleavage to be a plane of weakness in all observed microfractures. As earlier

described, the foliation is defined by oriented amphibole grains, implying that mineral cleavage can be a general plane of weakness in the amphibolite. Fig. 54 A shows a high frequency of transgranular microcracks in the amphibole cleavage, suggesting that the amphibolite at Gámanjunni 3 has a high frequency of microcracks that can easily link together, decreasing in number but increasing in length. Cleavage in amphibole grains is also suggested to facilitate fracture propagation better than foliation, similar to what was observed in the amphibolite's from Dusnjarga.

4.2.3 Combined strength evaluation

Dusnjarga and Gámanjunni 3 rocks are very different to each other and behave differently under compressional loading. The metagabbro at Dusnjarga is difficult to measure mechanically, as the degree of metamorphism and discontinuities changes constantly, and considered central in finding the rock mass strength. However, experiments do provide information on the strength of a "pre-weakened" rock mass based on the presence of pre-existing geological structures. At Dusnjarga this suggests that the processes that have affected the metagabbro, have weakened it more significantly than the processes that have affected the amphibolite. The pre-existing metamorphic overprint may in fact have strengthened the metagabbro so that pre-existing metamorphism in this case leads to a rock mass less favorable for failure. The mica schist from Gámanjunni 3 is difficult to measure, as the mica assemblage varies constantly and remain central in the rock's behavior and strength. Both localities have sections of other rock types (i.e. amphibolite and metapsammite) located in the back scarp region and with properties more resistant to deformation.

The meta-igneous rocks from Dusnjarga have properties that suggest better resistance to deformation and behave more elastic. The weaker, meta-sedimentary rocks from Gámanjunni 3 have a higher degree of deformation before failure occurs. This suggests that the rocks of the Dusnjarga URS behave as a stiffer material, with a sudden failure, but Gámanjunni 3 rocks on the other hand, deform more plastic before failing. Also, growth of amphibole crystals combined with a higher degree of metamorphism can have a strengthening effect on the metagabbro at Dusnjarga. The growth of micas, on the other hand, can weaken the mica schist as it facilitates for shear deformation. In this way the pre-existing metamorphic processes affect the rock strength and subsequent URS deformation.

In general, the metagabbro is suggested to behave in a stronger manner than the mica-schist, but the metagabbro at Dusnjarga is highly affected by ductile shear zones, which would directly weaken the rock mass. Mica schist is suggested to behave stronger where the quartz content is increased, but this would also increase the chance of microfractures propagating and weakening the rock.

4.3 The control of geology on failure and URS deformation processes

Dusnjarga and Gámanjunni 3 are metamorphosed bedrock of the Caledonides, but highly different lithologies show strong variation in pre-existing geological structures. The rock mass in a URS is exposed to brittle deformation as a result of gravitational forces. A recurring pattern of pre-existing discontinuities is easily developed in metamorphic bedrock and can facilitate for instabilities (Vick et al., 2020). Discontinuities can affect the URS in the controlling factor of stability and geometry. The degree of anisotropy and minerals more prone to fracture propagation, are therefore considered beneficial to investigate in relation to URS. PLT and UCS confirms that all tested rock types are anisotropic, and that the anisotropy translates into differences in directional strength in the rocks (e.g. box plot figure 57 and table 8, 10).

Small-scale geological features reveal important information from a mechanical aspect in the URS. Failure is observed to first occur in microscale, with the presence of isolated microcracks increasing and developing along a weakness plane before linking up and the scale of propagation increases for every linked microfracture. This is the brittle process of developing large-scale joints, and the progress of consistent joint sets occurs when the microcracks favors consistent structures in the fabric. This is suggested as the base evolution of joint sets, or in other words, the evolution of brittle discontinuities linking up and forming an URS.

4.3.1 Dusnjarga

From field work the URS appears complex and with constant local changing lithology. The distinctiveness of Dusnjarga is the progressive metamorphic grade with increased elevation. The backscarp region is the area of highest metamorphic grade and most affected by ductile deformation. The degree of metamorphic grade is suggested to affect the rock mass in a destabilizing manner, as the microfractures is observed to propagate easier with an ordered fabric (i.e. plagioclase layers and cleavage in amphibole grains). The microcracks link up easier when the small-scale weakness planes are equally oriented, as for the formation of joint sets parallel and normal to foliation. Ductile deformation, especially the presence of mylonite, affects the URS in controlling the geometry, as ductile structures is observed to facilitate the fracture propagation parallel to the structures. Ductile discontinuities appear to control the orientation of fractures in all scales, and therefore also act as point of rupture initiation in a URS. The combination of a destabilized metamorphic rock mass together with ductile discontinuities that control fracture orientation is suggested to act as the point of rupture initiation and control the geometry through the URS.

In addition, the presence of brittle faults ads to the controlling factor of geometry. Brittle faults are less abundant than ductile structures, but fault gouge is a pre-existing plane of significant weakness

facilitating for further movement for the URS. At Dusnjarga, the orientation of the brittle fault system is parallel to JN 2, and the orientation of the Langfjord fault is parallel to JN 1. This indicates that the large-scale URS geometry is defined by the orientation of brittle faults in immediate vicinity, while internal deformation in the slide is controlled more by the ductile structures.

The observed discontinuities at Dusnjarga affects the instability in different ways. The point of rupture initiation can be affected by several factors, but the presence of the thick mylonitic zone, crosscut by brittle faults and joints related to the nearby Langfjord fault, is suggested to be the most important factor. The metamorphic bedrock presents an ordered fabric that facilitates for microfractures to develop in small-scale and linking up to develop consistent joint sets. The presence of ductile structures controls fracture orientation, as microfractures favor ductile shear zones. And lastly, the brittle fault system present at Dusnjarga is parallel to both JN 1 and JN 2, indicating a significant controlling factor of the URS geometry.

4.3.2 Gámanjunni 3

The high degree of anisotropy that mica schist shows has been shown to present some geotechnical challenges to slope stability (Zhang et al., 2017). The PLT results confirm that the sampled mica schists and metapsammites are highly anisotropic at Gámanjunni 3.

The foliation is formed by mica, but the mica rich sections have a partially developed s-c' fabric. The small-scale folds developed in these sections are suggested to have a stabilizing effect on the low shear strength mica minerals presents. Even with the well-developed foliation combined with the s-c' fabric, the overall foliation of 10° is not considered steep enough for the URS to be foliation controlled rear rupture (Vick et al., 2020).

The presence of amphibolite with its amphibole foliation in the backscarp, facilitates intragranular microfractures that are oriented parallel to mineral cleavage and perpendicular to foliation, thereby facilitating fracture propagation that is consistent with the orientation of the backscarp. The presence of amphibolite therefore implies a point of rupture initiation control on the URS.

UCS tests suggest the bedrock at Gámanjunni 3 deforms more plastically before failing. From observations in microscopy, the plastic behavior is suggested to originate from mica minerals (i.e. lack of microfractures in mica schist). Fracture initiation and propagation is a brittle process, and plastic behavior in a rock is therefore considered disadvantageous for the formation of a URS. However, quartz behaves in a brittle manner and thin section confirms the presence of quartz increases fracture frequency at a microscale. The content of quartz is therefore presented as a key factor for microcrack propagation at a small-scale, and for brittle discontinuities to develop joint sets at a larger scale. The development of consistent joint sets is suggested to control the geometry of the

URS, with joint sets parallel to backscarp and foliation and therefore quartz content in a mica schist is most likely an important controlling factor in URS deformation.

Figure 51 (e.g. summary of fracture grade-DEM map) shows that all samples from the backscarp region are more fractured (i.e. fracture grade 2-3), than the rest of the sample selection. The increased frequency of small-scale microfractures is linked to the elevated assemblage of quartz and amphibole combined with a high frequency of ductile structures. Vick et al. (2020) found that as a point of rupture initiation typically follows pre-existing structural discontinuities within the rock mass, this is suggested to be the case Gámanjunni 3.

The entire URS is affected by ductile deformation, but only the backscarp region has the development of large-scale ductile structures. The presence of ductile structures (i.e. layers of metapsammite and amphibolite, lenses and folds) in the backscarp region implies a point of rupture initiation control on the URS.

4.3.3 Comparison of the influence of geology on Dusnjarga vs Gámanjunni 3

Dusnjarga and Gámanjunni 3 both displays a high degree of metamorphic foliation in the backscarp region, facilitating for microfractures to develop in an ordered fabric. The presence of ductile structures and lithological variation is also centered around the backscarp region at both URSs, suggesting a destabilizing effect on the entire top section and a central role in point of rupture initiation. In addition, the localities have strategically oriented brittle fault systems that play a significant role on the geometry of the URS. Dusnjarga is more affected by brittle faults as two fault systems affect the URS.

Foliation is another major discontinuity that displays a favorable orientation for both URSs, causing instability due to the anisotropic behavior of the rocks. Also, foliation is central for development of a joint set parallel to foliation at both URS.

However, each URS depends on certain minerals for microfractures to propagate. Dusnjarga URS consequently favors the foliation-forming plagioclase and favors amphibole more frequently with increased amphibole. Gámanjunni 3 on the other hand, favors a lower content of the foliation-forming mica minerals, but depends on the presence of quartz for brittle properties and microfractures to propagate. Amphibole is also highly favored in the amphibolite top layer. Both URSs present the development of intragranular microfractures in amphibole cleavage as a key factor for large-scale joint sets to develop normal to foliation (i.e. parallel to backscarp).

Observations from field, microcopy and mechanical tests imply foliation in all investigated rock types. However, the mica schist has a very well-developed foliation fabric and are highly anisotropic throughout the URS. Dusnjarga, on the other hand, has a foliation sometimes difficult to identify, but

which is observed to increase as the URS area shows more pre-existing ductile deformed with elevation. As foliation is considered a significant plane of weakness, the effect of foliation is suggested to be stronger at Gámanjunni 3. In terms of weakness planes, Dusnjarga has high frequency of ductile shear zones parallel to foliation, which is found to fracture easily.

4.4 Further work

The findings in this thesis show that pre-existing geological structures play a significant role in rock strength and URS development, but the data set should be more extensive and more detailed for a more comprehensive understanding of the causal links and mechanisms. The experimental data set was limited due to a well-developed fracture system in most samples, resulting in many failed UCS tests and only the most competent pieces making it through the thin section process. To develop this work further the following could be done:

- Study the behavior of microfractures in several bedrocks and how the microfractures behave to more discontinuities.
- The UCS data set should be larger, with more locations spread out at the URS and more cores per sample. Also, focus on testing with foliation completely parallel and perpendicular to load axis, if possible.
- Focus on larger samples and investigate the sample more thoroughly in field for fractures, to minimize the chance of fractures interrupting the study.
- Examine test results under the microscope.

5 Conclusions

Dusnjarga and Gámanjunni 3 are two unstable rock slopes with highly different lithologies, but both are previously metamorphosed and ductile deformed. From field investigations, microstructural analysis, and experimental investigation of rock strength this thesis reaches the following conclusions:

- Both localities have an elevated occurrence of ductile discontinuities in the back scarp region, and the ductile features are folds, lenses, and shear zones. Brittle structures occur more consistently in each URS, with brittle faults and consistent joint sets directly parallel to the back scarp, these brittle structures are suggested to act as a controlling factor for the geometry of the URS.
- 263 PLT experiments conclude with all rock types from Dusnjarga and Gámanjunni 3 are anisotropic. UCS tests confirm the anisotropic behavioral rock with strength values together with measurements of elasticity. Anisotropic behavior translates into a fabric that facilitates shear deformation, lowering the total strength implications in the rock mass.
- The microfractures appear to propagate easier in ordered fabrics (i.e. more planar foliations), and the fractures at Dusnjarga favor layers of plagioclase, grain boundaries or cleavage in amphibole. Microfractures also tend to favor pre-existing shear zones and changes in texture.
- Mylonite is the weakest rock type and microfractures appear to not follow any clear structures.
- The microfractures in mica schist favor foliation, which is controlled by mica minerals. UCS test implies a plastic behavior in the mica rich mica schist, which is supported by the absence of fractures in mica rich thin sections. Quartz adds a more brittle behavior to the mica schist, suggested to be the cause of more observed microfractures in thin sections with a higher assemblage of quartz.
- The amphibole defining foliation in the amphibolite at Gámanjunni 3 presents a well-developed intragranular fracture system in amphibole cleavage, facilitating for further development of a large-scale joint system in perpendicular to foliation.

  Small-scale microfractures can be linked to large-scale consistent joint sets.
- An instability begins with the development of small-scale fractures in the rock fabric. These microfractures favor certain minerals and structures, as minimum resistance presents an easier formation and propagation of microfractures that favor equal mineralogy. Each large-scale joint is the result of microfractures linking up and forming consistent joint sets. The presence of such joint sets is conclusive for rock slopes to develop as an unstable unit.

6 Sources

Ali, E., Guang, W., zhiming, Z., & Weixue, J. (2013). Assessments of Strength Anisotropy and Deformation Behavior of Banded Amphibolite Rocks. *Geotechnical and Geological Engineering*, 32(2), 429–438. https://doi.org/10.1007/s10706-013-9724-5

Ambrosi, & Crosta, G. . (2006). Large sackung along major tectonic features in the Central Italian Alps. Engineering Geology, 83(1), 183–200. https://doi.org/10.1016/j.enggeo.2005.06.031

Andresen, A. (1988). Caledonian terranes of northern Norway and their characteristics. *Trabajos de geología*, *17*, 103-117.

Andresen, M. L. (2018). Regional structural analysis of rock slope failure types, mechanisms and controlling bedrock structures in Kåfjorden, Troms. UiT Norges arktiske universitet.

Berisavljevic, D., Berisavljevic, Z., & Melentijevic, S. (2022). The shear strength evaluation of rough and infilled joints and its indications for stability of rock cutting in schist rock mass. *Bulletin of engineering geology and the environment*, *81*(3). https://doi.org/10.1007/s10064-022-02580-8

Blikra, L. H., Henderson, I., Nordvik, T. (2009) Faren for fjellskred fra Nordnesfjellet i Lyngenfjorden , Troms. *NGU reportnr. 2009.026*

Böhme, M., Bunkholt, H., Dehls, J., Oppikofer, T., Hermanns, R., Dalsegg, E., Kristensen, L., Lauknes, T. & Eriksen, H. (2016). Geologisk modell og fare-og risikoklassifisering av det ustabile fjellpartiet Gámanjunni 3 i Manndalen, Troms. *NGU Rapport, 64.*

Böhme, M., Hermanns, R., Gosse, J., Hilger, P., Eiken, T., Lauknes, T. & Dehls, J. (2019). Comparison of monitoring data with paleo–slip rates: Cosmogenic nuclide dating detects acceleration of a rockslide. *Geology, 47 (4), 339-342.*

Bois, B. S., & Guglielmi, Y. (2008). Influence of major inherited faults zones on gravitational slope deformation: A two-dimensional physical modelling of the La Clapière area (Southern French Alps). *Earth and Planetary Science Letters*, 272(3), 709–719. https://doi.org/10.1016/j.epsl.2008.06.006

Böse, M., Lüthgens, C., Lee, J. R., & Rose, J. (2012). Quaternary glaciations of northern Europe. *Quaternary Science Reviews*, *44*, 1–25. https://doi.org/10.1016/j.quascirev.2012.04.017

Braathen, A., Blikra, L.H., Berg, S.S. & Karlsen, F. (2004): Rock-slope failures of Norway; type, geometry,
deformation mechanisms and stability. *Norwegian Journal of Geology (NGT) 84, 67-88*.

Bredal, M. (2016). A structural, geomorphological, and InSAR study of the unstable rock slope in Oksfjellet, Kåfjord, Troms UiT Norges arktiske universitet].

Brideau, M. A., Stead, D., Kinakin, D., & Fecova, K. (2005). Influence of tectonic structures on the Hope Slide, British Columbia, Canada. *Engineering Geology*, 80(3), 242–259. https://doi.org/10.1016/j.enggeo.2005.05.004

Brideau, M. A., Yan, M., & Stead, D. (2009). The role of tectonic damage and brittle rock fracture in the development of large rock slope failures. *Geomorphology (Amsterdam, Netherlands*), 103(1), 30–49. https://doi.org/10.1016/j.geomorph.2008.04.010

Bunkholt, H., Osmundsen, P., Redfield, T., Oppikofer, T., Eiken, T., L'Heureux, J., Hermanns, R., and Lauknes, T. (2011) ROS Fjellskred i Troms: status analyser etter feltarbeid 2010. *NGU rapport,* 135.

Bunkholt, H. S. S., T. F. Redfield, P. T. Osmundsen, T. Oppikofer, R. L. Hermanns, and J. Dehls. 2012. 'Landslide Processes in Hard Rock in Troms, Norway'. *Landslides and Engineered Slopes: Protecting Society through Improved Understanding*. Taylor & Francis Group, London, 855–61.

Bunkholt, H., S. Otterå, F.X. Yugsi Molina, R.L. Hermans, J. Dehls, P.T. Osmundsen, T.F. Redfield, T. Eiken, and M. Böhme. 2013. *'Undersøkelser av ustabile fjellpartier i Troms - status og planer etter feltarbeid 2011 og 2012'*. *Norges Geologiske Undersøkelse.*

Corner, G. D., 1980, Preboreal deglaciation chronology and marine limits of the LyngenStorfjord area, Troms, North Norway: *Boreas*, v. 9, no. 4, p. 239-249.

D5731 Standard Test Method for Determination of Rock's Point Load Strength Index and Application to Rock Strength Classifications (2016). *American Society for Testing and Materials (ASTM)*. In.

D7012 Standard Test Methods for Compressive Strength and Elastic Moduli of Intact Rock Core Specimens under Varying States of Stress and Temperatures. (2014) *American Society for Testing and Materials (ASTM)*. In.

Dahle, H., Anda, E., Saintot, A., Sætre, S. (2008) *Faren for fjellskred fra fjellet Mannen i Romsdalen* NGU reportnr. 2008.087

Dannevig, P. (2020). Troms - klima. *Store Norske Leksikon*. https://snl.no/Troms_-_klima

Dehls, Olesen, O., Olsen, L., & Harald Blikra, L. (2000). Neotectonic faulting in northern Norway; the Stuoragurra and Nordmannvikdalen postglacial faults. *Quaternary Science Reviews*, *19*(14), 1447–1460. https://doi.org/10.1016/S0277-3791(00)00073-1

Dietrich, R. V. (2021) *Mica*. Encylopedia Britannica https://www.britannica.com/science/mica. Accessed 30 april 2022

Eikenæs, O. 2015, Nasjonal beredskap for fjellskred. *Norges vassdrags- og energidirektorat*.

Eilertsen, R. S., Hansen, L. & Olsen, L. (2012). Kvartærgeologisk kartlegging av Manndalen, Kåfjord, Troms, 2011.068. *Trondheim: Norges geologiske undersøkelse.* 24 s. [Lest 23.01.12].

Einstein, H. H., Veneziano , D., Baecher, G. ., & O'Reilly, K. . (1983). The effect of discontinuity persistence on rock slope stability. *International Journal of Rock Mechanics and Mining Sciences & Geomechanics Abstracts*, 20(5), 227–236. https://doi.org/10.1016/0148-9062(83)90003-7

El Bedoui, S., Bois, T., Jomard, H., Sanchez, G., Lebourg, T., Trics, E., Guglielmi, Y., Bouissou, S., Chemenda, A., Rolland, Y., Corsini, M., & Pérez, J. L. (2011). Paraglacial gravitational deformations in the SW Alps: a review of field investigations, 10Be cosmogenic dating and physical modelling. *Geological Society Special Publication,* 351(1), 11–25. https://doi.org/10.1144/SP351.2

Eriksen, H. Ø. (2018). Instrumentation and temperature data (2013-2017), Gámanjunni 3 rockslide and rock glacier, Manndalen, Troms. *Tromsø: Norut Northern Research Institute.* 59 s.

Eriksen, H. Ø., Larsen, Y., Hindberg, H. & Lauknes, T. R. (2017a). Kartlegging av 3Dbevegelsesmønstre på Gámanjunni 3, Kåfjord, Troms. Tromsø: Norut. 25 s.

Etzelmuller, B., Czekirda, J., Magnin, F., Duvillard, P.-A., Ravanel, L., Malet, E., Aspaas, A., Kristensen, L., Skrede, I., Majala, G. D., Jacobs, B., Leinauer, J., Hauck, C., Hilbich, C., Bohme, M., Hermanns, R., Eriksen, H. O., Lauknes, T. R., Krautblatter, M., & Westermann, S. (2022). Permafrost in monitored unstable rock slopes in Norway - new insights from temperature and surface velocity measurements, geophysical surveying, and ground temperature modelling. *Earth Surface Dynamics,* 10(1), 97–129. https://doi.org/10.5194/esurf-10-97-2022

Evans, David JA, Brice R Rea, James D Hansom, and W Brian Whalley. 2002. 'Geomorphology and Style of Plateau Icefield Deglaciation in Fjord Terrains: The Example of Troms-Finnmark, North Norway'. *Journal of Quaternary Science: Published for the Quaternary Research Association* 17 (3): 221–39.

Faber, C., Stünitz, H., Gasser, D., Jeřábek, P., Kraus, K., Corfu, F., Ravna, E. K., & Konopásek, J. (2018). An anticlockwise metamorphic P-T path and nappe stacking in the Reisa Nappe Complex in the Scandinavian Caledonides, northern Norway: evidence for a weakening of lower continental crust before and during continental collision. *Solid earth discussions SED*, 1-46. https://doi.org/10.5194/se-2018-74

GeoExpert-AG. (2016). Gámanjunni Rock Mass Movement Site / Kåfjord, Norway. Hybrid Seismic Mapping of the Subsurface Structures. 22.

Glueer, F., Loew, S., & Manconi, A. (2020). Paraglacial history and structure of the Moosfluh Landslide (1850–2016), Switzerland. Geomorphology (Amsterdam, Netherlands), 355, 106677. https://doi.org/10.1016/j.geomorph.2019.02.021

Grämiger, L. M., Moore, J. R., Gischig, V. S., Ivy‐Ochs, S., & Loew, S. (2017). Beyond debuttressing: Mechanics of paraglacial rock slope damage during repeat glacial cycles. *Journal of Geophysical Research. Earth Surface,* 122(4), 1004 – 1036. https://doi.org/10.1002/2016JF003967

Hansen. (2020). Analyse av strukturer og bevegelsesdata i det ustabile fjellskredområdet Gámmanjunni 3, Kåfjord kommune, Troms og Finnmark fylke. Med vekt på kontrollerende faktorer, skråningsprosesser, bevegelsesdynamikk og skredmodeller. *UiT Norges arktiske universitet.*

Hauck, C. & Hilbich, C. (2018). 4-PHASE MODEL SIMULATIONS Gámanjunni, NORWAY, 2018.

Henderson, I., Osmundsen, P. T., & Redfield, T. (2008). *ROS fjellskred i Troms : statusrapport 2007* (Vol. 2008.025). Norges geologiske undersøkelse.

Henderson, I., Osmundsen, P. T., & Redfield, T. (2010) *ROS Fjellskred i Troms: Status og planer 2010* (Vol.2010.021). Norges geologiske undersøkelse

Hilger, H. (2019). Rock-slope failures in Norway - temporal development and climatic conditioning.

Hilger, P., Hermanns, R. L., Czekirda, J., Myhra, K. S., Gosse, J. C., & Etzelmüller, B. (2021). Permafrost as a first order control on long-term rock-slope deformation in (Sub-)Arctic Norway. *Quaternary Science Reviews*, 251. https://doi.org/10.1016/j.quascirev.2020.106718

Hoyer, S., Römer, A. & Supper, R. (2016). Electrical Resistivity Tomography at Gámanjunni, Troms, Norway.

Hughes, A., Gyllencreutz, R., Lohne, Øystein S., Mangerud, J., & Svendsen, J.-I. (2015). *DATED-1: compilation of dates and time-slice reconstruction of the build-up and retreat of the last Eurasian (British-Irish, Scandinavian, Svalbard-Barents-Kara Seas) Ice Sheets 40-10 ka* [Data set]. PANGAEA - Data Publisher for Earth & Environmental Science. https://doi.org/10.1594/pangaea.848117

Hughes, A., Gyllencreutz, R., Lohne, Øystein S., Mangerud, J., & Svendsen, J. I. (2016). The last Eurasian ice sheets - a chronological database and time-slice reconstruction, DATED-1. *Boreas*, *45*(1), 1–45. https://doi.org/10.1111/bor.12142

Høgaas, F, L Hansen, BI Rindstad, H Sveian, and L Olsen. 2012. 'Database for Registrering Av Marine Grense (MG) i Norge'. NGU Rapport.

Kirkland, C. L., Stephen Daly, J., & Whitehouse, M. J. (2007). Provenance and Terrane Evolution of the Kalak Nappe Complex, Norwegian Caledonides: Implications for Neoproterozoic Paleogeography and Tectonics. *The Journal of geology*, *115*(1), 21-41. https://doi.org/10.1086/509247

Koehl, J. B. P, Bergh, S. G., Osmundsen, P.-T., Redfield, T. F., Indrevær, K., Lea, H., & Bergø, E. (2019). Late Devonian–Carboniferous faulting and controlling structures and fabrics in NW Finnmark. *Norwegian Journal of Geology*. https://doi.org/10.17850/njg99-3-5

Kranz. (1983). Microcracks in rocks: A review. *Tectonophysics*, *100*(1), 449–480. https://doi.org/10.1016/0040-1951(83)90198-1

Kristensen, L., Czekirda, J., Penna, I., Etzelmüller, B., Nicolet, P., Pullarello, J. S., Blikra, L. H., Skrede, I., Oldani, S., & Abellan, A. (2021). Movements, failure and climatic control of the Veslemannen rockslide, Western Norway. Landslides, 18(6), 1963–1980. https://doi.org/10.1007/s10346-020-01609-x

Lotfolahpour, A. & Asle Zaeem, M. (2021). Effects of cleavage plane and material strength on fracture of polycrystalline brittle materials: A phase-field modeling study. *Computational Materials Science*, 197, 110642. https://doi.org/10.1016/j.commatsci.2021.110642

Lysså, A. (2015), Quaternary geology, *NGU*, https://www.ngu.no/en/topic/quaternary-geology

Marulanda, C., Marulanda, A. and Phillips, C. (2013) "Experiences in Large Slope Stability Problems Under Complex Geology". *International Conference on Case Histories in Geotechnical Engineering. 21.*

Meteorologisk Institutt, N. v.-o. e. N., Norwegian Research Center AS NORCE and Bjerknes Center for Climate Research (2021). *Klimaprofil Troms*. https://klimaservicesenter.no/kss/klimaprofiler/troms

Mukherjee, S. (2015) Chapter 3 - Brittle Faults, *Atlas of structural Geology. p. 79-106.*

Neuhäuser B, Terhorst B, Damm B (2012) Landslide identification and modelling in flysch areas of the European Alpine foreland. *Z Geomorphol* 56:115–146. https://doi.org/10.1127/0372-8854/2012/00119

NGU (2019a), Unstable rock slope inventory map, www.ngu.no. Accessed 18. april

Oppikofer, T., Böhme, M., Nicolet, P., Penna, I. & Hermanns, R. (2016). Metodikk for konsekvensanalyse av fjellskred. *NGU Report 2016.0*47.

Panazzolo, D. & da Silva, P. R. (2017). Regularization of discontinuous foliations: Blowing up and sliding conditions via Fenichel theory. *Journal of Differential Equations*, 263(12), 8362–8390. https://doi.org/10.1016/j.jde.2017.08.042

Paronuzzi, Bolla, A., & Rigo, E. (2015). Brittle and Ductile Behavior in Deep-Seated Landslides: Learning from the Vajont Experience. *Rock Mechanics and Rock Engineering*, 49(6), 2389–2411. https://doi.org/10.1007/s00603-015-0815-x

Patton, H., Hubbard, A., Andreassen, K., Auriac, A., Whitehouse, P. L., Stroeven, A. P., Shackleton, C., Winsborrow, M., Heyman, J., & Hall, A. M. (2017). Deglaciation of the Eurasian ice sheet complex. Quaternary Science Reviews, 169, 148–172. https://doi.org/10.1016/j.quascirev.2017.05.019

Pedersen, I. (2015). Kæm e vi? https://www.manndalen.no/kaem-e-vi.358479.no.html

Pless, G., Blikra, L. H. & Kristensen, L. (2021) Possibility for using drainage as mitigation to increase the stability of the Åknes rock-slope instability, Stranda in western Norway, *Norwegian water resources and energy directorate*, https://publikasjoner.nve.no/rapport/2021/rapport2021_22.pdf

Quenardel, J.M., & Zwaan, K.B. (2008): Berggrunnskart Manndalen 1633 I, M 1:50000. Foreløpig utgave. Norges geologiske undersøkelse

Ramsay, D. M. (1979). The sub-Caledonian unconformity on Hjelmsøy: new evidence of primary basement/cover relations in the Finnmarkian nappe sequence (Vol. 51). Universitetsforlaget.

Rigopoulos, I., Tsikouras, B., Pemonis, P., Hatzipanagiotou, K. (2011) Microcracks in ultrabasic rocks under uniaxial compressive stress, Eng. Geol 117 (1-2) 104-113 https://doi.org/10.1016/j.enggeo.2010.10.010

Rigopoulos, Tsikouras, B., Pomonis, P., & Hatzipanagiotou, K. (2012). Petrographic Investigation of Microcrack Initiation in Mafic Ophiolitic Rocks Under Uniaxial Compression. *Rock Mechanics and Rock Engineering*, *46*(5), 1061–1072. https://doi.org/10.1007/s00603-012-0310-6

Riiber, K. 2000 'Løsmasse Kart. Manuskart 1:250 000'. http://geo.ngu.no/kart/losmasse/.

Roberts, D. 1974. 'Hammerfest: Description to the 1: 250.000 Bedrockgeological Map'. *Norges Geologiske Undersøkelse* 301: 1–66.

Roberts, R. J., Corfu, F., Torsvik, T. H., Ashwal, L. D., & Ramsay, D. M. (2006). Short-lived mafic magmatism at 560–570 Ma in the northern Norwegian Caledonides: U–Pb zircon ages from the Seiland Igneous Province. *Geol. Mag*, *143*(6), 887-903. https://doi.org/10.1017/S0016756806002512

Santos, C. A., White, R. W., Moraes, R., & Szabó, G. A. J. (2021). The gabbro to amphibolite transition along a hydration front. *Journal of metamorphic geology*, *39*(4), 417-442. https://doi.org/10.1111/jmg.12582

Sagaetsho, G. & Zvarivadza, T. (2006) Journal of the Southern African Institute of Mining and Metallurgy. *Southern African Institute of Mining and Metallurgy*.

Saintot, A., Henderson, I. & Derron, M.-H. (2011). Inheritance of ductile and brittle structures in the development of large rock slope instabilities: examples from western Norway. *Geological Society, London, Special Publications*, 351 (1), 27-78

Stead, D & Wolter, A. (2015). A critical review of rock slope failure mechanisms: The importance of structural geology. Journal of Structural Geology, 74, 1–23. https://doi.org/10.1016/j.jsg.2015.02.002

Stokes, Corner, G. D., Winsborrow, M. C. M., Husum, K., & Andreassen, K. (2014). Asynchronous response of marine-terminating outlet glaciers during deglaciation of the Fennoscandian ice sheet. *Geology (Boulder)*, *42*(5), 455–458. https://doi.org/10.1130/G35299.1

Storni, H. M., Hugentobler, M., Manconi, A., & Loew, S. (2020). Monitoring and analysis of active rockslide-glacier interactions (Moosfluh, Switzerland). *Geomorphology (Amsterdam, Netherlands*), 371, 107414. https://doi.org/10.1016/j.geomorph.2020.107414

Sturt, B. A., Ramsay, D. M., & Appleyard, E. C. (1965). *The alkaline complex of the Breivikbotn area, Sørøy, Northern Norway* (Vol. nr 231). Universitetsforlaget.

Sveian, H. 2004 'Isen Kom og Forsvant'. Ka Dokker Mein Førr Stein' Troms Fylke*: Løsmassekart.* Norges Geologiske Undersøkelse.

Vick, Böhme, M., Rouyet, L., Bergh, S. G., Corner, G. D., & Lauknes, T. R. (2020). Structurally controlled rock slope deformation in northern Norway. Landslides, 17(8), 1745–1776. https://doi.org/10.1007/s10346-020-01421-7

Vick, L., Bergh, S., Höpfl, S. Percival, J. & Daines, E. (2020.14-19/06) b. *The role of lithological weakness zones in rockslides in northern Norway*. Assessment of large unstable mountain slopes in Troms County, Hard Rock Engineering, Trondheim

Vorren, T. O., and Mangerud, J., 2007, Chapter. 15. "Istider kommer og går" in: Ramberg, Ivar B. Bryhni, Inge Nøtt.

Vorren, TO, J Mangerud, LH Blikra, A Nesje, and H Sveian. 2008. 'The Emergence of Modern Norway'. The Making of Land: Geology of Norway*. Geological Society of Norway,* Trondheim, 534–59.

Watanabe, T. & Tsurekawa, S. (1999). The control of brittleness and development of desirable mechanical properties in polycrystalline systems by grain boundary engineering. *Acta Materialia,* 47(15), 4171–4185. https://doi.org/10.1016/S1359-6454(99)00275-X

Yanuardian, A. R., Hermawan, K., Martireni, A. P., & Tohari, A. (2020). THE INFLUENCE OF DISCONTINUITIES ON ROCK MASS QUALITY AND OVERALL STABILITY OF ANDESITE ROCK SLOPE IN WEST JAVA. *Rudarsko-Geološko-Naftni Zbornik,* 35(3), 67–76. https://doi.org/10.17794/rgn.2020.3.7

Yin, X., Yan, E., Wang, L., Liu, L., Feng, B., & Wang, P. (2019). Anisotropy of quartz mica schist based on quantitative extraction of fabric information. *Bulletin of Engineering Geology and the Environment*, 79(5), 2439–2456. https://doi.org/10.1007/s10064-019-01699-5

Zehnder, A- T. (2013) Griffith Theory of Fracture. In: Wang, Q. J., Chung, Y. W. (eds) *Encyclopedia of Tribology.* Springer, Boston. MA. https://doi.org/10.1007/978-0-387-92897-5_259

Zhang, W., L. N. Y., Wang, S.-J., & Han, G.-Y. (2011). Engineering properties of quartz mica schist. Engineering Geology, 121(3), 135–149. https://doi.org/10.1016/j.enggeo.2011.04.020

Zwaan, K.B., Dangla, P., & Quenardel, J.M. (2006): Berggrunnskart Kåfjord 1634 II, M 1:50,000. Norges geologiske undersøkelse.

APPENDIX-1: SCAN OF DUSNJARGA THIN SECTIONS

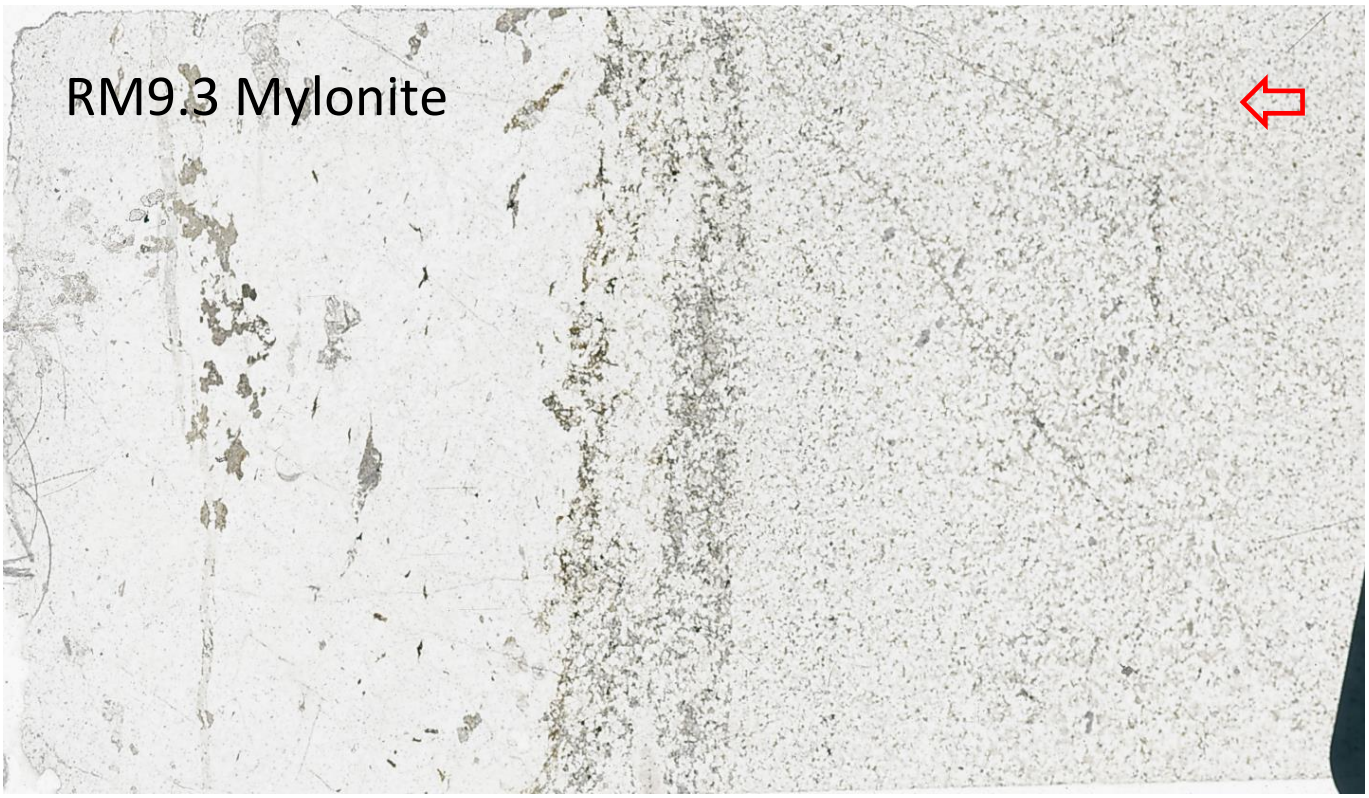


FM Mylonite


RM1.2 Metagabbro


RM1.2 Metagabbro

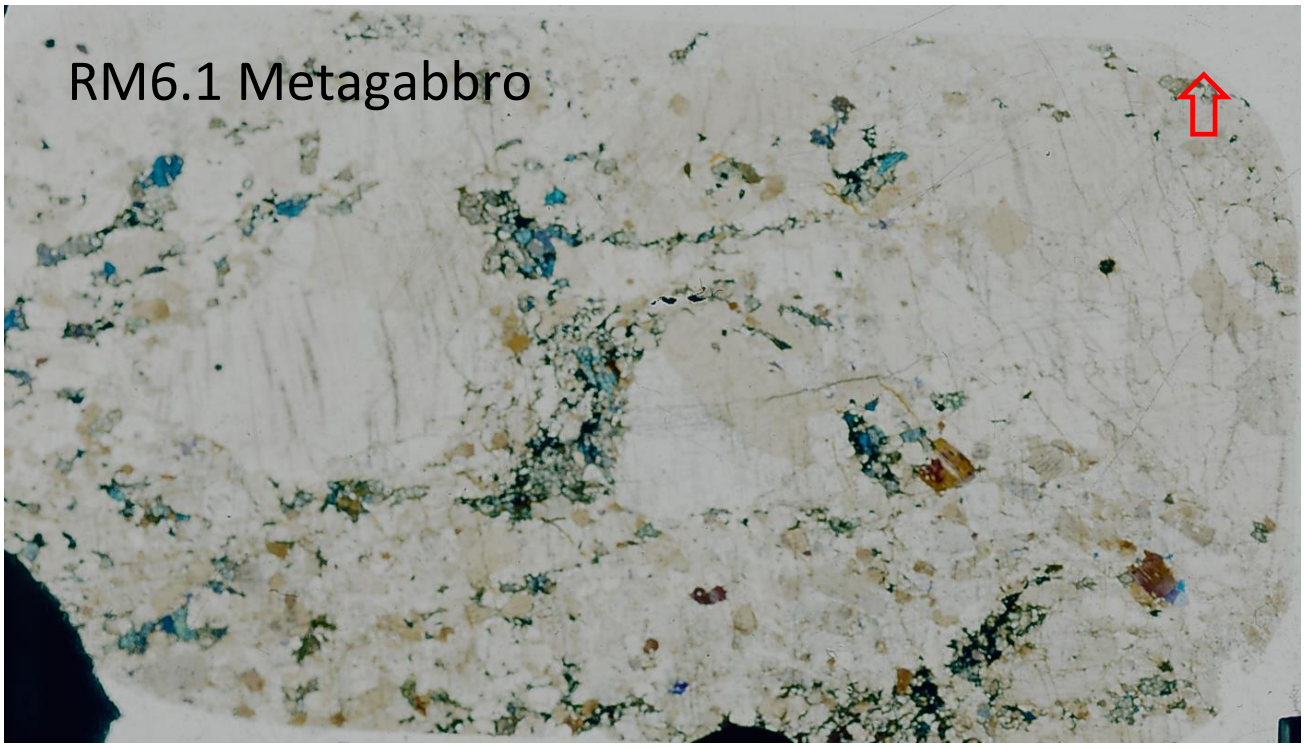
RM6.1 Metagabbro

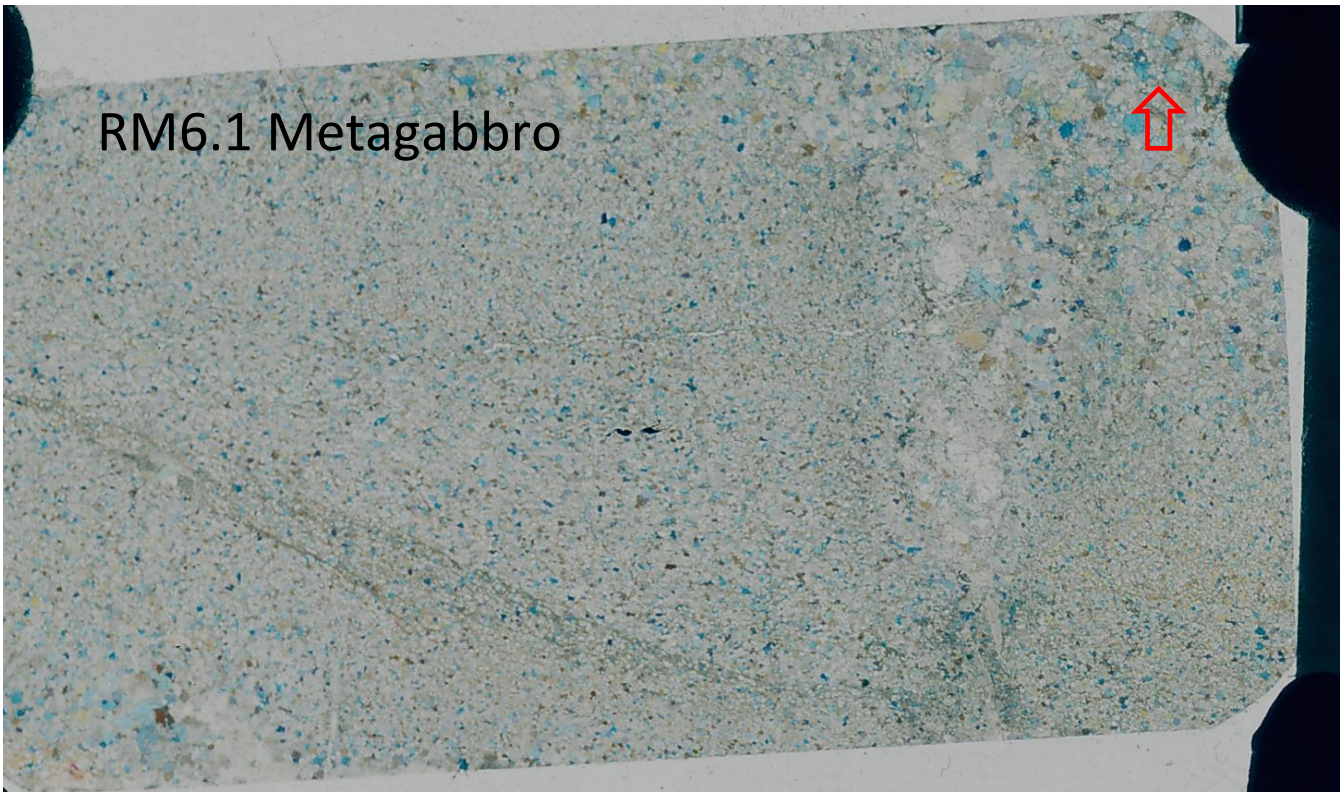
RM6.1 Metagabbro


RM12.2 Metagabbro

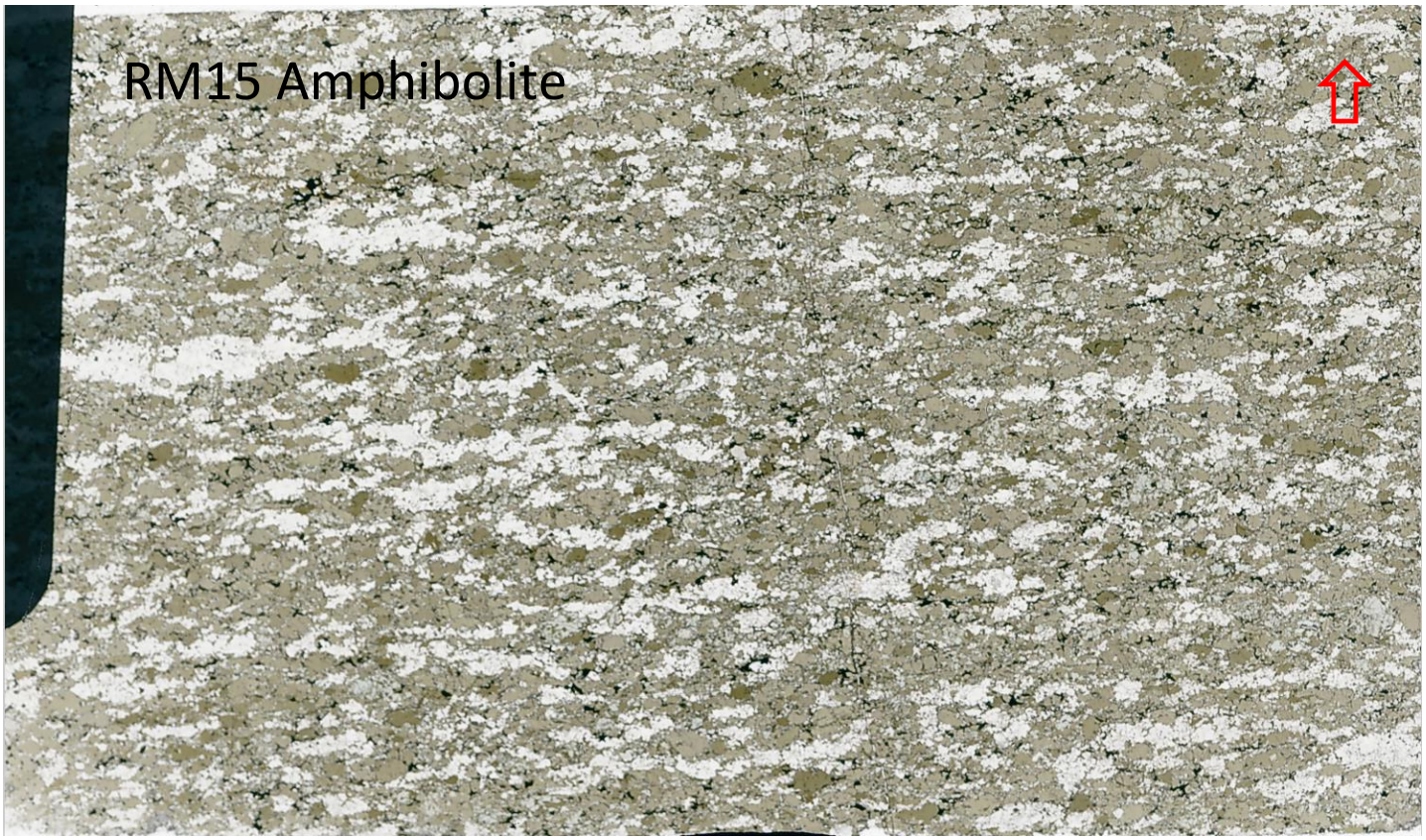
RM15 Amphibolite


RM3.1 Metagabbro

APPENDIX -2: SCAN OF GÁMANJUNNI 3 THIN SECTIONS:


G13 Muscovite-/biotite schist


G14 Muscovite schist

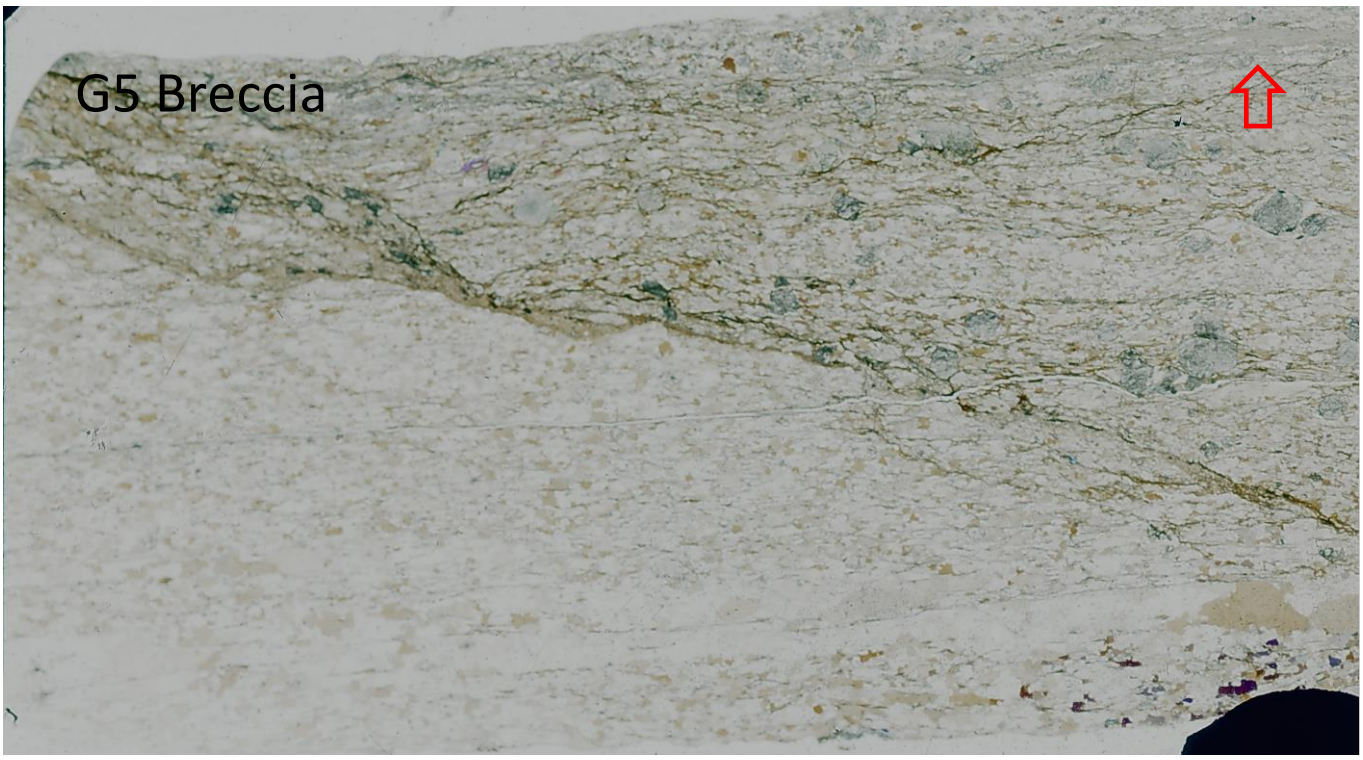
G5 Breccia

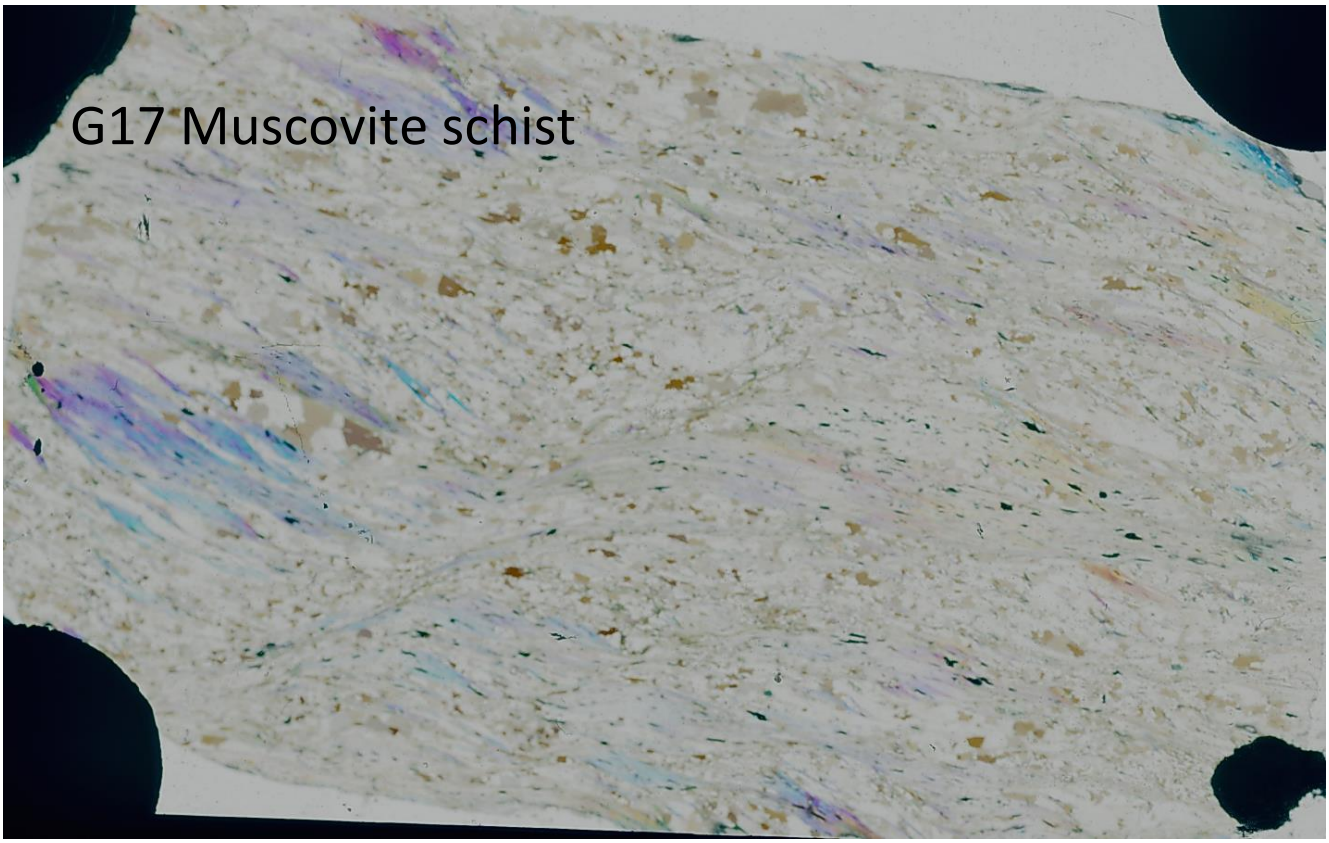
G17 Muscovite schist


G19 Biotite schist


G15 Biotite schist

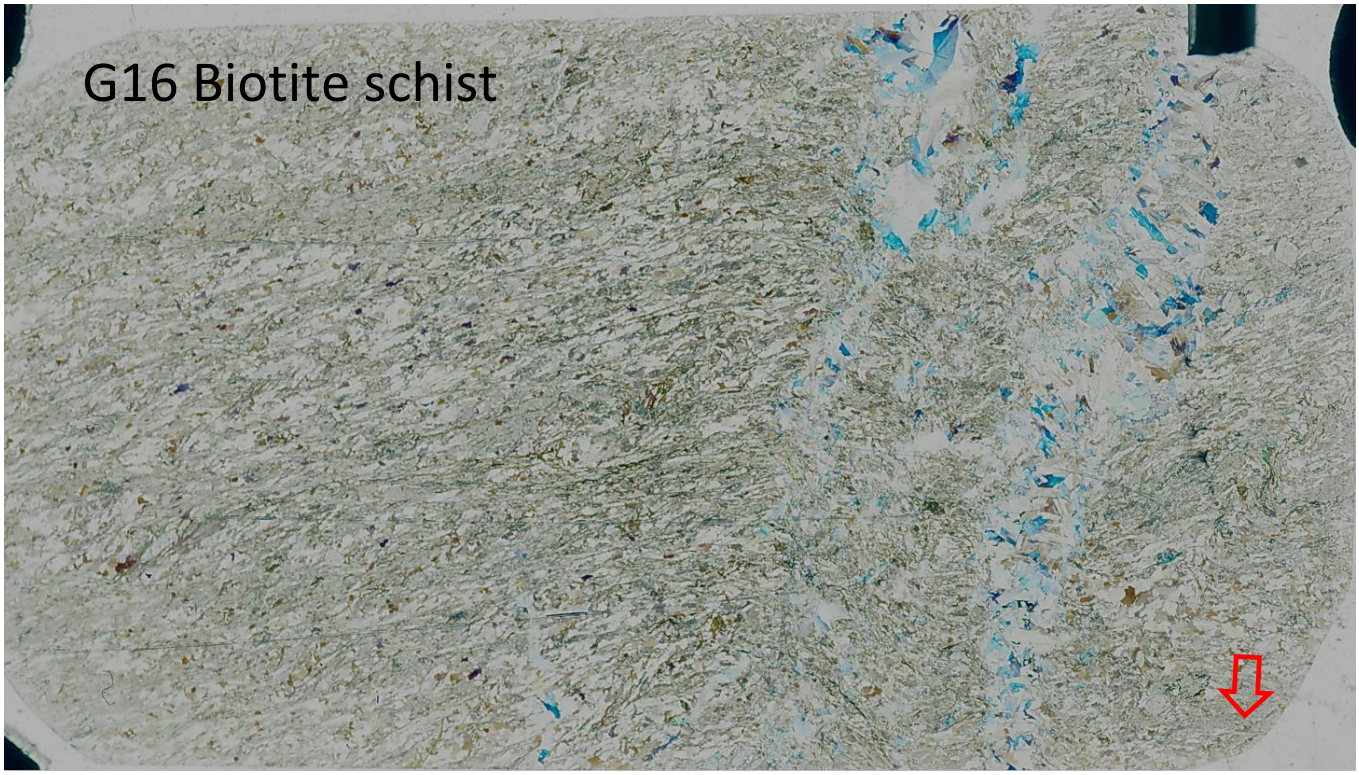
G16 Biotite schist

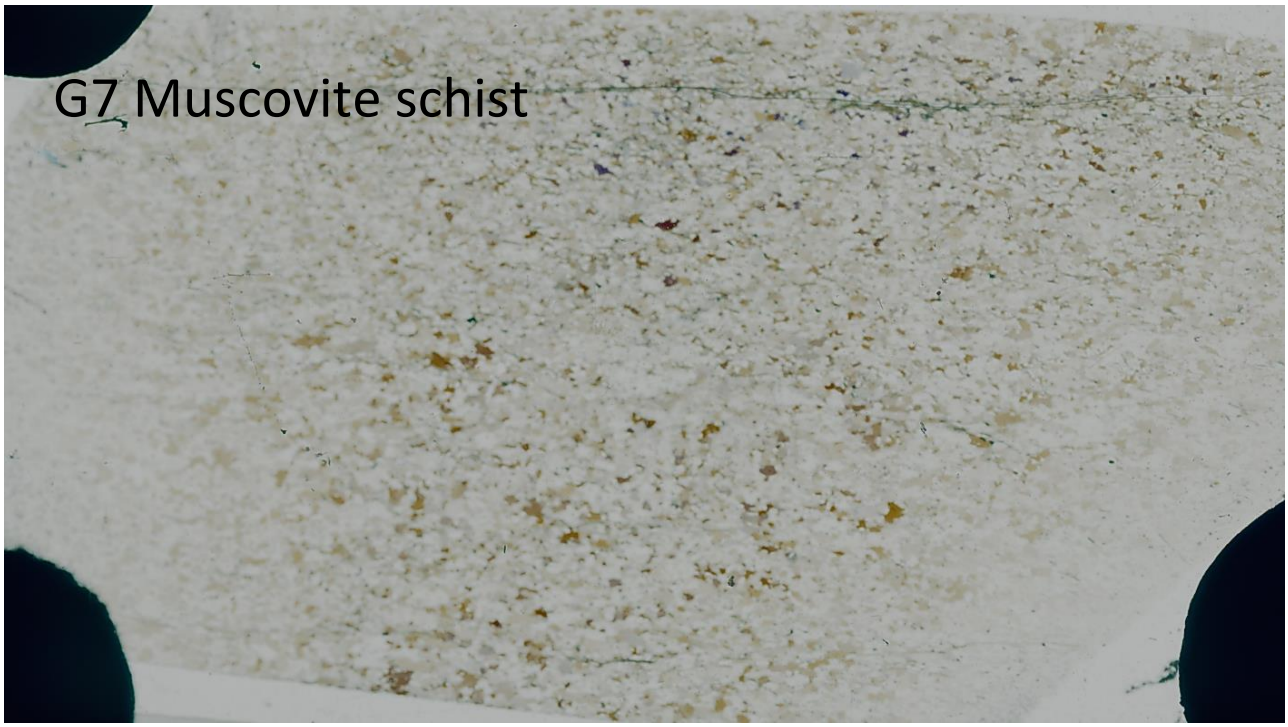

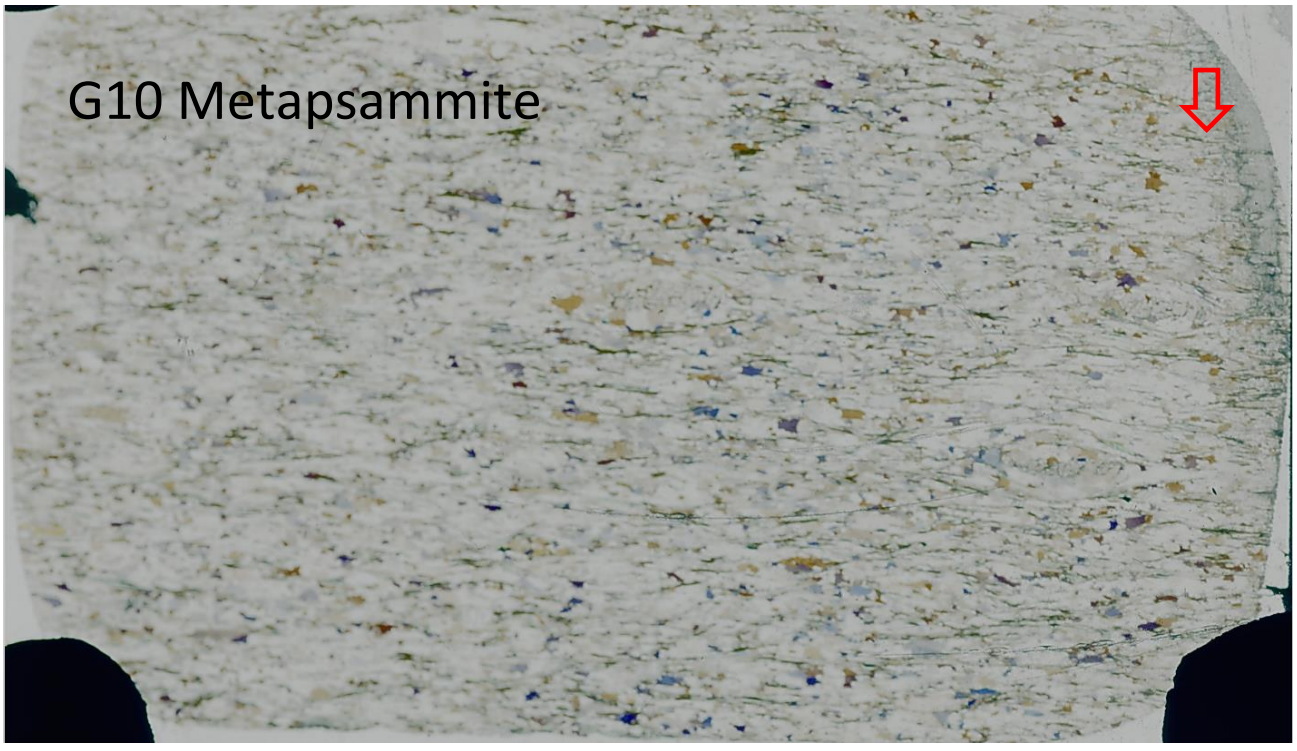

APPENDIX -3: PRE AND POST UCS PICTURES


G7.1
NGI
UCT1119 Post Test 11


NGI
UCT1119 Post Test 22


NGI
UCT1119 Post Test 33


NGI
UCT1119 Post Test 44

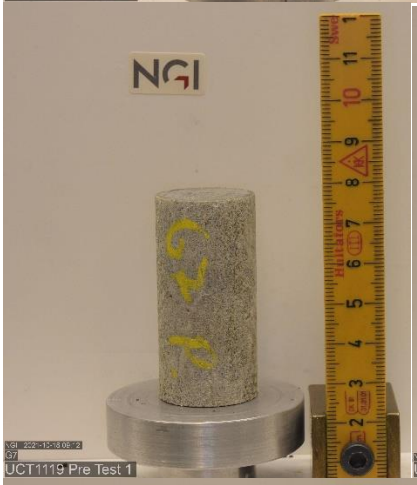
NGI
UCT1119 Pre Test 1


NGI
UCT1119 Pre Test 2


NGI
UCT1119 Pre Test 3


NGI
UCT1119 Pre Test 4

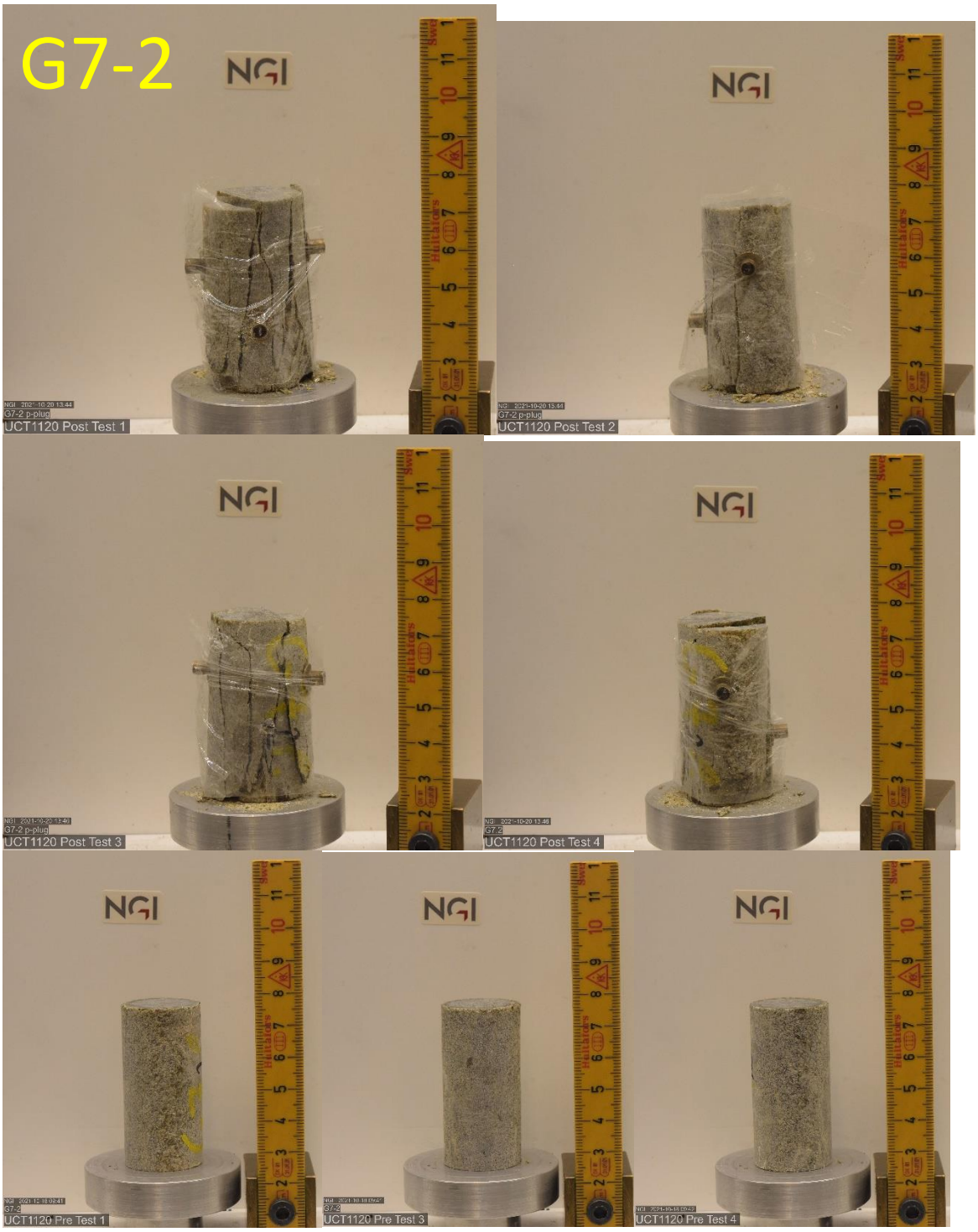
G7-2
NGI
UCT1120 Post Test 1
UCT1120 Post Test 2
UCT1120 Post Test 3
UCT1120 Post Test 4
UCT1120 Pre Test 1
UCT1120 Pre Test 3
UCT1120 Pre Test 4

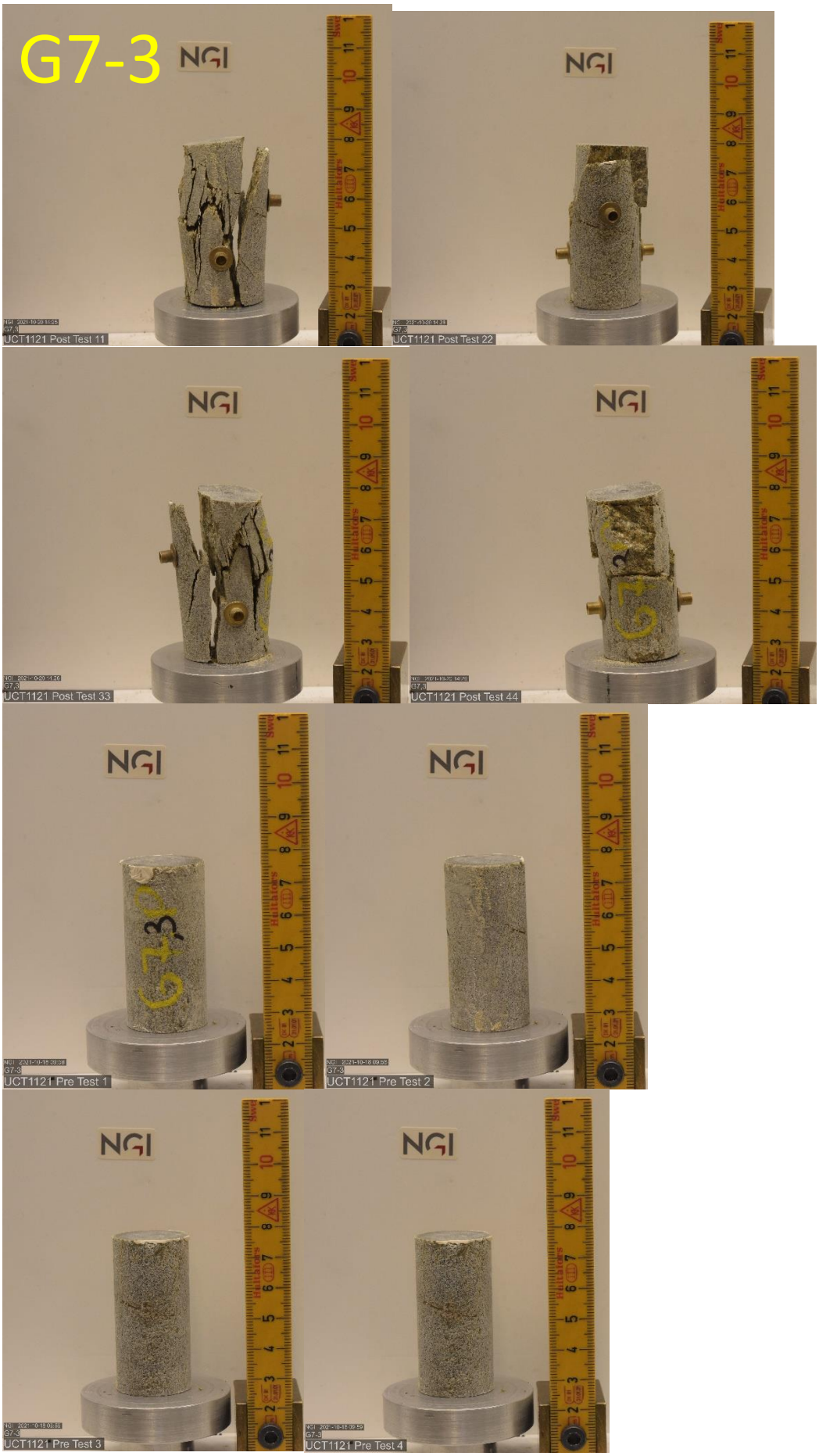
G7-3
NGI
UCT1121 Post Test 11
UCT1121 Post Test 22
UCT1121 Post Test 33
UCT1121 Post Test 44
UCT1121 Pre Test 1
UCT1121 Pre Test 2
UCT1121 Pre Test 3
UCT1121 Pre Test 4

G19-1


NGI
UCT1122 Post Test 11


NGI
UCT1122 Post Test 22


NGI
UCT1122 Post Test 33

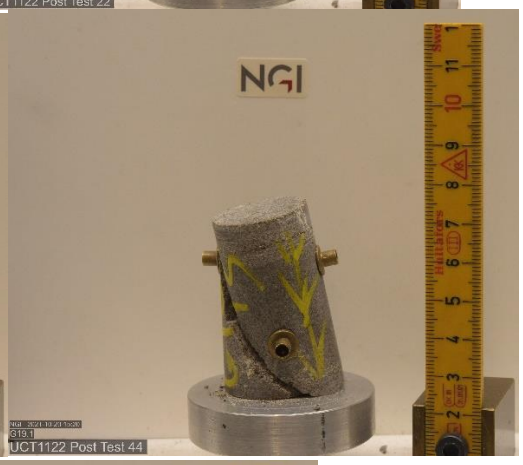
NGI
UCT1122 Post Test 44

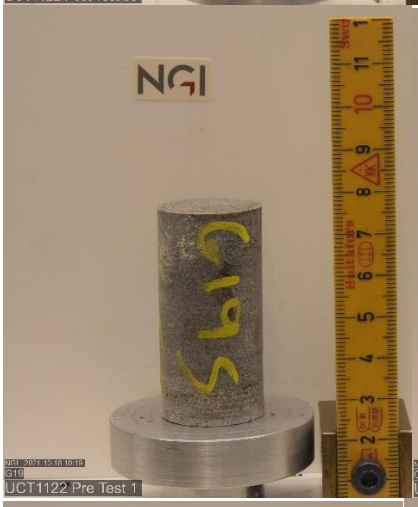
NGI
UCT1122 Pre Test 1


NGI
UCT1122 Pre Test 2


NGI
UCT1122 Pre Test 3


NGI
UCT1122 Pre Test 4

RM15-1

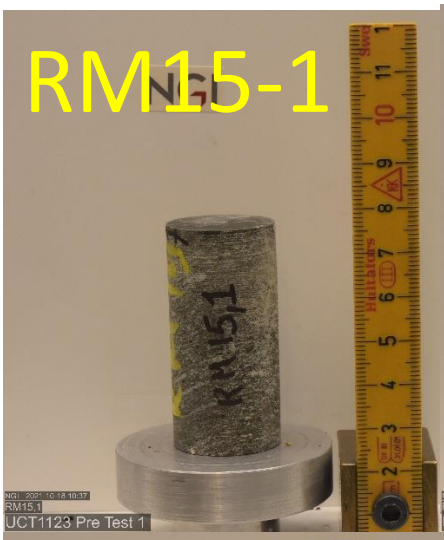
RM15.1
UCT1123 Pre Test 1


RM15.1
UCT1123 Pre Test 2

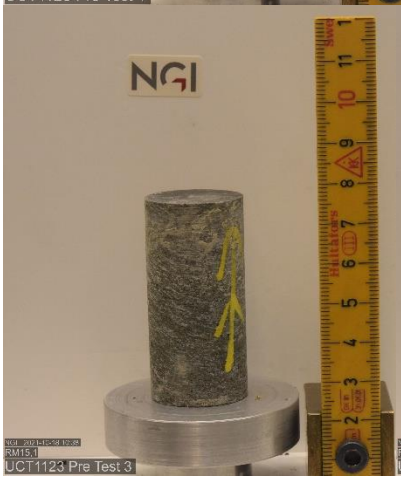
RM15.1
UCT1123 Pre Test 3


RM15.1
UCT1123 Pre Test 4

RM15-2

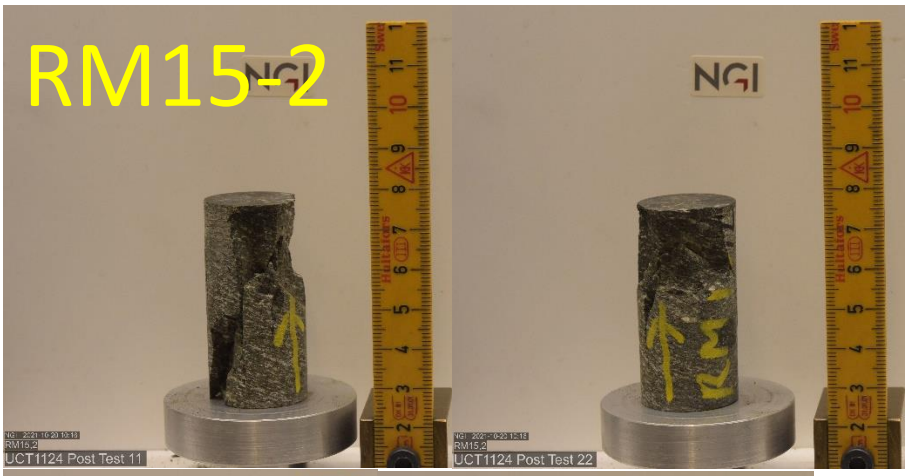
NGI
RM15.2
UCT1124 Post Test 11

NGI
RM15.2
UCT1124 Post Test 22


NGI
RM15.2
UCT1124 Pre Test 1


NGI
RM15.2
UCT1124 Post Test 33


NGI
RM15.2
UCT1124 Post Test 44


NGI
RM15.2
UCT1124 Pre Test 2


NGI
RM15.2
UCT1124 Pre Test 3


NGI
RM15.2
UCT1124 Pre Test 4

RM15-3


NGI
RM15.3
UCT1125 Post Test 1

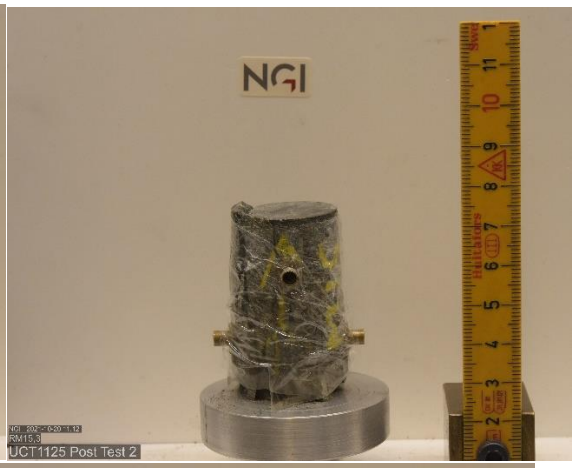
NGI
RM15.3
UCT1125 Post Test 2


NGI
RM15.3
UCT1125 Post Test 3


NGI
RM13.3
UCT1125 Post Test 4


NGI
RM15.3
UCT1125 Pre Test 1


NGI
RM15.3
UCT1125 Pre Test 2


NGI
RM15.3
UCT1125 Pre Test 3


NGI
RM15.3
UCT1125 Pre Test 4

RM13.2-1

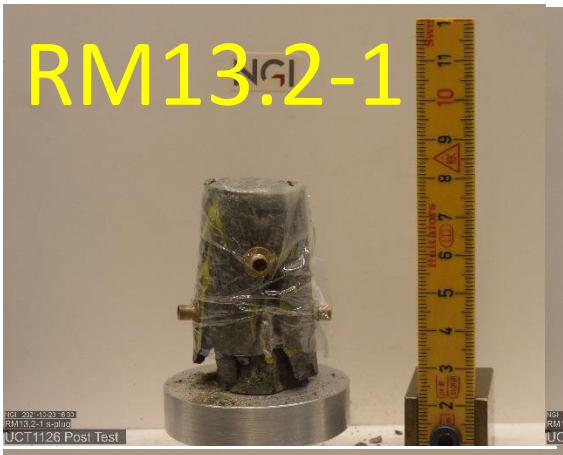
UCT1126 Post Test

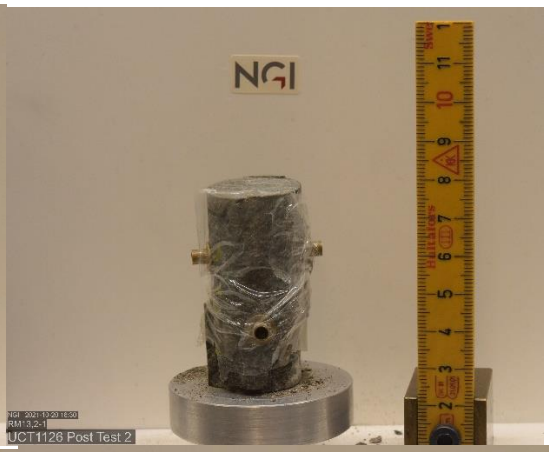
UCT1126 Post Test 2


UCT1126 Post Test 3


UCT1126 Post Test 4


UCT1126 Pre Test 1


UCT1126 Pre Test 2


UCT1126 Pre Test 3


UCT1126 Pre Test 4

RM13.2-2


UCT1127 Post Test 1
UCT1127 Post Test 2


UCT1127 Post Test 3
UCT1127 Post Test 4


UCT1127 Pre Test 1
UCT1127 Pre Test 2

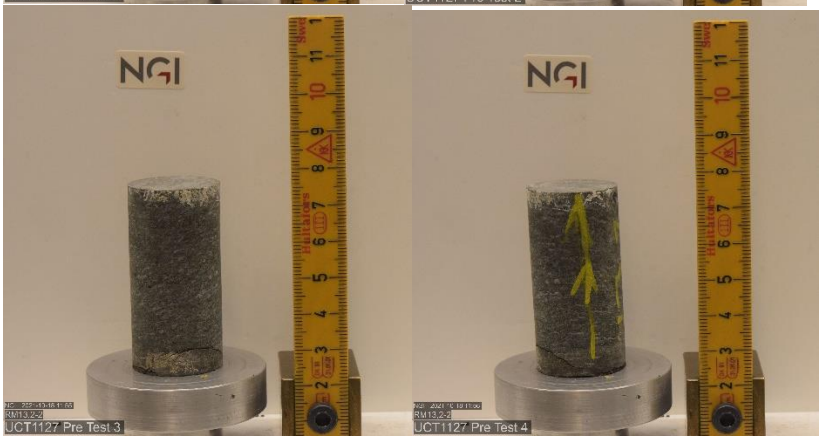
UCT1127 Pre Test 3
UCT1127 Pre Test 4

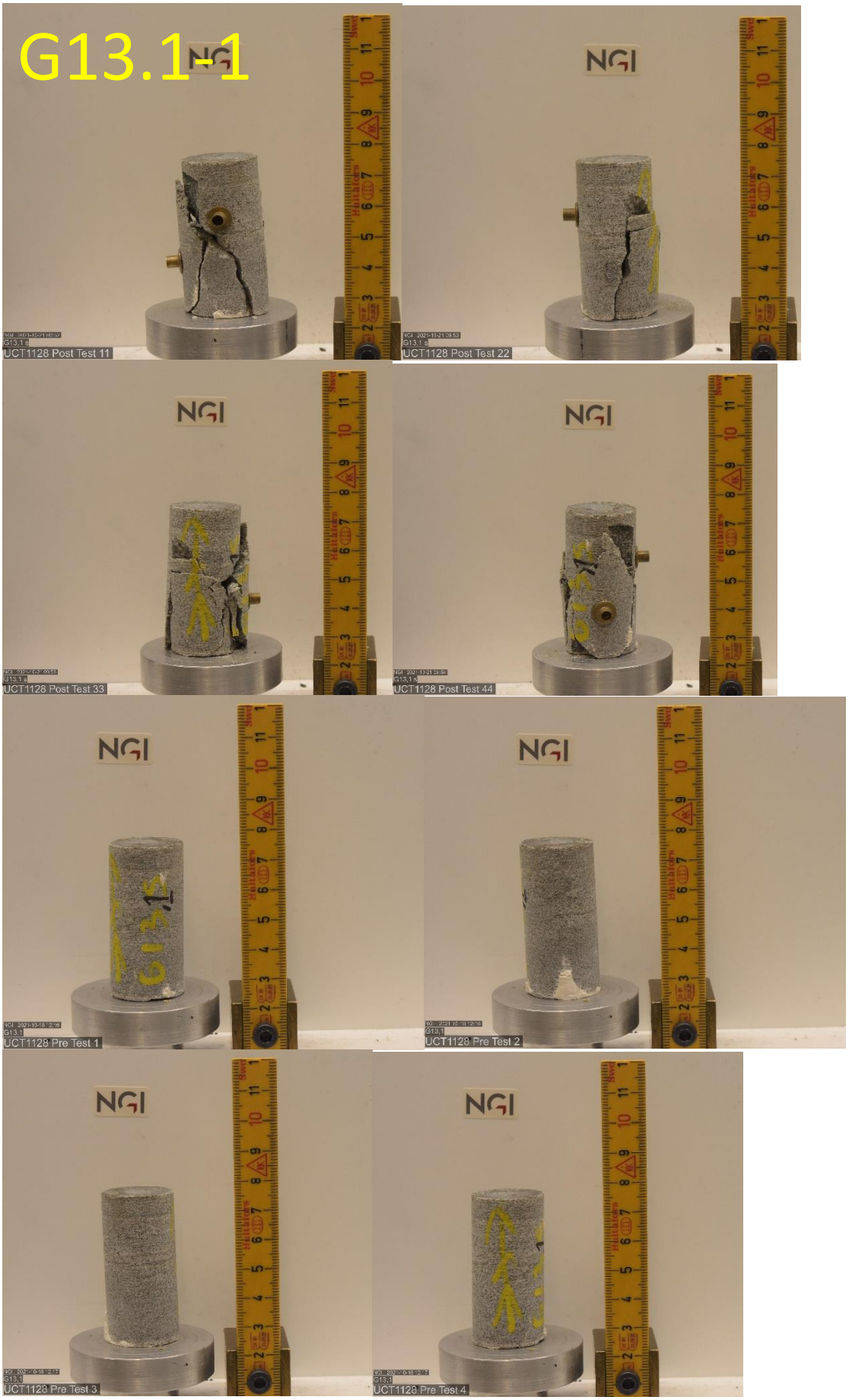
G13.1-1
UCT1128 Post Test 11
UCT1128 Post Test 22
UCT1128 Post Test 33
UCT1128 Post Test 44
UCT1128 Pre Test 1
UCT1128 Pre Test 2
UCT1128 Pre Test 3
UCT1128 Pre Test 4

G13.2-2

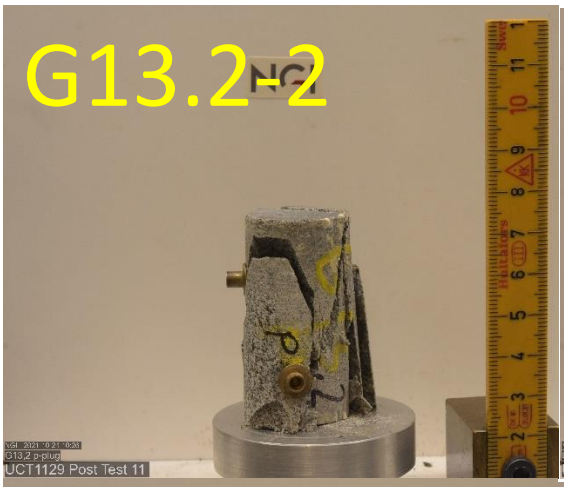
UCT1129 Post Test 11

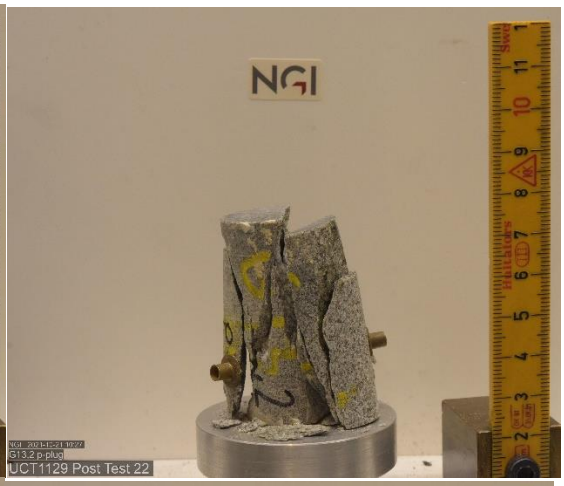
UCT1129 Post Test 22

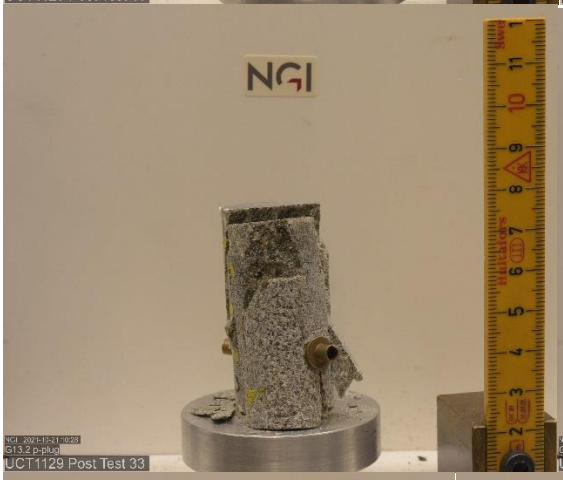
UCT1129 Post Test 33


UCT1129 Post Test 44


UCT1129 Pre Test 1


UCT1129 Pre Test 2


UCT1129 Pre Test 3


UCT1129 Pre Test 4

RM11.1


NGI
RM11.1 p-plug
UCT1130 Post Test 11


NGI
RM11.1 p-plug
UCT1130 Post Test 22


NGI
RM11.1 p-plug
UCT1130 Post Test 33

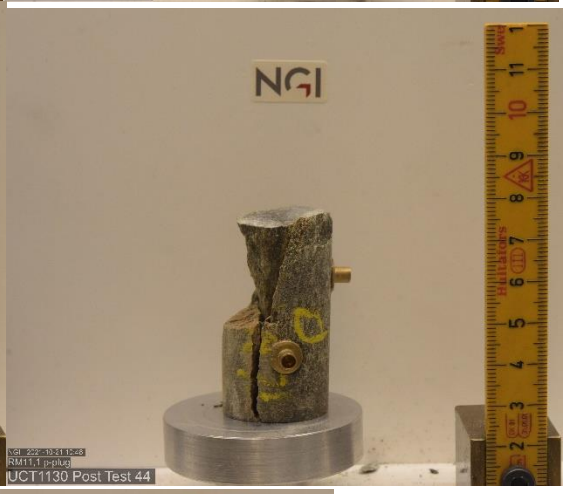
NGI
RM11.1 p-plug
UCT1130 Post Test 44


NGI
RM11.1
UCT1130 Pre Test 1


NGI
RM11.1
UCT1130 Pre Test 2


NGI
RM11.1
UCT1130 Pre Test 3


NGI
RM11.1
UCT1130 Pre Test 4

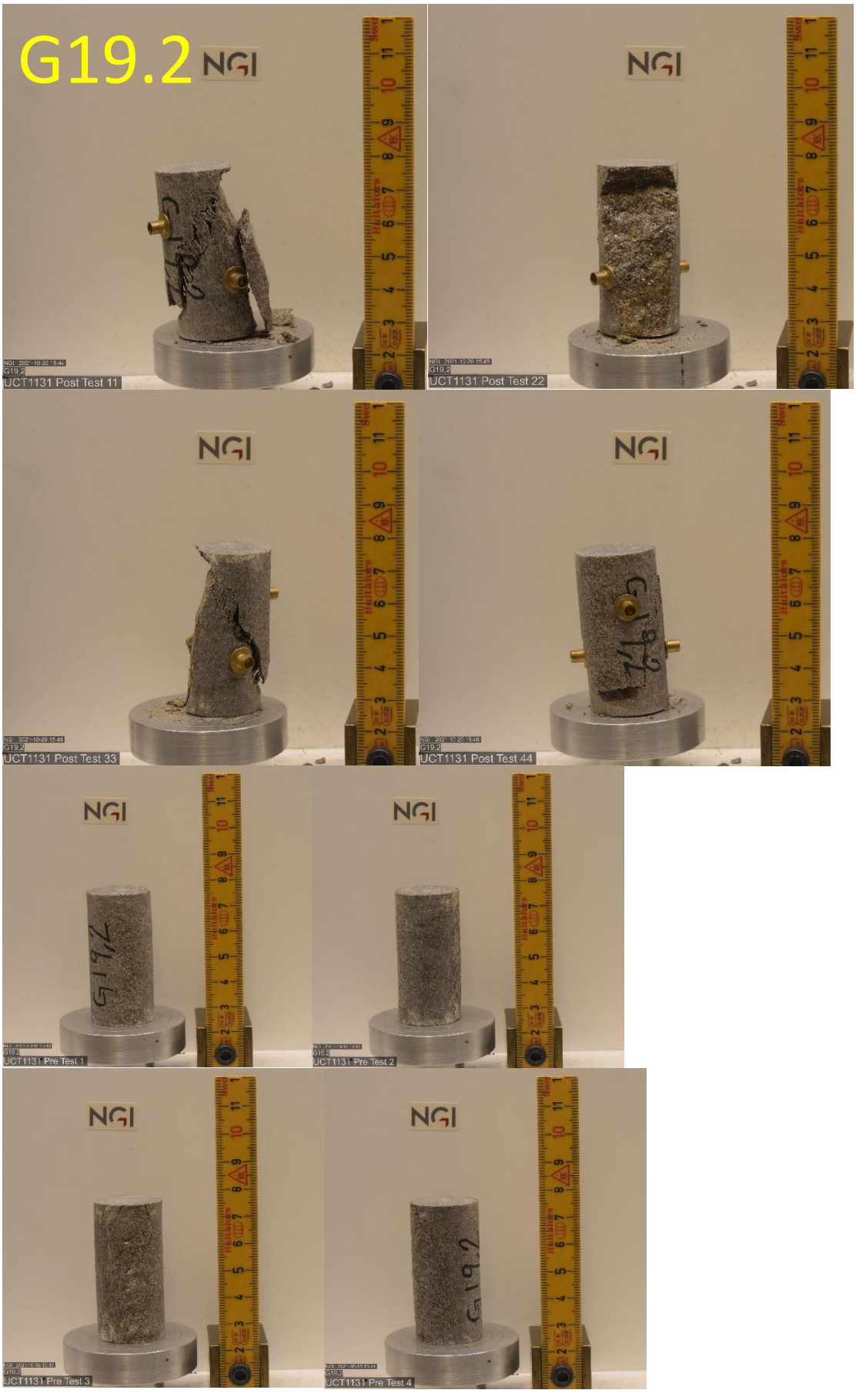
G19.2
NGI
UCT1131 Post Test 11
UCT1131 Post Test 22
UCT1131 Post Test 33
UCT1131 Post Test 44
UCT1131 Pre Test 1
UCT1131 Pre Test 2
UCT1131 Pre Test 3
UCT1131 Pre Test 4

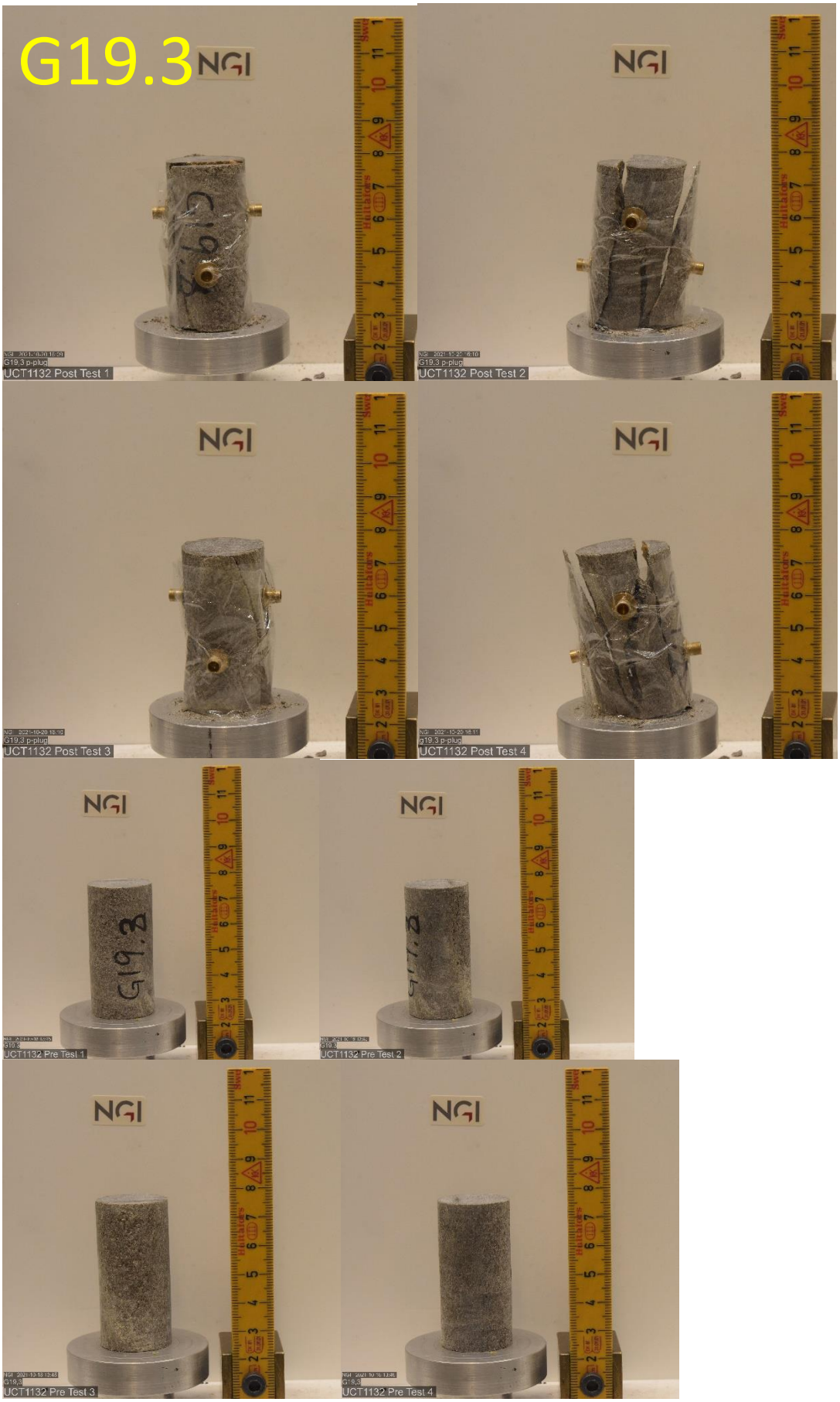
G19.3
NGI
UCT1132 Post Test 1
UCT1132 Post Test 2
UCT1132 Post Test 3
UCT1132 Post Test 4
UCT1132 Pre Test 1
UCT1132 Pre Test 2
UCT1132 Pre Test 3
UCT1132 Pre Test 4

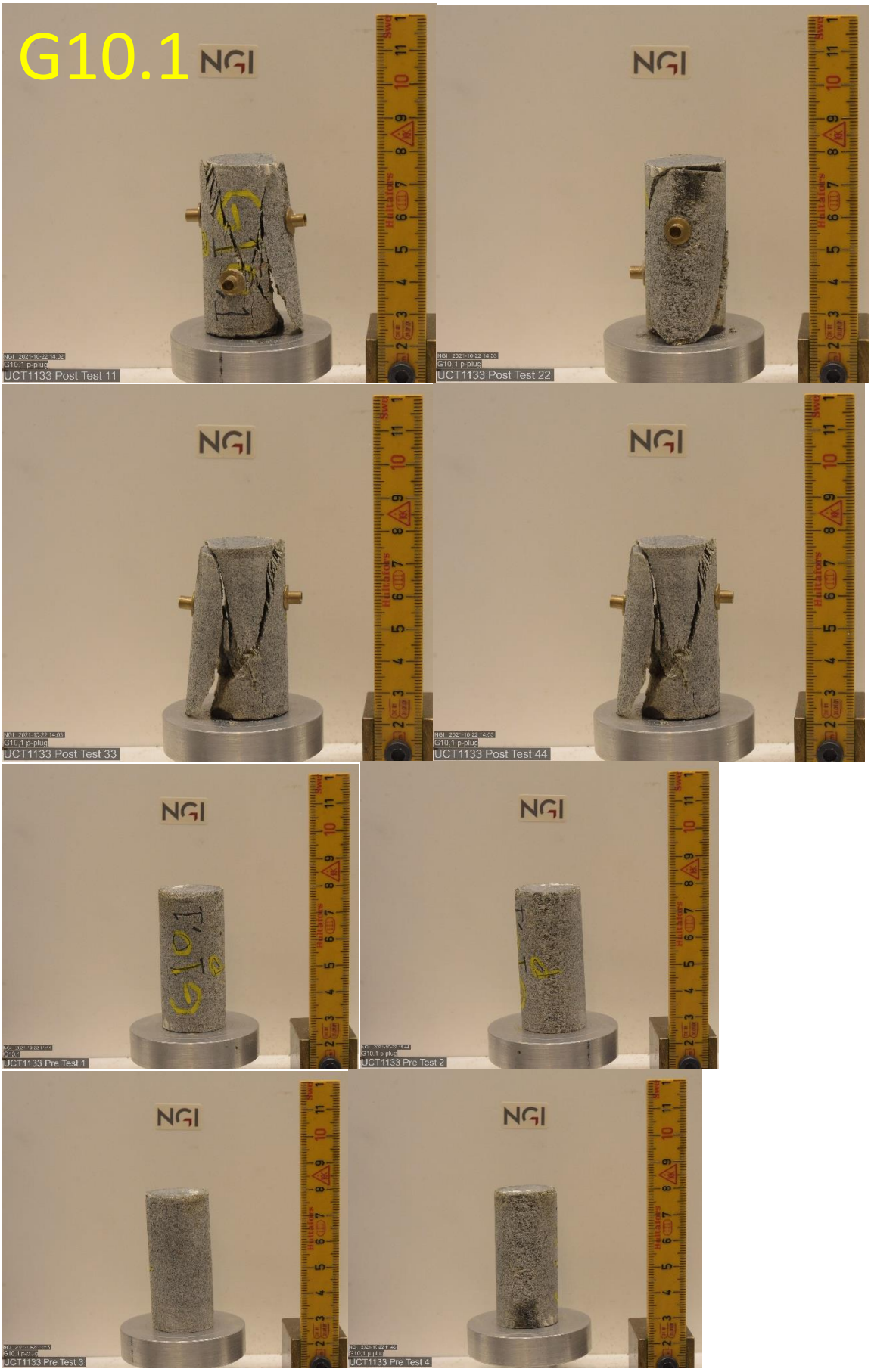
G10.1
NGI
UCT1133 Post Test 11
UCT1133 Post Test 22
UCT1133 Post Test 33
UCT1133 Post Test 44
UCT1133 Pre Test 1
UCT1133 Pre Test 2
UCT1133 Pre Test 3
UCT1133 Pre Test 4

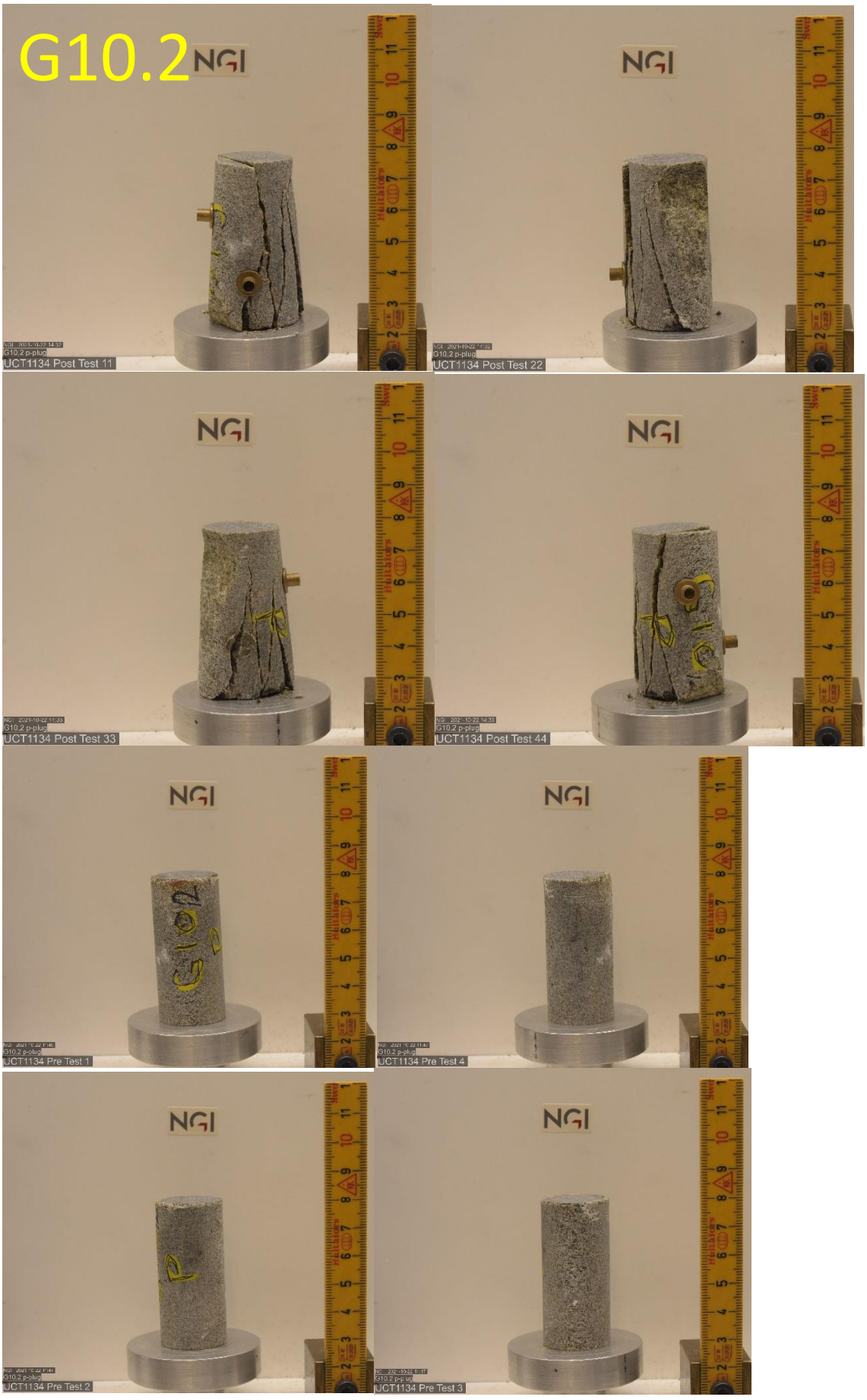
G10.2
NGI
G10,2 p-plug
UCT1134 Post Test 11
NGI
G10,2 p-plug
UCT1134 Post Test 22
NGI
G10,2 p-plug
UCT1134 Post Test 33
NGI
G10,2 p-plug
UCT1134 Post Test 44
NGI
G10,2 p-plug
UCT1134 Pre Test 1
NGI
G10,2 p-plug
UCT1134 Pre Test 4
NGI
G10,2 p-plug
UCT1134 Pre Test 2
NGI
G10,2 p-plug
UCT1134 Pre Test 3

RM12.2-1


RM12.2-1
UCT1135 Post Test 11


UCT1135 Post Test 22


UCT1135 Post Test 33


UCT1135 Post Test 44


UCT1135 Pre Test 1


UCT1135 Pre Test 2


UCT1135 Pre Test 3


UCT1135 Pre Test 4

RM12.2-2


UCT1136 Post Test 1


UCT1136 Post Test 2


UCT1136 Post Test 3


UCT1136 Post Test 4


UCT1136 Pre Test 1


UCT1136 Pre Test 2

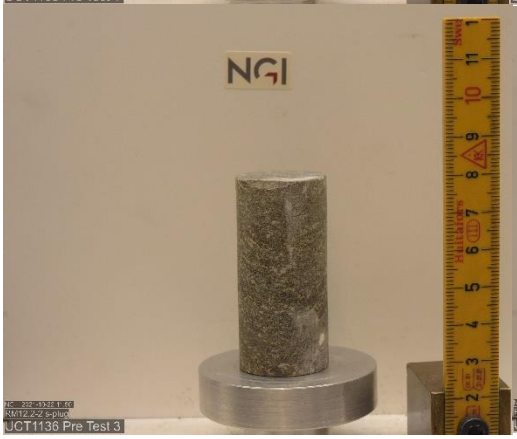
UCT1136 Pre Test 3


UCT1136 Pre Test 4

RM12.2-3


NGI
RM12.2-3 p-plug
UCT1137 Post Test 11

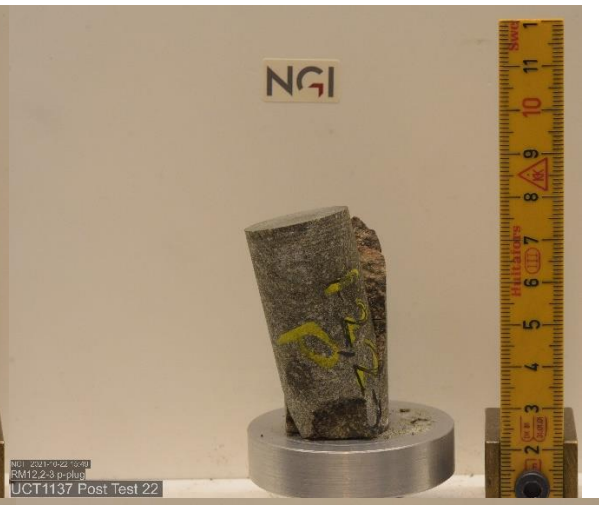
NGI
RM12.2-3 p-plug
UCT1137 Post Test 22

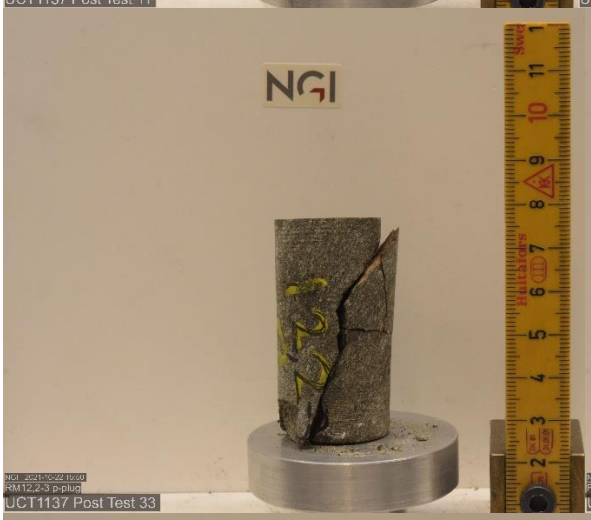
NGI
RM12.2-3 p-plug
UCT1137 Post Test 33


NGI
RM12.2-3
UCT1137 Post Test 44


NGI
UCT1137 Pre Test 1


NGI
UCT1137 Pre Test 2


NGI
UCT1137 Pre Test 3

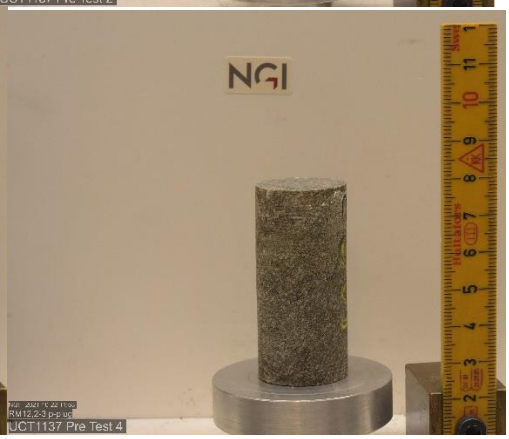
NGI
UCT1137 Pre Test 4

RM12.2-4


NGI
RM12.2-4
UCT1138 Post Test 11


NGI
RM12.2-4
UCT1138 Post Test 22


NGI
RM12.2-4
UCT1138 Post Test 33


NGI
RM12.2-4
UCT1138 Post Test 44

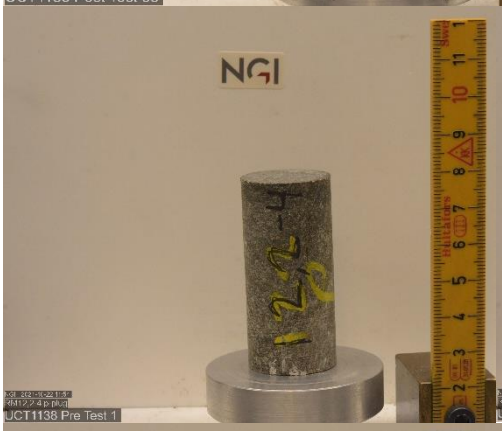
NGI
UCT1138 Pre Test 1


NGI
UCT1138 Pre Test 2


NGI
UCT1138 Pre Test 3


NGI
UCT1138 Pre Test 4